Understanding the Gas Sensing Mechanism for NO_2 on Unloaded and K-Loaded ZnO

Dissertation

der Mathematisch-Naturwissenschaftlichen Fakultät

der Eberhard Karls Universität Tübingen

zur Erlangung des Grades eines

Doktors der Naturwissenschaften

(Dr. rer. nat.)

vorgelegt von

Carolin Ewald

aus Heilbronn

Tübingen

2023

Gedruckt mit Genehmigung der Mathematisch-Naturwissenschaftlichen Fakultät
der Eberhard Karls Universität Tübingen.

Tag der mündlichen Qualifikation:	14.05.2024
Dekan:	Prof. Dr. Thilo Stehle
1. Berichterstatter/-in:	Prof. Dr. Udo Weimar
2. Berichterstatter/-in:	Prof. Dr. Reinhold Fink

Table of Contents

List of Abbreviations

AR	as received
a. u.	arbitrary unit
DC	direct current
DI	deionized
DL	drop loading or drop loaded
DRIFTS	diffuse reflectance infrared Fourier transform spectroscopy
DRUVS	diffuse reflectance ultraviolet-visible spectroscopy
dUV	deep ultraviolet
EDX	energy dispersive X-ray
e.g.	exempli gratia - engl. for example
et al.	et alia - engl. and others
EtOH	ethanol
FSP	flame spray pyrolysis
FT-IR	Fourier transform infrared
GMS	gas mixing system
HMT	hexamethylenetetramine
ICP-OES	inductively coupled plasma optical emission spectroscopy
i.e.	id est - engl. that is
i-PrOH	isopropyl alcohol
JCPDS	Joint Committee on Powder Diffraction Standards
LED	light emitting diode
MCT	mercury cadmium telluride
MeOH	methanol
MFC	mass flow controller
M-O	metal-oxygen
O1s (A)	O1s of adsorbed oxygen
O1s (L)	O1s of lattice oxygen
O1s (V)	O1s of oxygen close to oxygen vacancies
QD	quantum dots
RH	relative humidity
RT	room temperature
SA	Sigma Aldrich
SD	simple dispersion
SEM	scanning electron microscopy
SMOX	semiconducting metal oxide

syn. air	synthetic air
TMAH	tetramethylammonium hydroxide
UD	ultrasonic dispersion
UHV	ultra-high vacuum
UV	ultraviolet
Vis	visual
XPS	X-ray photoelectron spectroscopy
XRD	X-ray diffraction

List of Symbols

A	absorbance
at.%	atomic percent
°C	degree Celsius
cm	centimeter
eV	electronvolt
g	gram
h	hour
kV	kilovolt
l	litre
M	molar mass or molar
mA	milliampere
mbar	millibar
mg	milligram
min	minute
ml	millilitre
mm	millimeter
mol	mole
ms	millisecond
μ	reduced mass
µl	microlitre
µm	microgram
n	amount of substance
nA	nanoampere
nm	nanometer
Ω	ohm
ppm	parts per million
r	molar ratio
R	resistance
s	second
S	sensor signal
SC	intensity of the single channel spectrum
θ	Bragg angle
V	volt
$\hat{\nu}$	wavenumber
W	watt

X	mole fraction
%	percent
°	degree

1 Introduction

With growing industrialization and road traffic, the issue of air pollution has become increasingly present in recent decades. One of the relevant pollutants is NO_2, a toxic, oxidizing and corrosive gas [1] that is mainly emitted during the combustion of fossil fuels [2]. Due to its numerous harmful effects on health, such as respiratory inflammation, headaches and dizziness [3], limit values have been introduced; the occupational exposure limit in Germany is 0.5 ppm [4].

Because of its oxidizing property, it is possible to detect NO_2 with semiconducting metal oxide (SMOX) gas sensors. They are the most investigated group of gas sensors [5] and SMOX materials have been researched for almost 70 years [6]. The main advantages of SMOX gas sensors are low cost, good stability, high sensitivity and the possibility of miniaturization [7]. Besides the common SMOX materials like for example SnO_2 or WO_3, ZnO has also turned out promising for the detection of NO_2 [8],[9]. ZnO is an n-type semiconductor and was the very first SMOX material that was discovered for its gas-sensitive properties by Mollwo and Heiland in 1954 [6],[10]. To date, ZnO has been extensively researched and is particularly known for its high electron mobility. In addition, the gas-sensing properties of ZnO can be tuned by applying various nanostructures such as nanorods, nanotubes, quantum dots, nanopyramids or microflowers, in which the decreased particle size increases the specific surface area and can change the physical and chemical properties [9],[11]. Moreover, doping or loading ZnO with a foreign metal is also a strategy to change the sensing parameters. While an improvement of sensitivity can be achieved by loading with noble metals such as Ag [12] or Au [13], there are also approaches for transforming ZnO into a p-type semiconductor by doping with alkali metals [14],[15]. However, the use of potassium for example, can also result in undesirable changes of the properties, like an increased resistance [16].

Commonly, ZnO gas sensors are heated to temperatures between 200 and 400 °C to provide sufficient energy for the surface reactions. An alternative excitation source is light in the UV-Vis range. Research on light-activated gas sensing with ZnO strongly increased during the last decade. Excitation by photon energy can enable completely different surface reactions compared to heated SMOX sensors, which expands the field of application [17].

It is widely known that ZnO is a suitable material for the detection of NO_2. How exactly the gas sensing mechanism occurs, however, has so far only been documented to a limited extent by means of diffuse reflectance infrared Fourier transform spectroscopy (DRIFTS)

studies. The next section gives a review about the current state of research on unloaded, K-loaded and light-activated ZnO with regard to sensing NO_2.

1.1 Literature Review

When NO_2 is adsorbed on ZnO, the typical reaction between n-type semiconductors and oxidizing gases occurs: electrons are transferred from the conduction band to the ZnO surface, which leads to the formation of an electron depleted layer and an increase in resistance [9]. During this process, NO_2 can adsorb into oxygen vacancies or react with surface oxygen atoms to form nitrite ($-NO_2^-$) and nitrate ($-NO_3^-$) species. Their coordination at the surface is versatile and can be observed via DRIFTS [18],[19].

Two studies that addressed the sensing mechanism on ZnO with NO_2 by applying DRIFTS were reported by Chen et al. The authors exposed ZnO nanostructures to 9800 ppm NO_2 in a He atmosphere and investigated the surface reactions between RT and 300 °C. They could observe the time dependent evolvement of a variety of surface species and proposed mechanisms for their formation. For the formation of nitrite, the adsorption of NO_2 on a Zn site was proposed. Nitrate formation was suggested to occur either on nitrite together with an additional NO_2 molecule or on adsorbed oxygen with an NO_2 molecule. In both publications, the formation of nitrite and nitrate is considered to cause a resistance increase [20],[21].

Another investigation was performed by Zhang et al. using a ZnO nanorod array gas sensor for the detection of NO_2 and NO. During the experiments, the sensor was exposed to 4.2 ppm NO_2 in N_2 and operated at 200 °C. The authors observed a time resolved formation of various nitrates and proposed their formation especially on oxygen deficient sites [22].

Recently, Khamfoo et al. performed an operando DRIFTS study on ZnO based gas sensors fabricated from commercially purchased nanopowder from Sigma Aldrich. They dosed 2.5 ppm NO_2 in 10 % RH in synthetic air and operated the sensors at 300 °C. Their results showed the formation of nitrites and nitrates together with a resistance increase [23].

Although these studies are giving an overview of possible species during NO_2 exposure on ZnO, most of them do not address realistic conditions, i.e. humid air and an NO_2 concentration in the lower ppm range [20]–[22]. Moreover, in conditions close to realistic applications, the exact coordination of species, e.g. monodentate, bidentate or chelating was not clarified until now [23].

The gas sensing mechanism of K-loaded ZnO with NO_2 has not yet been researched before this work and the associated publication [24]. However, there are publications about the

sensing behavior in reducing gases and the changed properties of ZnO in general induced by K. Saaédi et al. reported about an improved gas sensing behavior of K- and Na-doped ZnO nanorods in ethanol at 300 °C. Their results showed that K-doped ZnO exhibited a higher sensor signal and a shorter response and recovery time than undoped ZnO. In addition, they found an increased amount of oxygen vacancies on the doped samples and an increased resistance. It was suggested that both properties result in the enhanced response to ethanol [25]. Gu et al. reported similar findings for K-doped ZnO nanowires that were exposed to various levels of humidity. They also suggest that the increased number of oxygen vacancies improves the sensor performance [26]. That the resistance increases as a result of K-doping is related to the fact that K acts as an electron acceptor, i.e. it attracts electrons that are no longer available for conduction [16]. From a certain K concentration, p-type properties can be identified, as reported by Au et al. They have applied concentrations between 0 and 25 at.% K and observed the transition from n- to p-type ZnO at 10 at.% K. The authors assume that K is present as an interstitial or substitutional atom in ZnO [15]. Even if the reaction of K-ZnO with NO_2 is still unknown, the interaction between K and NO_2 is a known phenomenon that is used in NO_x storage/reduction catalysts, e.g. $Pt/K/Al_2O_3$. In this process, exhaust NO_2 is adsorbed on the surface of alkaline earth or alkali adsorption sites in the form of nitrites or nitrates, where K promotes the formation of free nitrates, indicating the formation of KNO_3. With the help of reducing agents, the stored NO_2 is reduced to N_2 and released [27].

Until now, only the effect of reducing gases on K-ZnO was investigated and identified as beneficial for the sensor performance. However, the increased resistance could be disadvantageous in oxidizing gases because of the decreased concentration of electrons induced by the acceptor property of K. As a consequence, less oxidizing gases could be adsorbed which would decrease the sensor signal.

Applying light to the sensitive layer instead of heating it has certain benefits: with LEDs the power consumption is significantly reduced and due to the low operating temperatures sensors become more user-friendly, especially in portable devices. Therefore, research on this topic is of great interest. During the light-activation process, electron hole pairs are generated. When the photon energy of the light exceeds the band gap of the sensing material, electrons from the valence band are excited to the conduction band and the resistance decreases [17]. Defect states within the band gap can be activated already by applying lower photon energies [28]. For a long time, the focus of research was primarily on UV activation [29]–[31]. However, due to high pricing of UV LEDs, a lack of selectivity and photolysis of gases such as NO_2, light in the visible spectrum was also increasingly used for excitation [28],[32].

For ZnO it was reported that with the decreased resistance induced by e.g. UV light, more electrons are available, which leads to an increased adsorption rate of NO_2 and O_2. At the same time, a light induced desorption of O_2 is possible. However, as with conventionally operated gas sensors, the adsorption of NO_2 is suggested to take place both on surface oxygen atoms or in oxygen vacancies [17],[33]. It was demonstrated by Wang et al. that a high concentration of oxygen vacancies improves the sensing behavior because they are highly active under UV for the adsorption of O_2 and NO_2 [34].

Even though a number of studies of UV or visual light-activated gas sensing on ZnO with NO_2 was reported, none of these studies included a comprehensive investigation that addressed the whole UV-Vis range in various humidity levels.

1.2 Scope of the Work

The aim of this work is to provide a better understanding of the gas sensing mechanism on ZnO with NO_2.

First of all, the gas sensing properties of unloaded ZnO based gas sensors with NO_2 will be investigated in detail by applying DC resistance measurements combined with DRIFT spectroscopy. The aim is to identify the surface groups involved in the gas sensing mechanism. Together with the electrical results, the spectroscopic insights will be used to establish the surface reactions.

In the second part, the impact of K on the gas sensing behavior of ZnO together with O_2 and NO_2 will be identified. For this, a method to load ZnO with K will be developed. DC resistance measurements in combination with DRIFT spectroscopy will enable to determine the gas sensing mechanism and to propose the respective surface reactions. A direct comparison to unloaded ZnO allows for identifying the differences related to K.

In addition, some insights into light-activated gas sensing on ZnO based gas sensors with NO_2 will be given. For this, FSP prepared sensors will be investigated via DC resistance measurements during the application of light in the UV-Vis range. This approach will enable to identify the influence of various photon energies on the sensing behavior.

2 Experimental Methods

2.1 Preparation of the Powders

ZnO **rods** were received from Saito et al. and prepared in a solvothermal route. 2.202 g zinc acetate anhydride and 1.682 g hexamethylenetetramine (HMT) were dissolved separately in deionized water and combined. The mixture was stirred and heated to 95 °C for 12 h in an oven. Afterwards, the precipitate was centrifuged and rinsed with EtOH via ultrasonic bath three times. The powder obtained was dried in vacuum at RT [35].

Commercial ZnO nanopowder was purchased from Sigma-Aldrich (<100 nm particle size, SA as received or **SA-AR**). In order to homogenize the powder, 300 mg ZnO was dispersed in 5 ml isopropyl alcohol (*i*-PrOH) via ultrasonic bath for 15 min. The dispersion was repeated once and the mixture was stirred for 24 h at RT followed by two times centrifugation, washing with 5 ml *i*-PrOH and stirring for 2 h at RT. The washed powder was dried at 80 °C for 24 h and calcined at 500 °C for 5 h in an alumina crucible (SA ultrasonic dispersion or **SA-UD**) [24].

ZnO **quantum dots (QD)** were received from Lee at al. and synthesized via a wet chemical route. 1.975 g zinc acetate was dissolved in 90 ml *N,N*-dimethylformamide. This precursor solution was added to a solution of tetramethylammonium hydroxide in methanol (MeOH:TMAH = 1:8) with a syringe pump for 1 h at 30 °C. The powder obtained was washed with acetone and dispersed in methanol [36].

2.1.1 Loading Procedures

Various approaches were applied to load the sensors or powders with potassium. For calculating the appropriate concentration of potassium, the molar ratio *r* and the mole fraction x are considered:

$$r = \frac{n(\mathrm{K})}{n(\mathrm{Zn})} \tag{2.1}$$

$$x = \frac{n(\mathrm{K})}{n(\mathrm{K}) + n(\mathrm{Zn})} \tag{2.2}$$

Drop loading (DL)

Potassium acetate was dissolved in DI-water so that 0.1 M and 0.01 M solutions resulted. From the respective solution, 1 µl was dropped onto the sensitive layer (SA-AR) using a

pipette and the sensor was dried first at RT followed by calcination according to the procedure described below. Additionally, 1 µl droplets of the 0.01 M potassium acetate solutions were applied multiple times (1+4+5 times, in sum 1, 5 and 10 µl) onto the same sensitive layer, including calcination and characterization in between. Assuming that one sensitive layer consists of 20 mg ZnO and 1 µl 0.1 M or 0.01 M potassium acetate solution was added, the approximate concentration corresponds to 0.04 at.% or 0.004 at.% K, respectively.

Simple dispersion (SD)

An aqueous solution of potassium acetate with a concentration of 0.71 mg/ml was prepared. 300 mg ZnO (SA-AR) was mixed with 5 ml potassium acetate solution using a spatula. The mixture was dried at 80 °C under occasional stirring with a spatula for 18 h. When all solvent was evaporated, the dried powder was homogenized in a mortar. The target concentration was 0.99 at.%. Similarly, 0.5 ml potassium acetate solution and 4.5 ml DI-water were mixed with 300 mg ZnO, having a target concentration of 0.099 at.%.

Ultrasonic dispersion (UD)

This loading procedure corresponds to what is described above for SA-UD (dispersion of unloaded ZnO) with the only difference that potassium is added. Unloaded SA-UD serves as a reference to compare with K-loaded SA-UD. For its preparation, 300 mg ZnO was dispersed in 5 ml *i*-PrOH via ultrasonic bath for 15 min. 2 ml of a potassium acetate solution in *i*-PrOH (c=1.81 and 18.1 mg/ml) and 3 ml *i*-PrOH were added after which the mixture was homogenized again for 15 min via ultrasonic bath. The dispersion was stirred for 24 h at RT followed by two times centrifugation, washing with 5 ml *i*-PrOH and stirring for 2 h at RT. The washed powder was dried at 80 °C for 24 h, calcined at 500 °C for 5 h in an alumina crucible and subsequently homogenized in a mortar. The target concentrations were 0.99 and 9.09 at.%, respectively. The real concentrations are expected to be lower due to washing. In order to keep a higher concentration of K throughout the loading procedure, another sample with the target concentration of 9.09 at.% was prepared but without centrifugation, washing and stirring the powder before drying and calcination. An overview of the K-loaded samples prepared via SD and UD is given in Table 2.1. The real potassium concentrations are expected to differ from the target concentrations, which is why for the two samples with the highest target concentrations they were determined by means of ICP-OES. The analyses were performed by dissolving 10 mg of the sample powder in 10 ml of 18 % aqueous HCl solution. The mixture was heated to 140 °C for 30 min, cooled to RT and diluted to 50 ml using Milli-Q water. The analysis was performed using an Agilent 5800 ICP-OES (radial viewing, RF power 900 W).

Table 2.1 Overview of the K-loaded samples prepared via SD and UD.

Sample name	Target concentration	
	r [%]	x [at.%]
SA-SD	0.1	0.099
SA-SD	1	0.99
SA-UD	1	0.99
SA-UD	10	9.09
SA-UD (without washing)	10	9.09

2.2 Sensor Fabrication

2.2.1 Screen Printing

From each powder, sensors were fabricated according to the procedure described as follows. ZnO powder was mixed with 1,2-propanediol (Sigma-Aldrich, ACS reagent ≥99.5 %) and ground with a mortar and a pestle until a homogeneous paste was obtained. Using an Ekra Microtronic II screen printer, the paste was applied onto the interdigitated electrode structure (300 µm gap) of an Al_2O_3 substrate which was manufactured by Ceramtec. The screen printing process is schematically represented in Figure 2.1. A layer thickness of approximately 50 µm was achieved on the basis of the screen mesh.

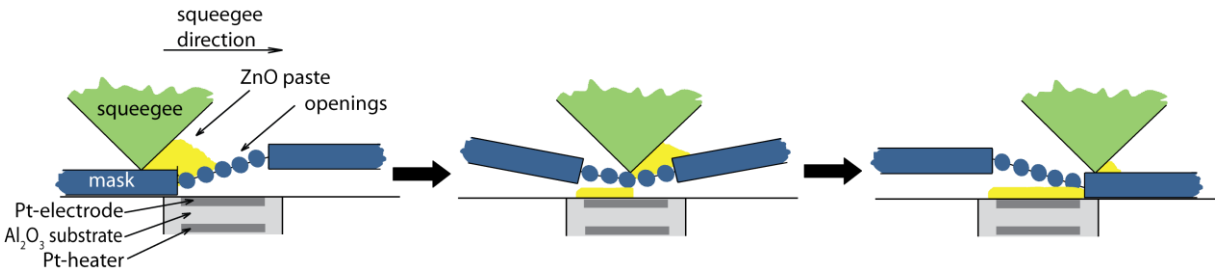

Figure 2.1 Sketch of the screen printing process. The figure was adapted from [37].

After screen printing, the sensors were kept overnight at RT and afterwards dried at 80 °C for 4 h in a Heraeus UT 12 oven. To finally stabilize the layer and remove the remaining binder, the sensors were annealed in a Heraeus ROK 6/30 tube furnace at 400, 500 and 400 °C, for each 10 min and slowly cooled down to RT. A sketch of a typical screen printed sensor from different views and with all dimensions is shown in Figure 2.2.

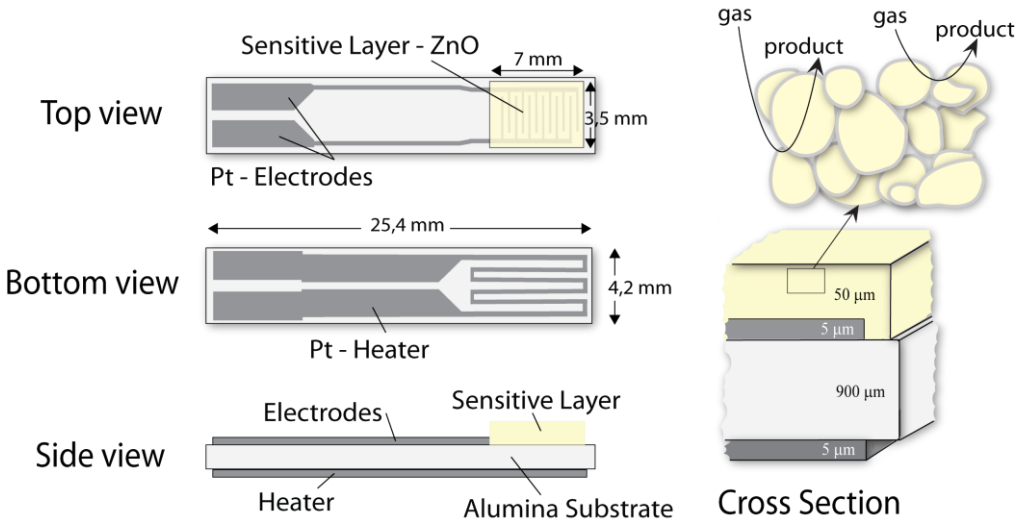

Figure 2.2 Schematic representation of a sensor substrate. On top of the platinum electrodes, the sensitive layer was deposited via screen printing and the heater on the backside enables temperature adjustment during the experiments. The figure was adapted from [38].

2.2.2 Flame Spray Pyrolysis

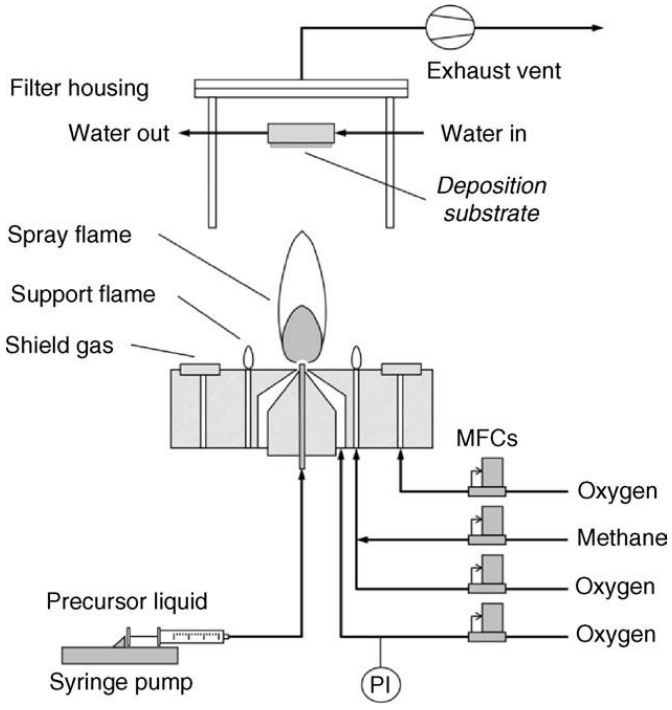

Figure 2.3 Schematic representation of the FSP setup. The figure was adopted from [39].

For light-activated gas sensing experiments, the sensitive layers were deposited via flame spray pyrolysis (FSP) and received from IWT in Bremen, Germany. A schematic of the experimental setup is shown in Figure 2.3. In this method, a precursor solution, typically

made of a metal salt and an organic solvent, is sprayed into a flame, followed by combustion of the small droplets. To receive ZnO, a solution of 0.5 mol/l zinc naphthenate (10 % Zn in mineral spirits, Strem Chemicals) in xylene (Fisher Chemical) was prepared via 10 min ultrasonic treatment. 100 ml of this precursor solution was filled into a KDS-100-CF syringe pump from KD Scientific that was connected to the FSP nozzle. A premixed flame of 1.5 l/min CH_4 and 3.2 l/min O_2 was applied as support flame and dispersion oxygen was set to 5.0 l/min with a constant pressure drop of 1.5 bar at the nozzle. In the flame, metal-oxyanions are formed, which co-react/nucleate to clusters of metal oxides. Via coalescence of these clusters, nuclei are formed that further build metal oxide particles [40]–[42]. For deposition, the substrates were mounted 14 mm above the nozzle. At this height, the formed particles are having a temperature of approximately 500 °C. To enable efficient deposition and avoid condensation of water from humid air, the substrates were cooled to a temperature of 120 °C using a variable air flowmeter (ABB). Afterwards, the as prepared sensors were annealed in a tube furnace as described above. With regard to light-activated gas sensing measurements, the advantage of FSP is that a highly porous and almost transparent layer is obtained. This allows the light to penetrate the whole layer, which increases the photoresponse [43]. Since the particle size is smaller compared to conventionally prepared powders (about 10 nm), these sensors have a relatively high baseline resistance [44],[45]. To still ensure a reliable measurement, substrates with a smaller electrode gap were used (Innovative Sensor Technology, 30 µm).

2.2.3 Temperature Calibration

To enable the setting of the desired temperature during the experiments, the platinum heaters were calibrated. A voltage in steps of 0.5 V and in a range between 2 and 8 V was applied and the current was measured with an Agilent Single Output DC Power Supplier. At the same time, the temperature of the sensitive layer was measured with a Maurer KTR 2300 digital infrared Pyrometer. In Figure 2.4, a schematic of the calibration setup is shown together with an exemplary calibration plot, where the linear relation between the resistance of the platinum heater and the temperature is seen. This calibration was performed on every single sensor as the resistance-temperature correlation is different for each substrate.

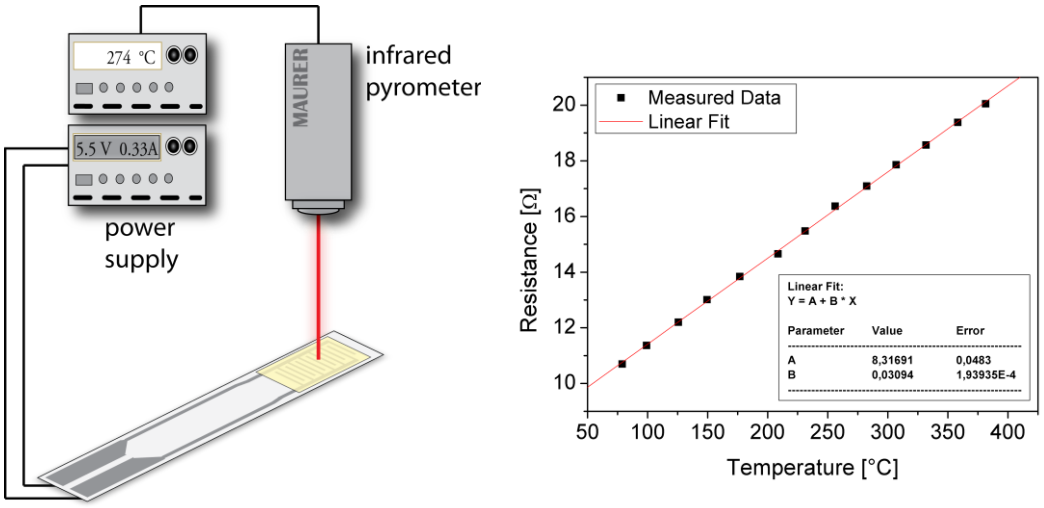

Figure 2.4 The temperature calibration of the platinum heater is represented with a schematic of the calibration setup showing the sensor, power supply and infrared pyrometer [38] on the left hand side and an exemplary calibration plot after linear fit on the right hand side.

2.3 Material Characterization

The SEM images were taken with a HITACHI SU8000 scanning electron microscope directly on the sensitive layers, with an acceleration voltage of 3 or 5 kV, a working distance between 3 and 9 mm and an emission current of 10100 nA. EDX measurements were performed as well in order to get qualitative information about the composition at the surface.

To prepare the samples for XPS measurements, the powders were mixed with EtOH, deposited on a Si-wafer and dried at 80 °C. The spectra were recorded with a Sigma Probe instrument from Thermo Scientific in UHV conditions (around 10^{-9} mbar). The binding energy was calibrated using Au4f as a reference. Deconvolution and fitting of the spectra were done with the software Avantage from Thermo Fisher, wherein a Sherley-background was chosen for peak fitting.

For most of the samples, XRD was performed on the powder using a Rigaku D/teX Ultra 250 equipped with a monochromatic Cu K_α radiation source (λ = 1.541862 Å). Diffraction patterns were recorded from 5 to 85 ° 2θ with a step size of 0.01 ° and a rate of 1°/min. For rods and QD the XRD measurement was carried out also on powder using a StadiP Stoe with a Ge-monochromatic Cu $K_{\alpha1}$ radiation source and similar settings. FSP prepared ZnO powder was characterized with a Bruker D8 Discover diffractometer equipped with a Cu $K_{\alpha1,2}$ Ni-filtered radiation source. The diffraction patterns were recorded from 5 to 135 ° 2θ and with time steps of 1.5 s.

DRUV spectroscopy was performed on FSP prepared ZnO powder to determine the band gap. The sample was placed in a Harrick Praying Mantis optic chamber and the measurement was carried out with a DH-2000-Bal broadband UV-Vis lamp (Ocean Insight) and a Maya2000 Pro single channel spectrometer (Ocean Insight). The spectra were recorded at RT with the reference BaSO4 (97 %, Alfa Aesar) and a spectral resolution of 0.5 nm, an integration time of 50 ms, a boxcar width of 10 and were averaged over 40 scans. The Tauc plots were generated from the reflectance data by applying the Kubeka-Munk transformation. For this, a direct allowed transition from valence to conduction band was assumed.

2.4 DC Resistance Measurements

To investigate the sensor performance, the DC resistance of the sensitive layers was measured while the sensors were exposed to different gases. The setup is represented in Figure 2.5.

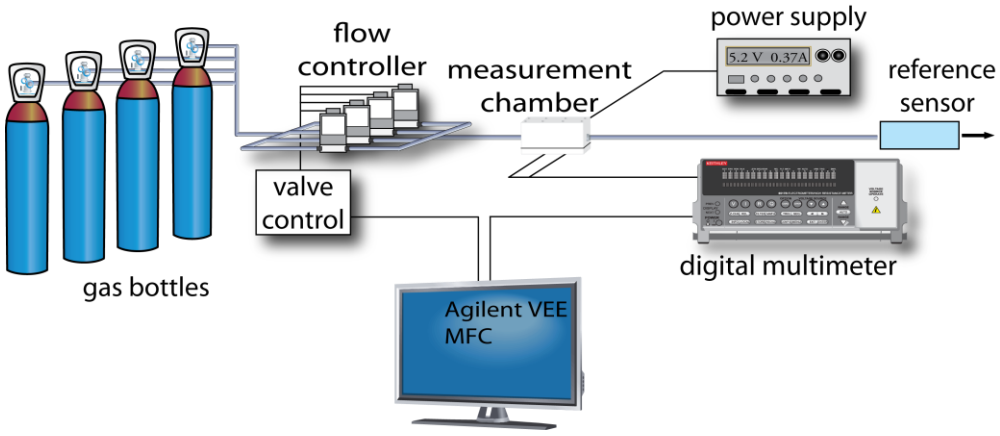

Figure 2.5 Setup for the DC resistance measurements. The figure was adapted from [38].

During the experiments, the gases were composed with a computer-controlled gas mixing system (GMS), so that the desired gas mixture was obtained. Among the applied gases, N_2, synthetic air, NO_2, and CO_2 were dosed via gas bottles, whereas humidity was controlled with a bubbler filled with deionized water (as RH @ 25 °C). Application relevant concentrations were chosen. The gas mixture was led through an in-house made measurement chamber, in which the sensors were mounted. For setting a certain temperature, a voltage was applied to the heaters using an Agilent E3642A power supply. Unless otherwise stated, the operating temperature was 250 °C. The resistance of the sensitive layer was measured with an Agilent 34972A digital multimeter. In addition, the

exhaust leaving the chamber was controlled by commercial reference sensors, including a Figaro TGS 2600 SMOX sensor and an IST HYT 939 humidity sensor.

The sensor signal *S* was calculated to enable comparison between the gas sensing properties of different sensors. For its calculation, resistance values of the sensitive layer in equilibrium with the gas atmosphere were taken. In the case of oxidizing gases, the resistance during exposure to the target gas is divided by the resistance during baseline condition:

$$S_{ox} = \frac{R_{target\ gas}}{R_{baseline}} \tag{2.3}$$

For the sensor signal of reducing gases, the inverse relation applies.

2.4.1 Light-Activated Gas Sensing

In a different experimental series, the NO_2 performance of ZnO based gas sensors that are activated by light instead of being heated was investigated. For this purpose, FSP samples were used because in this way the light can access the whole layer. The experimental setup is very similar to the common DC resistance setup with the main difference of a specialized measurement chamber. This chamber is equipped with holes in the side of the lid to introduce the light by LEDs, with a distance of 3 mm to the sensing layer (see Figure 2.6). Using a constant current source (Knight J152), the LEDs were operated at 20 mA. The experiment started in the dark, followed by exposure to red (631 nm), green (520 nm), blue (468 nm), UV (375 nm) and deep UV (dUV, 310 nm) light and a final measurement in the dark again. In addition, the sensors were operated at 70 °C in order to avoid degradation processes which were observed at RT [46].

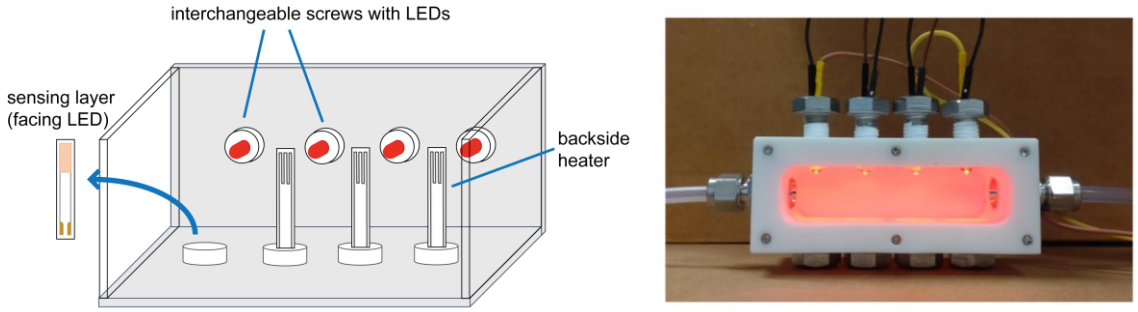

Figure 2.6 Specialized measurement chamber for light-activated gas sensing experiments depicted as a side view of the open chamber (left) and a bottom view of the lid with LEDs mounted through the side (right). The figure was adapted from [46].

2.5 DRIFTS Measurements

Operando DRIFT spectroscopy was performed to investigate the surface reactions at the sensitive layer. The spectra were recorded with a Bruker Vertex70v and 80v FT-IR spectrometer, that were equipped with a Harrick Praying Mantis optic chamber and evacuated during the measurements. The narrow-band mercury cadmium telluride (MCT) detector was cooled with liquid nitrogen. Simultaneously to the DRIFT spectra, the DC resistance was measured as described in section 2.4. Inside the optic chamber, an in-house made air tight gas sensing chamber with a KBr window was placed, in which the sensor was mounted and exposed to different gases. The operating temperature was set with an Agilent U8001A DC power supply and the resistance was measured using a Keithley 617 electrometer. The setup is shown in Figure 2.7.

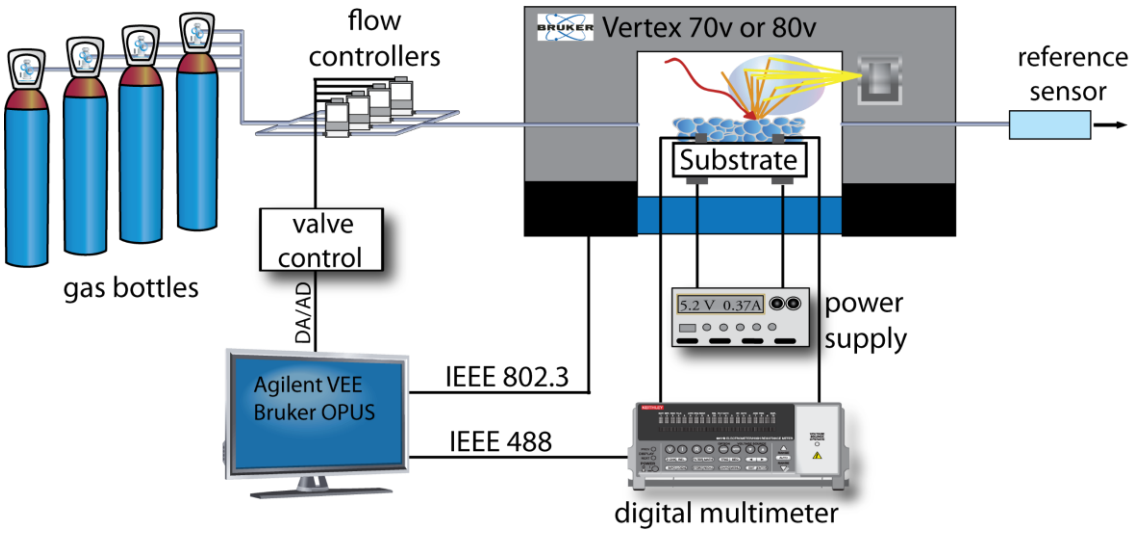

Figure 2.7 Setup for the DRIFTS measurements. The figure was adapted from [38].

Using the software OPUS, the single channel spectra were recorded with a spectral resolution of 4 cm^{-1} every 15 min with 1024 sample scans or every 15 s with 17 sample scans, respectively. The absorbance spectra were calculated according to the relation proposed by Olinger and Griffiths [47]:

$$A = -\log\left(\frac{SC_{target\ gas}}{SC_{reference}}\right) \tag{2.4}$$

To obtain the absorbance *A*, the intensity values of the single channel spectrum recorded during exposure to the target gas ($SC_{target\ gas}$) were referenced to the values of the single channel spectrum in the reference condition ($SC_{reference}$). Isotopically labelled gases exhibit a mass difference to the respective unlabeled gas, that leads to a characteristic

wavenumber shift, enabling the distinct identification of surface groups. In this manner, D_2O was used to distinguish between different hydroxyl species. The theoretical shift factor was calculated on the basis of the harmonic oscillator approximation:

$$\frac{\tilde{\nu}_{\mathrm{O-D}}}{\tilde{\nu}_{\mathrm{O-H}}} = \sqrt{\frac{\mu_{\mathrm{O-H}}}{\mu_{\mathrm{O-D}}}} \tag{2.5}$$

For the shift between O-D and O-H vibrations the theoretical factor is 0.728. In most cases it is in good agreement with the experimental values. Slight differences might occur though, as the anharmonic oscillator model is neglected in this approach.

3 Sensing with ZnO

3.1 Material Characterization

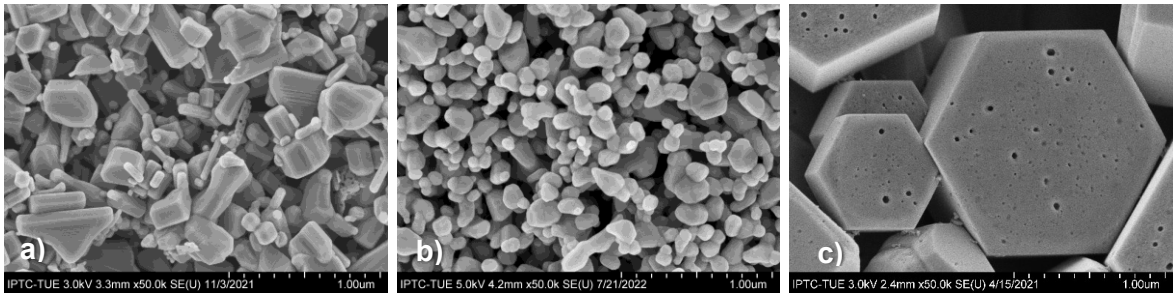

Figure 3.1 SEM images of the sensitive layers of unloaded ZnO samples a) SA-AR, b) SA-UD, c) rods.

Initially, morphological and structural characterizations were carried out via SEM, XPS and XRD. The SEM measurements have revealed that the morphology of ZnO SA-AR, seen on the image in Figure 3.1 a), includes various shapes as elongated rods or round and hexagonal structures of various grain sizes (range between 49 and 457 nm). It is not clear if some of the largest particles are agglomerates of many smaller grains. In order to obtain a more homogeneous morphology, the as-received powder was ultrasonically dispersed as described above (2.1 Preparation of the Powders). The SEM image in Figure 3.1 b) shows that this approach was successful, as the grains appear more homogeneous in shape and size. After ultrasonic treatment, the grains have a roundish shape with a grain size range between 48 and 222 nm. In contrast, ZnO rods show larger hexagonal shaped grains of diameters from 330 nm up to 2 µm with pores that are hexagonally shaped, as well. For a better overview of the size distribution, a SEM image of lower magnification is attached to the appendix (SF 1).

The XPS measurements are depicted in Figure 3.2. For SA-UD, the C1s spectrum was already published in [24]. In the C1s spectra it is seen that all unloaded samples contain hydrocarbons, which is a common impurity in ZnO [48]. Additionally, zinc carbonate [49] was found in SA-UD; this indicates that carbon was introduced with the ultrasonic treatment by isopropanol or atmospheric CO_2 [50] and transformed into carbonate during the final annealing. The C1s of the rods is very noisy and it is not clear if there is a peak in the carbonate region. Moreover, O1s spectra are considered and deconvoluted to compare between the samples. In literature, asymmetric O1s spectra are deconvoluted into three characteristic peaks: lattice oxygen (L), oxygen atoms adjacent to oxygen vacancies (V)

and adsorbed oxygen (A). Depending on their neighboring atoms, these species reveal different binding energies, which makes them distinguishable [51]. In relation to O1s (L), O1s (V) is higher for the rods than in both SA samples. This indicates that the rods have more oxygen vacancies in the surface layer of approximately 5 nm that is accessible via XPS. In addition, O1s (A) was identified only for the rods. Both SA samples are similar in their O1s spectra.

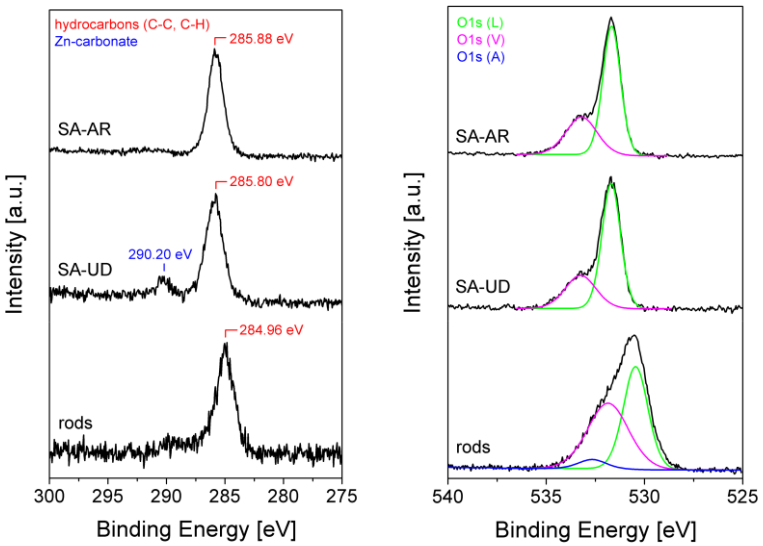

Figure 3.2 XPS measurements of the unloaded ZnO samples including C1s spectra (left) and O1s spectra (right).

From the XRD patterns, the hexagonal wurtzite phase was identified for all unloaded ZnO samples and the diffractograms are depicted together with the reference pattern JCPDS 96-900-4181 in the appendix (SF 2). The sharper reflexes of the rods compared to both SA samples indicate a higher crystallinity, which is in line with the SEM results.

3.2 DC Resistance Measurements

SA-AR and SA-UD were characterized thoroughly via DC resistance measurements in order to evaluate their performances and to point out differences ascribed to the treatment via ultrasonic dispersion. Based on the results, the reproducibility, repeatability and recovery are discussed.

3.2.1 Baseline Investigation

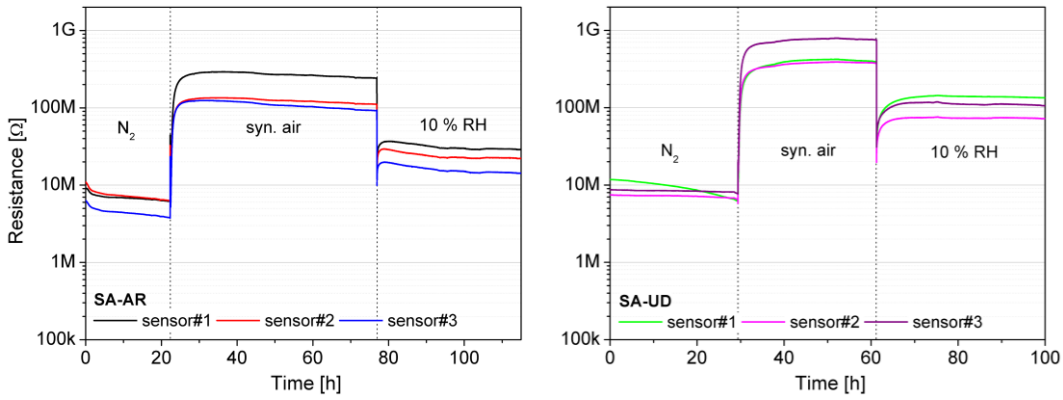

Figure 3.3 The results obtained during DC resistance measurements in various baseline conditions are shown for SA-AR (left) and SA-UD (right). Each three identically prepared sensors were measured simultaneously.

Figure 3.3 shows the simultaneous measurements of each three identically prepared sensors while they were exposed to nitrogen, followed by dry synthetic air (20.5 % O_2) and humidified air (10 % RH). This approach enables evaluating the reproducibility and the performance in oxygen and humidity. Both SA-AR and SA-UD have a comparable baseline resistance in nitrogen, however, the resistance increase in oxygen is stronger for SA-UD. The resistance change in humidity is comparable for both samples. With the sensors signals, which were calculated and averaged over three sensors, a more detailed comparison is possible. In order to represent the range of signals, for each condition the minimum and maximum signals are plotted together with the average signal in Figure 3.4.

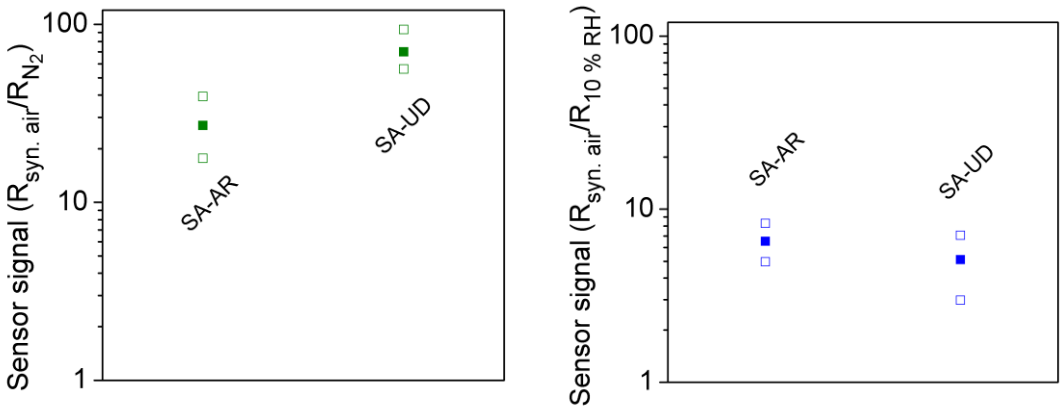

Figure 3.4 Sensor signals to 20.5 % O_2 (synthetic air, left) and 10 % RH (right) are represented for both SA samples. The filled squares represent the average signals of the three simultaneously measured sensors, whereas the blank squares represent minimum and maximum signals.

SA-UD shows significantly higher signals to O_2 than SA-AR. During the dispersion, agglomerates were homogenized to smaller particles of similar shape (seen in Figure 3.1); this means that the surface area was enlarged, making more sites available for oxygen to adsorb, which increases the sensor signal. In contrast, SA-UD has an almost similar but slightly lower signal to humidity compared to SA-AR. This tells that the reaction with water vapor is not significantly affected by the dispersion and the maximum number of hydroxyls at the surface is limited in both SA-AR and SA-UD. In terms of reproducibility, both samples are overall comparable. In oxygen, the signals are slightly less spread for SA-UD, whereas in humidity this is the case for SA-AR. Still, the variations among the three identically prepared sensors are rather ascribed to the sensor fabrication itself than to the dispersion.

3.2.2 Exposure to NO_2

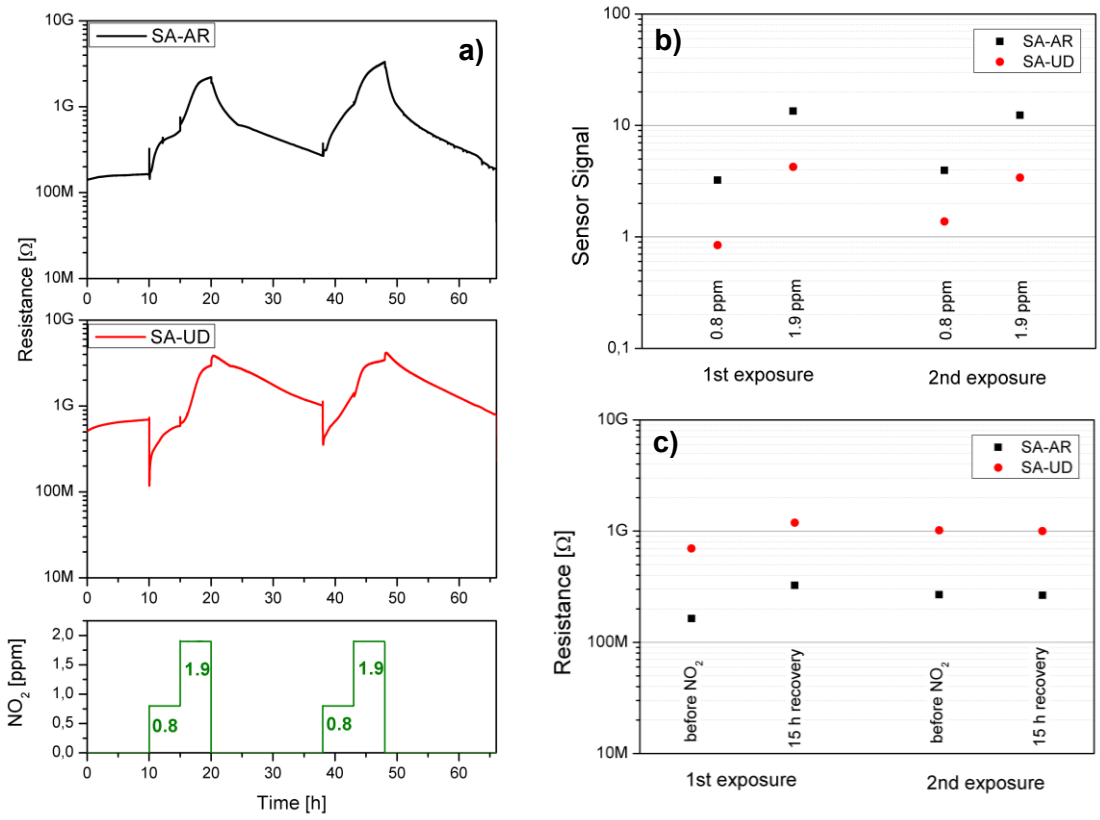

Figure 3.5 Raw data and evaluation of the DC resistance measurement in 0.8 and 1.9 ppm NO_2. The raw data for both samples (a), the respective sensors signals (b) and the resistance values before and after recovery (c) are shown.

During previous studies, 250 °C and 10 % RH have turned out to be the conditions in which the signals to NO_2 are still relatively high [52], provided that it is desired to stay in humid conditions as they are found in ambient air. In dry air the signals are expectedly even higher, however this condition is less realistic. It is known that increasing the humidity decreases

the sensor signal. The reason discussed in literature is that water molecules and their related surface species adsorb at the surface, making less sites available for NO_2 molecules [53]. Knowing this, the baseline condition that was chosen during the NO_2 experiments was 10 % RH @ 25 °C in synthetic air and the operating temperature was set to 250 °C. One sensor of each SA material was exposed twice to two concentrations of NO_2, followed by a 18 h recovery period in the baseline condition. In this way, the repeatability and recovery can be investigated. During preliminary tests, it was observed that the sensors require several hours to reach a state comparable to equilibrium. This indicates a relatively long response time compared to the typical values in seconds or minutes range found for gas sensors [54]. Although this does not indicate a good sensor, it does make it possible to examine the reactions more thoroughly. Therefore, the sensors were allowed to stay 5 h exposed to each concentration of NO_2. Dosing two concentrations enables to examine if there is an effect of saturation or memory induced by NO_2 related species.

Comparing the two measurements shown in Figure 3.5 a), it turns out that both materials respond qualitatively similar to NO_2. One main difference is the higher baseline resistance in 10 % RH of SA-UD, related to a higher resistance in oxygen as discussed above. Another conspicuity is the sudden drop in resistance when NO_2 is dosed: the resistance of SA-UD decreases to approximately the one of SA-AR, from where it starts to increase while exposed to NO_2. This behavior indicates that the surface is re-equilibrating when NO_2 approaches. It seems as some oxygen species need to be desorbed in order to adsorb NO_2. Additionally, hydroxyl species might be involved as they are known to interact with NO_2 [55]. Altogether, it is a very dynamic situation and for clarification spectroscopic investigations are necessary. The overall qualitative response to NO_2, however, is very comparable among the samples, as the resistance increases for both concentrations. Still, generally lower signals are observed for SA-UD (see Figure 3.5 b), mainly ascribed to the initial resistance drop. This leads to a signal even below one during the first exposure to 0.8 ppm.

In contrary to typical recovery times for gas sensors in the seconds or minutes range [56],[57], both materials recover very slowly, with SA-UD being slower than SA-AR. As it is seen in in Figure 3.5 a) and c), after 15 h both resistances decreased to a similar extent but do not reach the initial baseline resistance again. A reason for this could be that some of the NO_2 related species are still present at the surface and keep the baseline resistance increased. This indicates that some of the surface reactions are irreversible. The recovery after the second exposure is not faster but the baseline resistance of before the second exposure was recovered since the surface was still saturated with nitrites and nitrates at that time.

Compared to the first exposure, the sensor signals of the second exposure are qualitatively similar, being even quantitatively comparable for SA-AR. This indicates a certain repeatability. SA-UD shows a slightly higher signal for 0.8 ppm NO_2 but a lower signal for 1.9 ppm NO_2 during the second exposure. A possible reason is that the initial resistance drop is less expressed. If regarding only the resistance increases caused by NO_2, the second exposure shows a clearly lower response. This would be in line with the assumption that the surface is still covered with some NO_2 related species, which would limit the additional adsorption of NO_2 and thus result in a lower signal.

Even though the signals to NO_2 are smaller for SA-UD, it is considered as a promising material for more detailed spectroscopic investigation. One of the reasons is the larger surface area found in SEM. As it was seen in the enhanced response to oxygen, this enables more sites and possibilities for gas molecules to adsorb, making the reaction mechanism much more interesting and versatile. In addition, it is of interest to elucidate the processes during the sharp resistance drop and the recovery period. Therefore SA-UD was chosen for the DRIFTS studies.

3.3 Spectroscopic Investigations

Beneath SA-UD, another sample was chosen for a thorough spectroscopic investigation, i.e. ZnO rods. In a previous study, the response to NO_2 was already characterized [52]. Their special morphology and higher concentration of oxygen vacancies indicate that the sensing mechanism might be different. In order to clarify their mechanisms in NO_2, both samples were examined spectroscopically and compared.

3.3.1 Identification of Zn-O and Hydroxyl Bands

Initially, it is of importance to identify the bands under exposure to oxygen and water vapor. As both gases are present during the whole experiment, they might be involved in the mechanism during exposure to NO_2, as well. For this purpose, the sensors are operated in N_2 first, followed by 20.5 % O_2 (syn. air). The bands increasing in the absorbance spectrum during exposure to oxygen are attributed to the formation of M-O bonds, represented by their overtone vibrations. These bands are typically observed in the region below 2000 cm^{-1}.

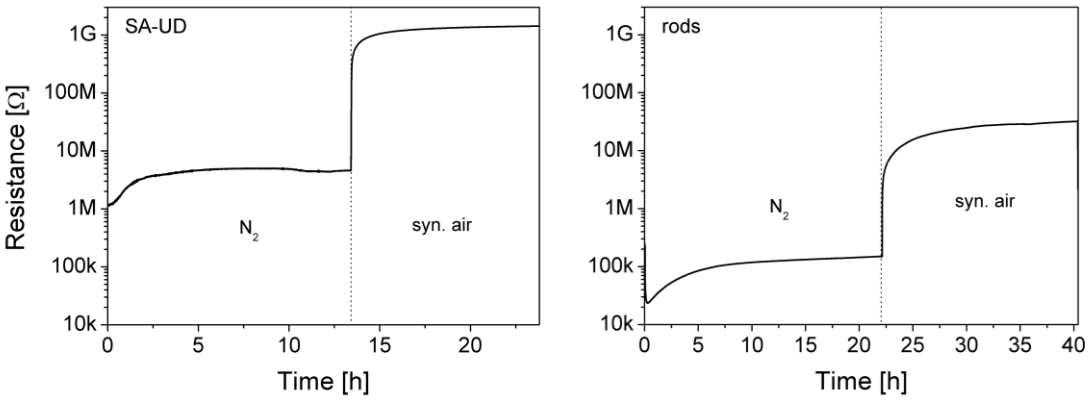

Figure 3.6 DC resistance measurement recorded during DRIFTS investigations in N_2 and 20.5 % O_2 for SA-UD (left) and rods (right).

In Figure 3.6 it is seen that the rods are having a clearly lower baseline resistance in nitrogen than SA-UD. A possible explanation is the higher concentration of oxygen vacancies. Still, the responses to oxygen are comparable for both samples. This indicates that the amount of adsorbed oxygen species is limited at the ZnO surface. Even if the rods are having large particles and thus a lower surface area than SA-UD, they are responding still moderately to oxygen. All of this shows that not only the surface area or concentration of oxygen vacancies matters, but also the available surface sites. When comparing the response for SA-UD shown here with the one discussed in section 3.2.1, it can be seen that the baseline resistance in nitrogen is lower in the DRIFTS setup, resulting in a stronger response to oxygen. The reason for this is that the DC resistance setup is less airtight than the DRIFTS setup due to the use of different materials, which enables comparatively more laboratory air to diffuse into the system and increases the baseline resistance in nitrogen. In both spectra, shown in Figure 3.7, multiple increasing bands are observed in the M-O overtone region. For SA-UD, they appear rather thin and separated whereas they are broader but more intense for the rods. To date, there are very few reports about Zn-O overtone vibrations in literature. Khamfoo et al. identified three Zn-O bands [23] that were also found on SA-UD: 1324, 1288 and 1230 cm^{-1}. Two of them appear also for the rods at 1333 and 1293 cm^{-1}. Most of the other bands are attributed to further Zn-O overtone vibrations, with the exception of 1650 and 1617, respectively. Around this wavenumber, molecular physisorbed water was identified on SnO_2 and WO_3 at 150 °C [58],[59]. Although dry air was dosed, there is still a low concentration (<10 ppm) of H_2O present from the gas bottles and via diffusion through tubing. Therefore, it is assumed that on both materials small amounts of molecular water are found. As the band for the rods at 1617 cm^{-1} appears stronger, it is very likely that Zn-O vibrations are included there additionally.

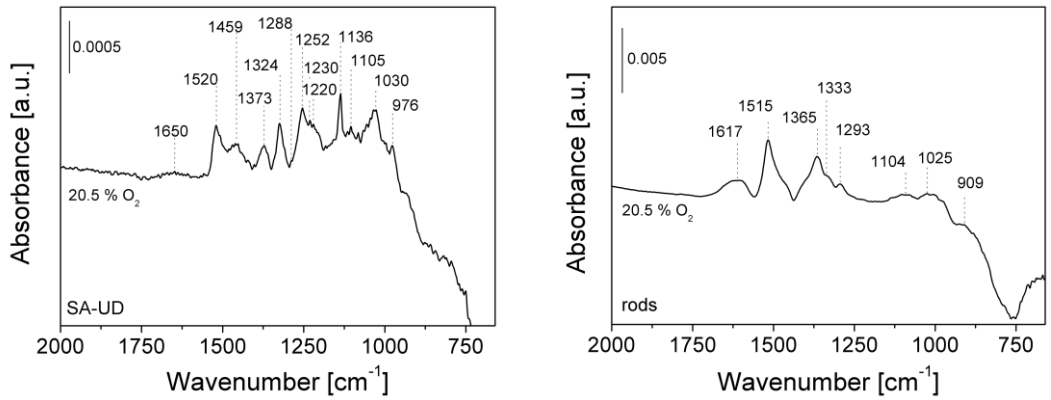

Figure 3.7 Absorbance spectra of SA-UD (left) and rods (right) during exposure to 20.5 % O_2; reference spectrum: N_2.

For the identification of hydroxyl groups, the samples are operated in dry syn. air, followed by 10 % H_2O and 10 % D_2O @ 25 °C (see Figure 3.8). It is remarkable that the resistance decreases stronger for the rods when water vapor is dosed. To understand and explain this behavior, the species that are formed or cancelled need to be identified. For the unambiguous assignment of hydroxyls, D_2O is commonly used [23],[60].

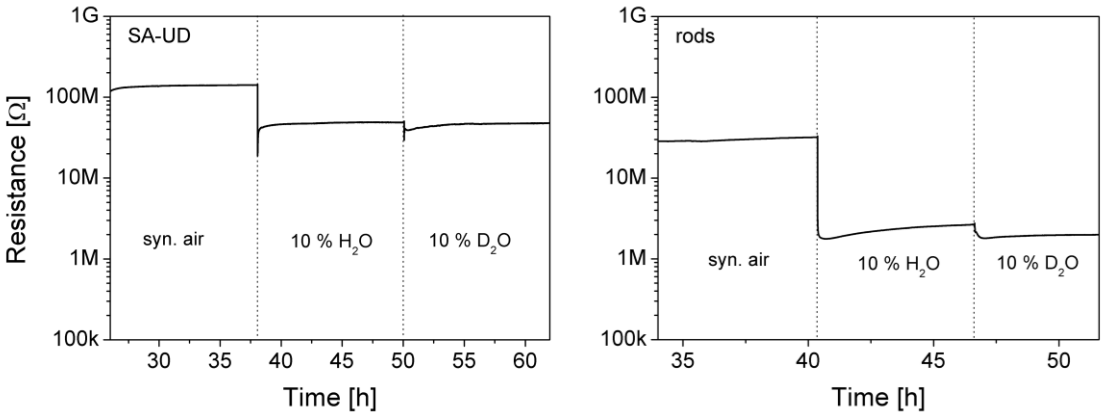

Figure 3.8 DC resistance measurement recorded during DRIFTS investigations in dry synthetic air, 10 % H_2O and 10 % D_2O for SA-UD (left) and rods (right).

In the wavenumber region around 3700 cm^{-1}, stretching vibrations of isolated, rooted and interacting hydroxyl groups are usually found. Interacting hydroxyls appear with a characteristic broad band and thus are easy to identify in the absorbance spectra in Figure 3.9. They are found at 3410 cm^{-1} (SA-UD) and 3406 cm^{-1} (rods) and shifted to 2530 and 2519 cm^{-1} during exposure to D_2O. Due to rotational vibrations, the other hydroxyl

bands in that region are masked in the water spectrum and cannot be clearly identified from it. However, the decreasing bands in the D_2O spectrum between 3500 and 3715 cm^{-1} prove that OH groups existed there before. Literature about the vibrations of hydroxyls on ZnO surfaces is scarce and therefore it is unclear which of these bands belong to terminal or rooted OH vibrations. For both samples, the hydroxyl bands were shifted during exposure to D_2O and some additional OD bands appeared between 2638 and 2779 cm^{-1}. As the resistance does not significantly change in D_2O, these bands indicate an exchange of OH bands that were masked before.

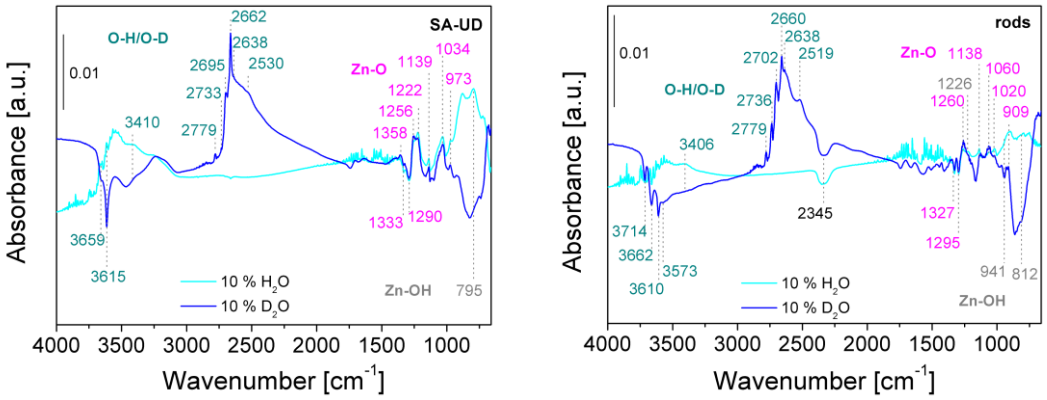

Figure 3.9 Absorbance spectra of SA-UD (left) and rods (right) during exposure to 10 % H_2O and 10 % D_2O; reference spectrum: dry synthetic air.

In order to reduce the rotations and make some of the hidden hydroxyls visible, the single channel spectrum recorded in the end of water vapor exposure was referenced to a spectrum recorded at the beginning (Figure 3.10). For this purpose, the first spectrum without strong changes in the rotational vibrations was selected individually.

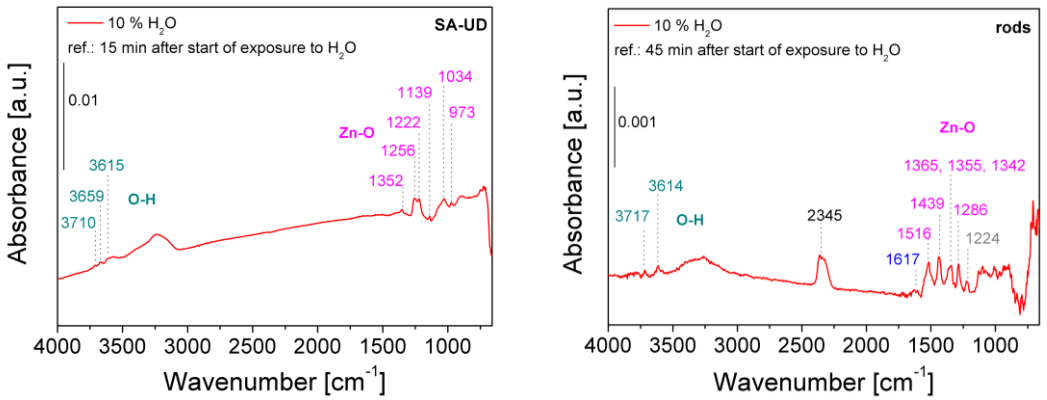

Figure 3.10 Absorbance spectra of SA-UD (left) and rods (right) during exposure to 10 % H_2O; reference spectrum: 10 % H_2O at the beginning of exposure.

For both samples, OH vibrations could be revealed and especially the vibration at 3710 cm^{-1} for SA-UD was not visible before. In Table 3.1 all identified OH bands are listed together with their OD bands and the shift. The calculated factors are between 0.736 and 0.742, being in good accordance with the theoretical value.

Table 3.1 Overview of the O-H and O-D stretching vibrations with the respective shift factors.

Sample	Wavenumber (O-H) [cm^{-1}]	Wavenumber (O-D) [cm^{-1}]	Shift factor
SA-UD	3710	2733	0.737
	3659	2695	0.737
	3615	2662	0.736
	3410	2530	0.742
rods	3714	2736	0.737
	3662	2702	0.738
	3610	2660	0.737
	3573	2638	0.738
	3406	2519	0.740

The broad species observed for SA-UD around 3235 cm^{-1} is not attributed to hydroxyl vibrations, but it is caused by ice inside the detector due to loss of vacuum. After evacuation of the detector, this band disappeared again. In the spectrum of the rods a species at 2345 cm^{-1} decreases in both H_2O and D_2O. This wavenumber is characteristic for the asymmetric stretching vibration of molecularly adsorbed CO_2 [61] and thus not expected in this condition. However, this feature appears also in the single channel spectra, so the origin must be real. It is assumed that the pores inside the particles incorporate molecular CO_2 which is formed by a residual from the synthesis. A similar case was reported by Hlaing for the synthesis of zinc oxide from zinc acetate via zinc carbonate: CO_2 impurities were formed by organic precursors which was demonstrated via isotopic labelling [62]. However, this impurity of the rods is in a region that does not overlap with other important vibrations, so that a reasonable evaluation is still possible and the CO_2 band can be neglected. Since it is considered that this impurity is not involved in the gas sensing mechanism, it will not be regarded further from now on.

Regarding the region around 1500 cm^{-1} further rotational vibrations in the H_2O spectrum make it impossible to identify bands. In this case the absorbance spectrum with a reference in early exposure to water vapor in Figure 3.10 is considered again. The bands between

1617 and 1342 cm^{-1} could be made visible this way. Most of them are known from the absorbance spectrum in oxygen and attributed accordingly, except for 1439 cm^{-1}. This could be another M-O vibration as the D_2O spectrum shows an increasing band at this wavenumber, as well. However, the remaining D_2O bands that do not overlap with already assigned vibrations cannot be assigned.

Moreover, additional Zn-O overtones, marked as pink numbers in Figure 3.9 and Figure 3.10, are identified as they were not shifted during the exchange with D_2O. Most of the bands increase during exposure to water vapor which is rather uncharacteristic. However, among them two decreasing M-O vibrations were identified for both samples. This indicates that these are the bonds involved in the mechanism of hydroxyl formation. The decrease of these bands could be related to a formation of hydroxyls on top of the surface lattice oxygens or the formation of oxygen vacancies at these sites, connected with the formation of hydroxyls at different sites. The increase of all other M-O bands indicates that oxygen vacancies were filled by atmospheric oxygen, which is also seen in the DC resistance measurement of the rods where the resistance increased over time during exposure to water vapor. A possible explanation is that the formation of hydroxyls is limited to certain sites or even inhibited on some sites. However, the reducing effect during hydroxyl formation predominates over the oxidizing effect during Zn-O formation, so that the overall resistance decreases. An overview of all identified M-O vibrations is given in Table 3.2.

Furthermore, deformation vibrations of rooted hydroxyls are observed at 795 cm^{-1} (SA-UD) and at 1226, 941 and 812 cm^{-1} (rods) as they were found to increase in H_2O and decrease in D_2O. This region is characteristic for these species [58]. Regarding hydroxyl stretching vibrations again, on SnO_2 it was found that there is a difference in the electrical changes related to their formations. According to the mechanisms proposed by Heiland and Kohl [63], the formation of rooted and terminal hydroxyls on top of lattice oxygen and tin atoms, provides less electrons compared to the formation of two terminal hydroxyl groups where one surface oxygen leaves its place in the lattice to form a hydroxyl on top of a tin atom, leading to the formation of an oxygen vacancy. Assuming the two mechanisms found on SnO_2 are also true for ZnO, together with the formation of Zn-O bonds there would be mainly three mechanisms to explain the electrical findings and differences between the samples. The stronger initial decrease in resistance for the rods in water vapor compared to SA-UD could indicate that more terminal hydroxyls are formed and the resistance decreased stronger due to the formation of oxygen vacancies. Another possibility is that the formation of M-O bonds contributes electrically different among the samples and compensates the resistance decrease caused by the formation of hydroxyls, such that for example the resistance for SA-UD decreases less because more electrons are taken for

the formation of Zn-O bonds. Still, altogether the surface chemistry of both samples in water vapor is qualitatively very comparable.

Table 3.2 Overview of Zn-O overtone vibrations extracted from the absorbance spectra in oxygen and water vapor. More than one wavenumber is given in a line when the same vibration appeared in various spectra but was slightly shifted or the peaks overlapped to one broad peak.

Sample	Wavenumber (Zn-O) [cm^{-1}]	Sample	Wavenumber (Zn-O) [cm^{-1}]
SA-UD	1520	rods	1515, 1516
	1459		1439
	1352, 1358, 1373		1342, 1355, 1365
	1324, 1333		1327, 1333
	1288, 1290		1286, 1293,1295
	1252, 1256		1260
	1230		1138
	1220, 1222		1104
	1136, 1139		1060
	1105		1020, 1025
	1030, 1034		909
	973, 976		

3.3.2 Reaction with NO_2

When NO_2 is adsorbed on the ZnO surface, typically nitrite and nitrate species are formed [64] and the surface gets oxidized, which leads to an increase in resistance. The absorbance spectra during exposure to two different concentrations of NO_2 will enable the identification and differentiation of these species. The spectroscopic and electrical results are combined to propose reaction equations for the NO_2 sensing mechanism. Parts of the results for SA-UD presented and discussed in this section were already published [24].

For SA-UD the same NO_2 sequence as in section 3.2 was measured, but without repetition, and for the rods same concentrations were applied, with additionally 1.2 ppm NO_2 in between and a lower duration of exposure (3 instead of 5 h). The results are shown in Figure 3.11. It can be seen that the DC resistance measurement of SA-UD is qualitatively comparable to the one discussed before. Minor differences as observed in the initial resistance drop are mainly ascribed to differences in the setup. It is striking that the rods'

response to NO_2 is much stronger compared to SA-UD. Moreover, the rods are almost fully recovered after 15 h, whereas SA-UD stays at a higher resistance value during the recovery period.

Although the protocol is not exactly the same, still a spectroscopic comparison for 0.8 and 1.9 ppm between both samples is possible and in both cases the data allows to identify species at the respective concentration. In order to separate the species that are being formed in both NO_2 concentrations, they are regarded separately. For this purpose, the spectrum recorded in 0.8 ppm NO_2 is referenced to 10 % RH, whereas the spectrum in 1.9 ppm NO_2 is referenced to 0.8 ppm NO_2.

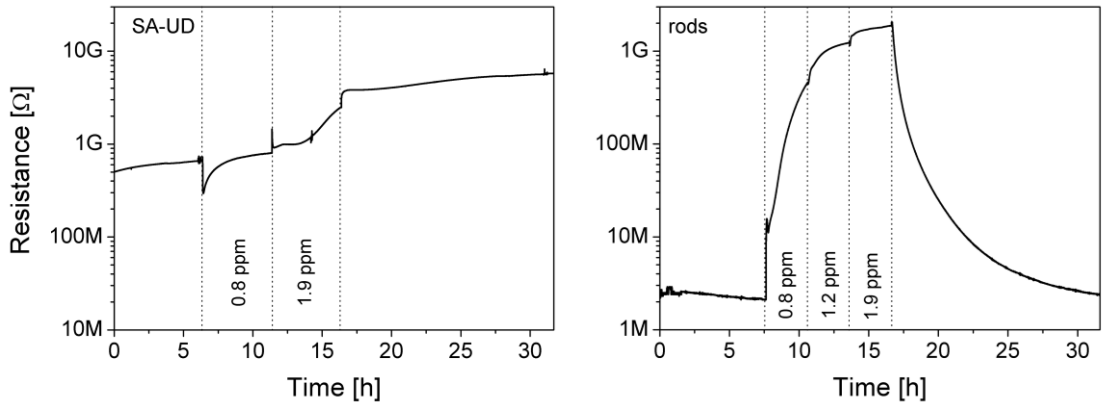

Figure 3.11 DC resistance measurement recorded during DRIFTS investigations under exposure to 0.8 – 1.9 ppm NO_2 in a background of 10 % RH for SA-UD (left) and rods (right).

The resulting absorbance spectra are depicted in Figure 3.12 and can be separated into two regions: the hydroxyl region between 4000 and 3000 cm^{-1} and the nitrite, nitrate and Zn-O based region between 1750 and 1000 cm^{-1}. Starting from this wavenumber, the intensity of the single channel spectra drops drastically (see SF 3), which makes an interpretation of very low frequencies questionable. In the hydroxyl regions of both samples, increasing and decreasing OH bands are visible during exposure to NO_2, but the concentration of water vapor was not varied during this experiment. This finding indicates a reorientation of hydroxyl groups related to the adsorption of NO_2. The bands at 3672 and 3618 cm^{-1} (SA-UD) and 3665 and 3612 cm^{-1} (rods), which were mostly identified as stretching vibrations of O-H before, decrease and new hydroxyl vibrations appear at 3646 and 3606 cm^{-1} (SA-UD) and 3640 and 3596 cm^{-1} (rods). It is remarkable that this feature appears for SA-UD mainly at higher NO_2 concentration, whereas for the rods it is already observed at 0.8 ppm NO_2. In addition, the stretching vibration of interacting hydroxyls appears for SA-UD at a lower wavenumber (3377 cm^{-1}) compared to the exposure to water vapor (3410 cm^{-1}), indicating a reorientation of this species, as well. Probably the

respective decreasing band is not clearly observable due to the broadness. When this experiment was repeated in D_2O with SA-UD, the corresponding bands were shifted by factors between 0.736 and 0.737 to the region of O-D vibrations (see SF 4), which serves as an additional proof for the presence of hydroxyls and their reorientation. These findings confirm the assumption made in chapter 3.2.2 about the involvement of hydroxyls when NO_2 is adsorbed. A similar phenomenon was reported by Roso et al. on In_2O_3: changes in the hydroxyl region during NO_2 exposure were observed, as well. Based on their results, they concluded that hydroxyls interact with nitrites and the adsorption of NO_2 leads to a transformation of these hydroxyls to different hydroxyls, which can be seen as a shift to lower wavenumbers (red-shift) [65]. The hydroxyl species in Figure 3.12 indicate a red-shift, as well.

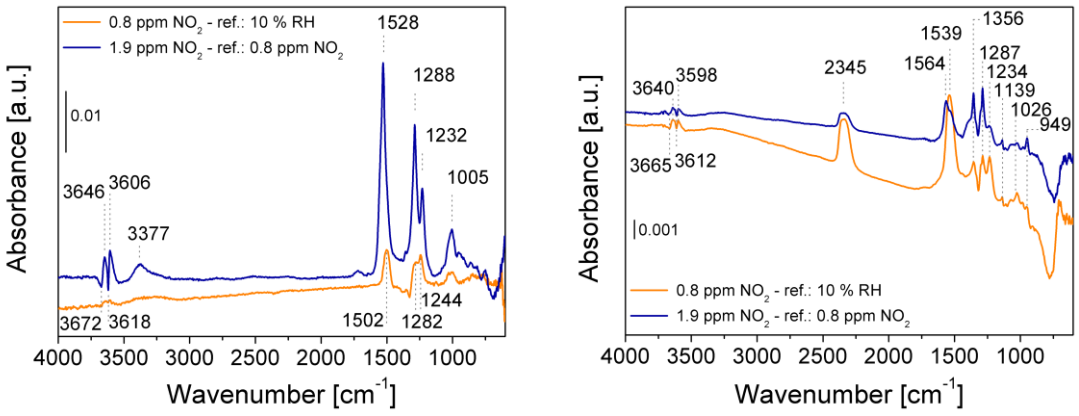

Figure 3.12 Absorbance spectra of SA-UD (left) and rods (right) during exposure to 0.8 and 1.9 ppm NO_2; reference spectra: 10 % RH and 0.8 ppm NO_2.

Regarding the region where nitrite, nitrate and Zn-O vibrations can be found, both samples exhibit various bands, which will be discussed now in detail. For the assignment of nitrites and nitrates, wavenumbers from literature were considered [61],[66],[67] and have been summarized in [24]. To start with SA-UD, for 0.8 ppm NO_2 nitro-nitrites (1502 and 1244 cm^{-1}) and monodentate and bidentate nitrates (1535**–**1474, 1282, and 1005 cm^{-1}) were identified, with the bands of nitro-nitrites being slightly higher. Since the wavenumber regions for the two mentioned nitrates overlap, they cannot be distinguished at this point. At higher NO_2 concentration, the same species are found at the surface and all appear much more intense, with the nitrate vibrations now higher than the nitrite vibrations. The fact that all these bands did not shift during the exchange experiment (SF 4) tells that pure nitrites and nitrates are observed and the interaction with hydroxyls does not change their wavenumbers. For the rods, the situation looks a bit different: nitro-nitrite (1529 and 1234 cm^{-1}) and monodentate and bidentate nitrate species (1564–1529, 1287 and 1026 cm^{-1}) are also observed here,

but the bands appear much less intense. Moreover, the band centered around 1356 cm^{-1} was attributed to nitro species. At low NO_2 concentration, nitrate species are dominant, whereas at higher concentration both nitrate and nitro species reveal the highest bands. In addition, a Zn-O overtone vibration is observed at 1139 cm^{-1} and the band at 949 cm^{-1} could be a Zn-OH deformation vibration included in the one observed around 941 cm^{-1} in Figure 3.9. A complete list of assigned NO_2 related species and their wavenumbers for both samples is given in Table 3.3.

Table 3.3 Summary of the nitrite, nitrate and nitro groups observed on SA-UD and rods with the corresponding wavenumbers and literature. The '+' indicates that the species were found at different wavenumbers depending on the concentration, whereas a range is given when the peak was broad.

Sample	Species	Wavenumbers [cm^{-1}]	References
SA-UD	nitro-nitrite	1502+1528, 1244+1232	[61][66]
	monodentate and bidentate nitrate	1535–1474, 1282+1288, 1005	[61][67]
rods	nitro-nitrite	1520–1480, 1234	[61][66]
	monodentate and bidentate nitrate	1564–1520,1287, 1026	[61][67]
	nitro	1365	[61][66]

Based on the electrical results and the identified species, their formation will be explained and suggestions for the corresponding mechanisms are made, as published in [24]. For this, a (0001) ZnO surface is assumed. Nitro-nitrite is formed when the oxygen of a NO_2 molecule bonds to a zinc atom, with the nitrogen atom being coordinated to a neighbored zinc, as it is represented in Figure 3.13 a). Since the nitro-nitrite is a singly negatively charged species, it is assumed that for the formation of a Zn-ONO bond one electron is transferred from the conduction band of ZnO to the NO_2 molecule, which results in a resistance increase. Without coordination of the nitrogen, the species is called monodentate nitrite and carries the same charge (see Figure 3.13 b). If NO desorbs from the monodentate nitrite, a surface oxygen remains (see Figure 3.13 c). The formation of nitrites and surface oxygen species by reaction with NO_2 was found and reported for several metal oxides and is a commonly known mechanism [9],[18],[19]. Consequently, the formation of nitrates can take place on both nitrites [19] and surface oxygens [20]. Both species are oxidized by NO_2 and form monodentate nitrate, which is easily transformed into bidentate nitrate and vice versa (Figure 3.13 b) and d). In these reaction sequences, all species are singly negatively charged, hence no electrons are exchanged and the resistance does not change. When NO_2 coordinates via the nitrogen atom to a zinc, a nitro group is formed (Figure 3.13 e). The study of Rodriguez et al. [64] indicates that the electron concentration is comparable to that

of a free NO_2 molecule, which means that it is neutral and therefore its formation does not cause a change in resistance.

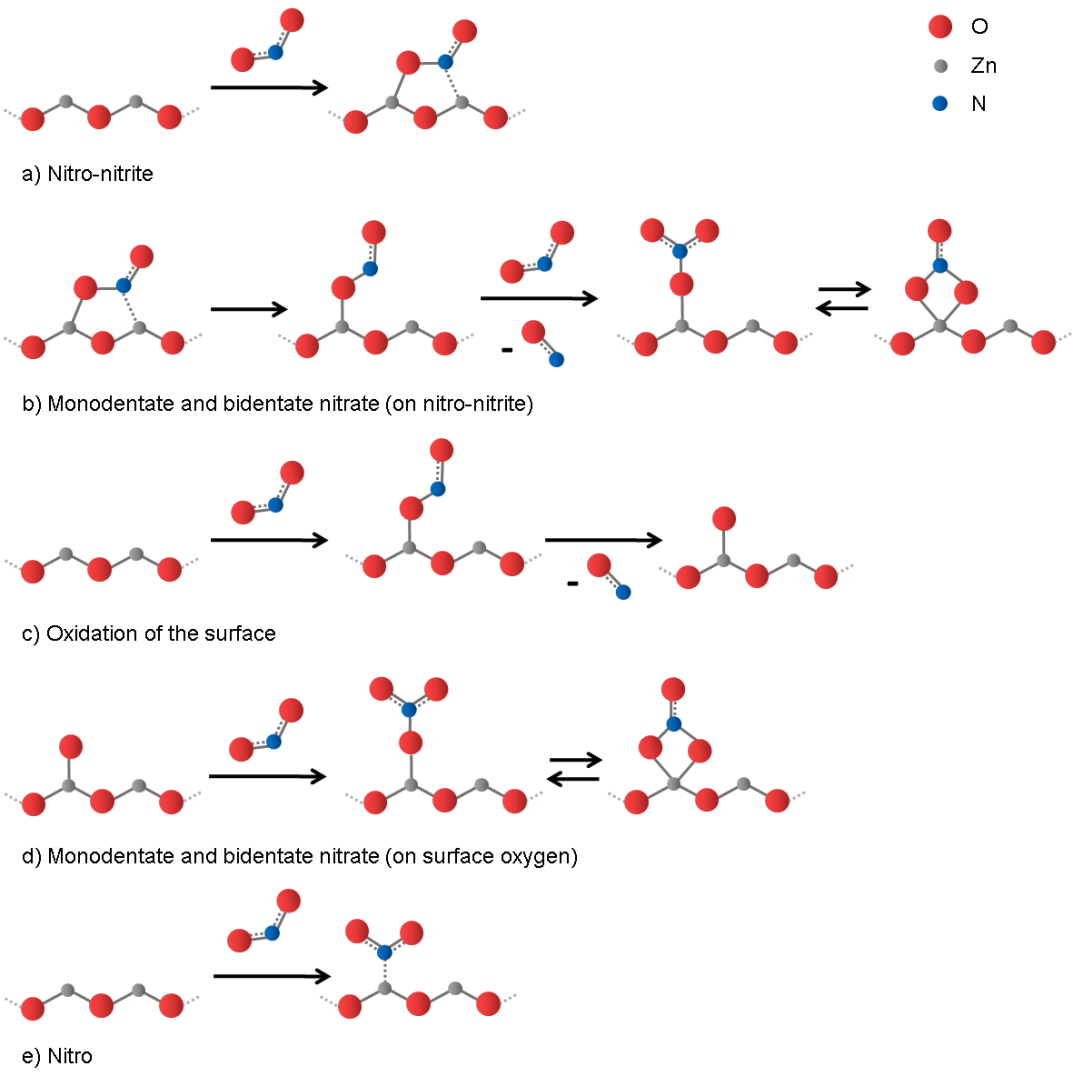

Figure 3.13 Schemes of the proposed mechanisms for reaction of the (0001) ZnO surface with NO_2, including the formation of a) nitro-nitrite, b) monodentate and bidentate nitrate (on nitro-nitrite), c) oxidation of the surface, d) monodentate and bidentate nitrate (on surface oxygen) and e) nitro species.

On SA-UD nitro-nitrite is observed in both concentrations and explains the resistance increase throughout the whole exposure. That nitrate bands increase at the same time means that they were formed from nitro-nitrite and accumulate at the surface. In relation to the nitrates, nitro-nitrites appear slightly stronger at low NO_2 concentration. At higher concentration, more NO_2 molecules are adsorbed and additional sites are necessary. As the nitro-nitrite attaches to two Zn atoms, at higher NO_2 concentration a transformation to nitrate is beneficial for more adsorption sites and would explain the dominance of nitrates

there. Since monodentate nitrites were not observed, they are assumed to be an intermediate species that is immediately transformed to nitrate because of the strong oxidizing effect on NO_2. Nitrite and nitrate species were identified on ZnO via DRIFTS before [20],[23], however, nitro-nitrite is not commonly known on ZnO but was identified on a Cu^{2+}/ZrO_2 catalyst [68] and on Co(II) nitrite complexes [69]. That nitro-nitrite was found here could be due to the rather low NO_2 concentration compared to other studies [20],[23].

Even if some NO_2 based species could be attributed for the rods, their rather small extent of vibration does not fully explain the strong resistance change. When comparing with the spectrum recorded in oxygen, it turns out that the bands at 1617, 1515, 1365 and 1293 cm^{-1} overlap with the bands observed during exposure to NO_2. This indicates an increase in Zn-O overtone vibrations caused by the oxidation of the surface with NO_2 and would explain the strong resistance increase. Therefore, it is concluded that this is the mechanism responsible for most of the resistance changes. An oxidation through NO_2 is also shown by the Zn-O band at 1139 cm^{-1}. The increasing band at 941 cm^{-1} attributed to Zn-OH, without any red-shifted decreasing band as it was observed before in the hydroxyl rearrangement, indicates the adsorption of water during NO_2 exposure. This would make less sites available for NO_2 adsorption [53], and might partly explain the rather low nitrite and nitrate bands. Further possible reasons for the different surface chemistry of the rods are the high concentration of oxygen vacancies or the larger particle size.

In order to investigate the fast initial resistance decrease of SA-UD when NO_2 is dosed, time resolved DRIFTS was applied. For this purpose, a spectrum was recorded every 15 s, instead of the typical record time of 15 min. The sharp resistance drop at the beginning of 0.8 ppm NO_2 exposure is less pronounced in the DC resistance measurement during DRIFTS than it was in the measurement discussed before. Nevertheless, the same phenomenon is observed. Minor differences are mainly ascribed to the different setup and the common small variations between sensors of the same batch. The corresponding part of the measurement can be split into two parts: first the resistance sharply decreases and then it starts to increase rather slowly. The spectra of both parts are shown in Figure 3.14. During the sharp initial resistance decrease, two decreasing bands at 1510 and 1328 cm^{-1} are observed. They overlap with the Zn-O vibrations identified in Figure 3.7 a). The decrease of these bands indicates the cancellation of Zn-O bonds immediately before NO_2 attaches. Directly after this sequence, when the resistance increases again, nitrite and nitrate species are formed, which partially overlap with the Zn-O bands. The decreasing band at 1328 cm^{-1} however still exists in the spectrum of the full response (as it is shown in Figure 3.12 a), indicating that this bond is not rebuilt during exposure to 0.8 ppm NO_2. A possible explanation for the cancellation of Zn-O species before adsorption of NO_2 is that

these surface oxygens are used for the formation of nitrate species, e.g. on top of Zn-O as it is shown in Figure 3.13 d). Thus, the assumption made in section 3.2.2 that oxygen species need to be desorbed to enable the adsorption of NO_2 is partially confirmed. From the results it is not possible to tell whether a desorption occurs or the band decreases because of the formation of nitrates on top of the oxygen.

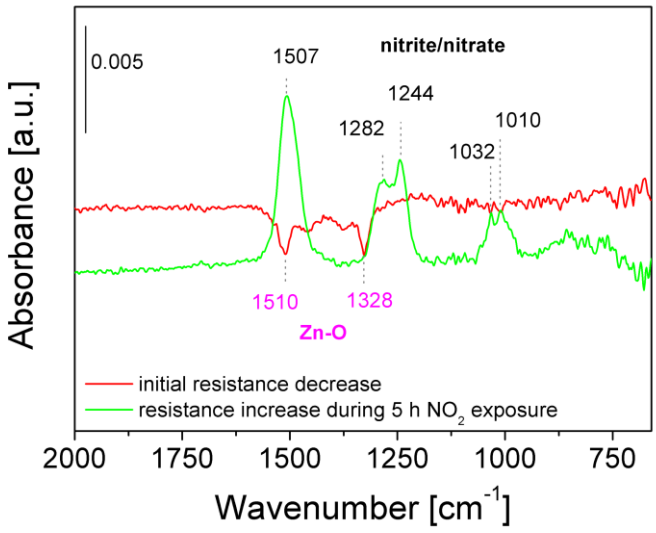

Figure 3.14 Absorbance spectra of SA-UD during exposure to 0.8 ppm NO_2, two sequences are represented: the spectrum covering the sharp initial resistance decrease and the spectrum recorded during the resistance increase. Reference spectra: 10 % RH and last spectrum recorded during the initial resistance decrease.

3.3.3 Recovery

To understand why both samples recover very differently, absorbance spectra during the recovery period are considered. First, the spectrum after 15 h recovery time was referenced to the last spectrum recorded in NO_2. In the corresponding absorbance spectrum, decreasing bands indicate the species that leave the surface during that time. Second, the surface after 15 h recovery time was compared to the surface before NO_2 exposure. A perfect recovery would result in a completely flat absorbance spectrum. Increasing bands indicate remaining groups after recovery. The resulting absorbance spectra for both samples are shown in Figure 3.15. In this part, the spectra are evaluated qualitatively and no exact assignment of bands is made in order to allow a simple characterization of the recovery. On SA-UD, the hydroxyl rearrangement caused by NO_2 is to some extent reversible, indicated by decreasing bands. Some of the nitrates leave the surface, as well. However, compared to the initial surface, part of the rearranged hydroxyl groups stays, which is correlated with the nitrates that also stay, both seen as increasing bands. For the

rods, decreasing bands in the hydroxyl and nitrate regions are also observed, but as a main difference to SA-UD the surface after recovery resembles more to the surface before NO_2 exposure, seen by rather small bands. The amount of species remaining on the surfaces of both samples is consistent with the differences observed in the DC resistance results during recovery: the more NO_2 based species remain, the higher the resistance will be which means the less the initial surface was recovered.

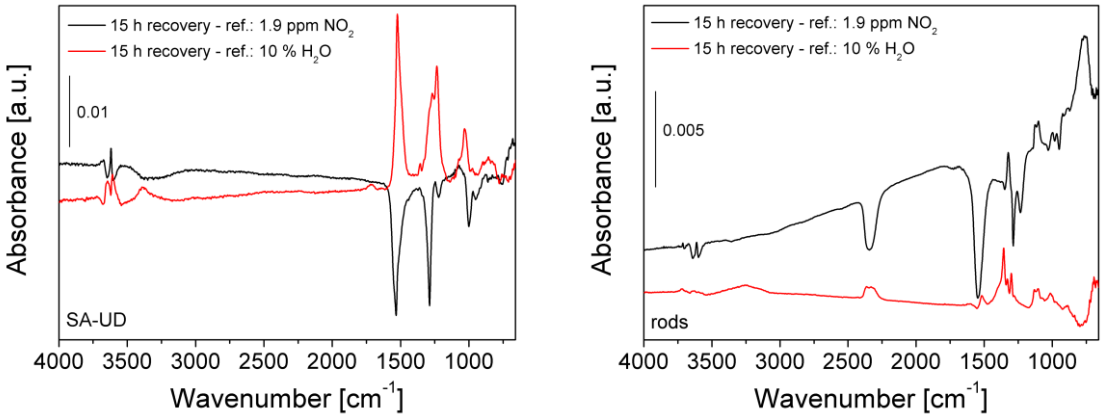

Figure 3.15 Absorbance spectra of SA-UD (left) and rods (right) during recovery period; reference spectra: 1.9 ppm NO_2 and 10 % H_2O.

One of the main reasons for irreversible adsorption of NO_2 is the formation of stable and strong bonds with ZnO at the surface [64]. It is possible that the rods recover better because of the involvement of less nitrite and nitrate species compared to SA-UD. The oxidation of the surface by NO_2 via Zn-O formation identified for the rods seems to facilitate the recovery process.

3.4 Summary and Outlook

From a series of material characterization and DC resistance measurements, two unloaded ZnO samples proved to be of interest for spectroscopic analysis because of their special and different properties. SA-UD exhibited a comparatively uniform and homogeneous morphology with rather small particles, whereas the rods showed a high crystallinity and rather large particles but still a relatively high concentration of oxygen vacancies. While the reaction with and recovery from NO_2 was slow for SA-UD, the rods respond faster and stronger to NO_2 and recover better. DRIFTS was applied to identify the relevant species in oxygen, water vapor and NO_2 and to understand the gas sensing mechanism in NO_2. During the exposure to oxygen and water vapor, relevant Zn-O overtone and hydroxyl vibrations were identified on both samples. It turned out that, despite different concentrations of

oxygen vacancies and different morphologies, the response to oxygen was comparable between both samples and the reaction depended mainly on the amount of available adsorption sites. The ongoing formation of Zn-O bonds during exposure to water vapor demonstrated that the hydroxyl formation is limited to certain sites. It was observed that the surface chemistry in water vapor is comparable for both samples but the rods showed a stronger response than SA-UD. It was suggested that various reactions occur that contribute differently to the electrical changes on both samples. For the reaction with NO_2, it was demonstrated that hydroxyl groups rearranged when NO_2 was adsorbed. This phenomenon was proven on both samples and the reorientation was observed together with the formation of nitrate and nitrite. These species were however not changed or shifted by the rearranged hydroxyls. The formation of various species such as monodentate and bidentate nitrate, nitro-nitrite and nitro groups was identified with a dependency on the NO_2 concentration. Reaction mechanisms were proposed for their formation, including explanations of the associated electrical changes. The different performance in NO_2 between the samples was explained by the contribution of different kinds of surface species to the electrical changes. While on SA-UD mainly the formation of nitrite species explains the increasing resistance, for the rods especially the formation of Zn-O bonds by the oxidation via NO_2 causes the electrical changes. This was found to be induced by the adsorption of additional hydroxyl groups during NO_2 exposure and possibly by the higher concentration of oxygen vacancies or the different morphology. It was suggested that this preferred formation of Zn-O bond on the rods leads to a better recovery of the surface. The incomplete recovery of SA-UD was explained by remaining NO_2 based species at the surface, resulting in an increased resistance.

The results demonstrated that the reaction of ZnO with NO_2 can lead to the formation of differently coordinated nitrites and nitrates and/or Zn-O bonds at the surface. The differences in the samples' morphologies and O1s spectra indicate that these properties influence the preferred surface reaction.

In future research, the influence of the surface morphology and concentration of defects as oxygen vacancies can be investigated more detailed, by preparing various ZnO powders with different properties and investigating them via DRIFTS. In addition, the application of more than two NO_2 concentrations may enable the observation of a larger variety of species with a concentration dependent evolvement.

4 Sensing with K-Loaded ZnO

Normally ZnO is loaded with metals such as Ag [12] or Au [70] to improve the gas sensing properties. But loading with a foreign metal atom can also have the opposite effect: alkaline metals such as K or Na are often present as residues or impurities, which can lead to unintentional loading with them. The consequences are changes in the electrical properties and the gas sensing mechanism [15],[16],[25]. Therefore, this chapter will focus on the influence of K on the gas sensing mechanism of ZnO with NO_2. The starting point of this research was the unintentionally K contaminated sample QD that exhibited a peculiar sensing performance in NO_2. To obtain a deeper understanding of the reasons, SA ZnO was loaded with K in a controlled manner and investigated in detail.

4.1 Material Characterization

For K-loaded ZnO samples, the material characterization was performed in a similar manner to that described in section 3.1. The SEM, XPS (C1s and K2p) and ICP-OES results for SA-UD 10 % K (with and without washing) were already published in [24].

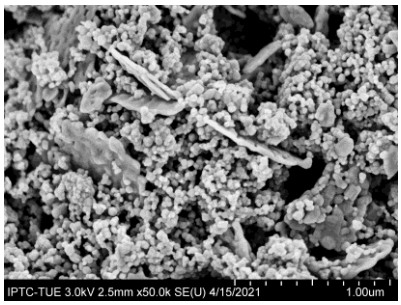

Figure 4.1 SEM image of the sensitive layer of a QD sample.

From the SEM image of the QD, shown in Figure 4.1, it can be seen that the morphology includes small roundish shaped particles in a range between 25 and 67 nm that in some parts agglomerate to sheet like structures. In a former study, it was found that the particles had an initial average grain size of 6 nm that increased during calcination to 27 nm [71], not corresponding to the quantum size range anymore. Nonetheless, the sample name QD was kept. For a better overview or the particle size, a higher magnification SEM image is included in the appendix (SF 5).

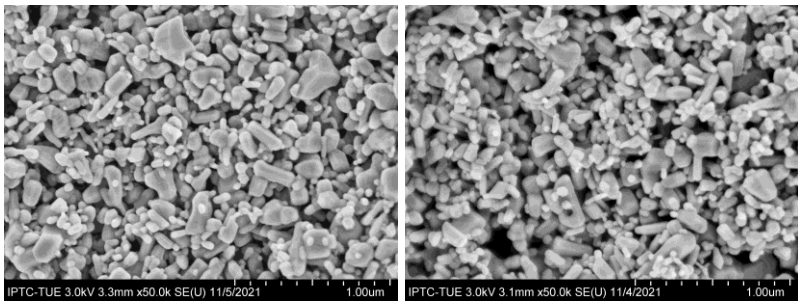

Figure 4.2 SEM images of the sensitive layers of K-loaded ZnO samples prepared via simple dispersion (SA-SD) with 0.1 % K (left) and 1 % K (right).

The particles of SA-SD (Figure 4.2) with a grain size range of 44–236 nm (0.1 % K) and 48–235 nm appear smaller than observed on unloaded SA-AR but a variety of shapes is still observed. Their difference in morphology is ascribed to the treatment and not to K itself because both concentrations of SA-SD show a similar morphology. Compared to unloaded SA-AR it seems as some of the bigger agglomerates were separated into smaller particles.

Figure 4.3 SEM images of the sensitive layers of K-loaded ZnO samples prepared via ultrasonic dispersion (SA-UD) with 1 % K (left), 10 % K (middle) and 10 % K without washing (right).

Both washed K-loaded samples (Figure 4.3 a) and b) look very similar to unloaded SA-UD as all of them exhibit roundish shaped particles with comparable grain size ranges (43–247 nm for 1 % K and 58–221 nm for 10 % K). Looking closer to the morphology of the sample without washing (Figure 4.3 c), it features more edges and hexagonal elongated structures and a similar grain size range of 50–224 nm. All three washed samples (unloaded, 1 and 10 % K) show a similar morphology regardless of the K concentration. The different morphology of the unwashed sample is attributed to either the higher K concentration or the differences in the preparation. However, no influence of only the K concentration on the morphology was observed in the other samples. SA-UD samples appear more homogeneous in their morphology compared to SA-SD, which is ascribed to the finer dispersion by ultrasonic treatment.

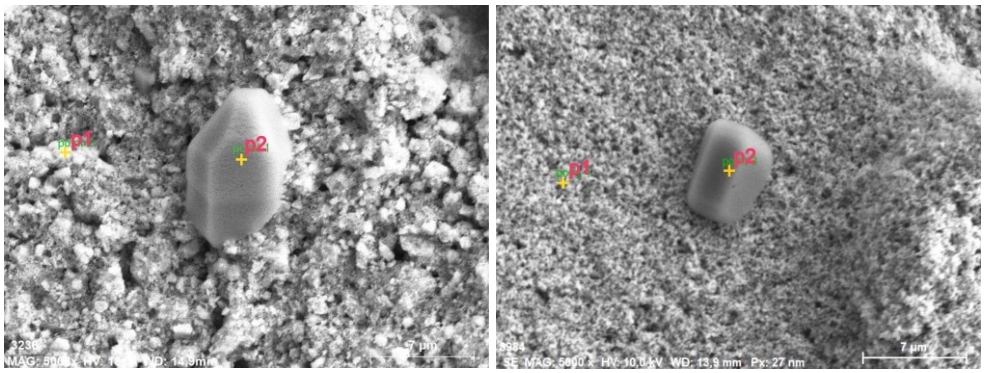

Figure 4.4 EDX scans of crystals found at the surfaces of QD (left) and SA-UD 10 % without washing (right). Each two points are marked at the places where the respective EDX spectra were measured.

At the surfaces of QD and SA-UD 10 % K (without washing), large isolated crystals with a diameter of 8.2 µm (QD) and 5.4 µm (SA-UD) were found (see Figure 4.4). EDX analysis revealed that the concentration of K, listed in Table 4.1, is significantly higher at these crystals compared to the surrounding layer. This indicates that a crystallization of excess K took place during the synthesis or sample preparation. Because of their size and different composition compared to the sensor material, it is assumed that they do not participate in the gas sensing mechanism. The respective EDX spectra can be found in the appendix (SF 6–SF 9).

Table 4.1 Comparison of K concentration from EDX analysis between positions on the regular layer and on isolated crystals of QD and SA-UD 10 % without washing.

Sample	Position	K [at.%]
QD	regular layer, p1	0.45
	isolated crystal, p2	28.81
SA-UD 10 % K (without washing)	regular layer, p1	0.18
	isolated crystal, p2	15.89

With EDX the surface layer up to 2 µm is captured. The gas sensing process however occurs through the whole porous layer. Therefore, the significance of the values in Table 4.1 is limited, but they still serve as an approximation.

In the XPS analysis, C1s, O1s and K2p spectra were investigated for the two samples with the highest nominal K concentration and for QD. Regarding the C1s spectra in Figure 4.5, every sample shows the common hydrocarbon impurity peak. Moreover, both SA-UD samples contain Zn-carbonate peaks. For the unwashed sample, K-carbonate and C-O compounds occur additionally. Together with both characteristic K2p peaks and based on

their binding energies, they indicate the presence of K_2CO_3. It was formed during the powder calcination process as a decomposition product of potassium acetate [72]. Since the binding energies of C1s and K2p are shifted to higher values compared to reports on pure K_2CO_3 (C1s 288.5 eV and $K2p_{3/2}$ 292.2 eV) [73], it is considered to be bound in a complex manner and not to be completely isolated from the regular ZnO surface.

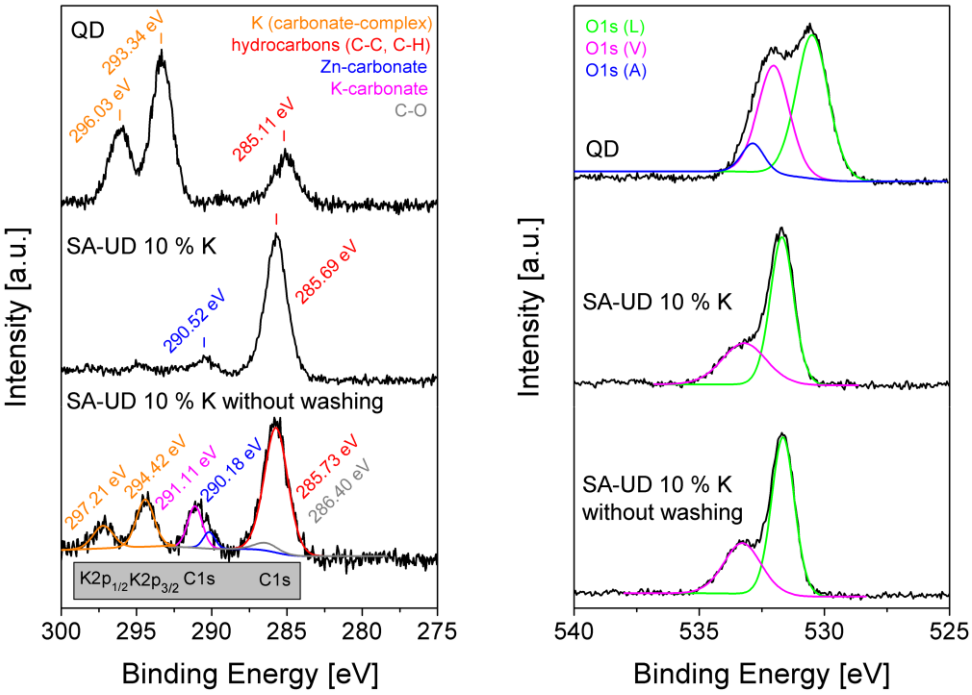

Figure 4.5 XPS measurements of K-loaded ZnO samples with C1s and K2p spectra on the left hand side and deconvoluted O1s spectra on the right hand side.

The C1s spectrum of SA-UD 10 % K resembles the one of unloaded SA-UD (see Figure 3.2). In the K2p region a very small peak can be recognized. However, related to the noise it is too small for an unambiguous identification. It seems as the K concentration at the surface of this sample is too small to capture it via XPS. In contrast, on QD no carbonate based peaks were found and the K2p peaks appeared more intense related to the hydrocarbon peak. The absence of carbonate indicates that potassium is present as a different compound in this sample, e.g. K_2O. The O1s spectra were evaluated similar to section 3.1. Both loaded SA-UD samples look similar to each other and appear comparable to unloaded SA-UD. For a better overview, all three spectra were scaled and plotted in the appendix (SF 10), wherein only a minor difference in the peak attributed to oxygen vacancies is observed. The slightly higher shoulder in the spectrum of the unwashed sample, attributed to O1s (V), indicates that it exhibits a slightly higher concentration of oxygen vacancies, which is in line with reports about K-loaded ZnO [25]. On the contrary to SA-UD, QD have an almost equal contribution of O1s (V) and O1s (L). This indicates that

related to lattice oxygen, for this sample more oxygen vacancies are present in the surface layer. In addition, O1s (A) was identified only for QD.

XRD characterizations revealed the hexagonal wurtzite phase for all K-loaded ZnO samples and the diffractograms are depicted together with the reference pattern JCPDS 96-900-4181 in the appendix (SF 11). For loaded SA-UD the results are similar to unloaded SA-UD. This indicates that the potassium concentration is too small to observe reflexes and/or the compound is amorphous. Due to the very small particle size of the QDs, the reflexes appear very broad. Moreover, small additional reflexes exist that could not be identified. It is assumed that they belong to a mixture of residual substances from the synthesis. Especially for QD it should be noted that the situation on the powder which was analyzed via XRD is different from the situation on the sensing layer, since it was observed that the grain size increased during calcination. In a former study, the sensing layers were measured via XRD after calcination of various temperature and discussed [71]. It was observed that the peaks appeared less broad after calcination, indicating the increasing grain size.

The determination of the K concentration via ICP-OES revealed 0.08 at.% K for 10 % SA-UD and 0.9 at.% K for 10 % SA-UD (without washing). For better overview, the concentrations are given together with the sample names from now on.

4.2 DC Resistance Measurements

4.2.1 K-Contaminated ZnO Sample

In a previous study [52], the performance of QD in NO_2 was characterized. The most conspicuous property was the inverse response – the resistance decreased, although ZnO typically shows a resistance increase for oxidizing gases, and the samples did not recover. Moreover, this was only observed for NO_2; the material responded as it is common with a decreasing resistance for CO and EtOH [71]. At that time, the origin of this behavior was not clear and further experiments needed to be done.

As it turned out from EDX and XPS measurements that QD contains small amounts of K – probably as residues of contaminated educts used in synthesis – it was suspected that this is related to the inverse response in NO_2. Potassium is a common impurity and it is known that it can affect ZnO by increasing the resistance [16], increasing the concentration of oxygen vacancies [25] or converting it into a p-type [15]. In order to investigate if these effects are also found here, the response to oxygen was examined and compared to

unloaded ZnO (SA-AR). In Figure 4.6 it is seen that the resistance of QD only slightly increases in O_2 with a signal below two being significantly lower compared to unloaded ZnO (SA-AR, signal: 27). The baseline resistance in nitrogen is higher and the response is lower. The former is in line with literature [16]. In XPS the sample with the highest concentration of oxygen vacancies was QD, which corresponds to what was reported in [25]. This would indicate a respectively enhanced response to oxygen. However, the opposite is true. That the QD sensor does only slightly respond to oxygen even if there are enough oxygen vacancies indicates that they are energetically unfavorable, i.e. the acceptor states of oxygen might lie above the ones of K. It is known that K acts as an electron acceptor [15], which means that in the loaded material K atoms attract electrons. As a consequence, these electrons cannot move freely anymore and the resistance increases. Similarly, less electrons are available for the adsorption of oxygen, which would explain the low response.

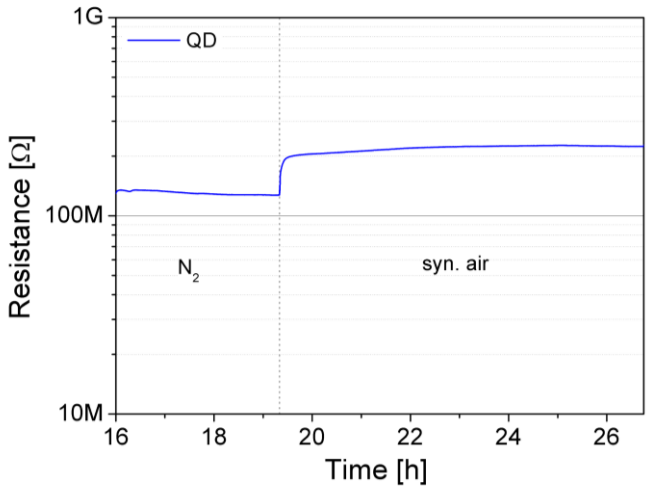

Figure 4.6 DC resistance measurement of QD in nitrogen and dry synthetic air at 250 °C.

In a further experiment, it should be verified whether K can be removed by washing. For this purpose, the powder was washed twice with DI-water followed by centrifugation, whereby the centrifugate changed from alkaline to neutral. For a comparison with the unwashed QD sample, both sensors were exposed to several concentrations of NO_2 at 250 °C in 10 % RH @ 25 °C, as these conditions were found to result in the strongest resistance decrease in a former study [52]. The results in Figure 4.7 show that washing significantly changes the sensor response. Instead of the resistance decrease observed for unwashed QD, the resistance of the washed sample first slightly increases and then continuously decreases with increasing NO_2 concentration. A similarity of both samples is the lack of recovery. These findings indicate that K could be partially removed and thus its effect on the response to NO_2 could be reduced. Nevertheless, it seems as there is some K left at the surface, leading to the still peculiar response.

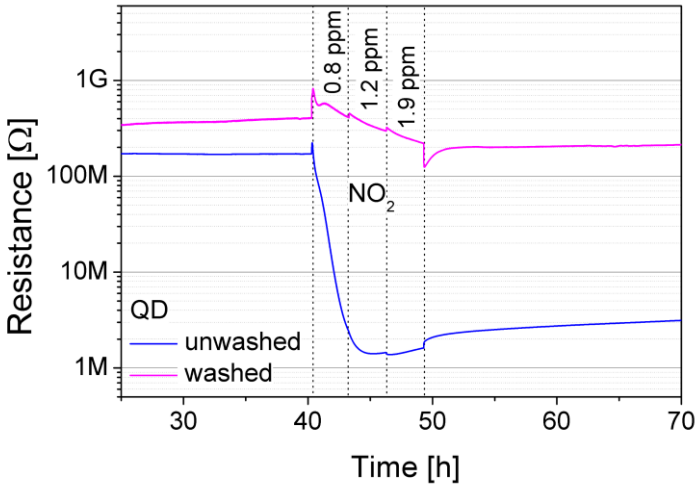

Figure 4.7 Comparison of the DC resistance measurement in NO_2 (10 % RH @ 25°C) between unwashed and washed QD. The operating temperature was 250 °C.

These results are giving first insights into K-loaded ZnO based gas sensors. However, the reasons for the observed performance are not yet fully known and understood. Therefore, it is of interest to figure out why the response to O_2 is reduced in K-loaded ZnO compared to unloaded ZnO. In addition, the loading concentration of K that is necessary to invert the response to NO_2 should be identified. For this purpose, unloaded ZnO was loaded with different concentrations of K in a controlled manner by applying various approaches, which are electrically studied and discussed in the following sections. The unloaded ZnO samples discussed in section 3 are considered in comparison.

4.2.2 Drop Loaded Samples

As a first approach, sensing layers were drop loaded with K containing solutions. Initially, an appropriate K compound had to be found. KOH is one of the simplest compounds, but is too alkaline in the required concentration range and could dissolve ZnO [74]. Potassium acetate was chosen as alternative, as it is less alkaline and decomposes at temperatures above 400 °C [72], which are exceeded during the calcination process.

The target concentration was chosen below the approximate K concentration found in QD to slowly approach the relevant range. First of all, it should be verified if 250 °C is also in this case the operating temperature with the largest resistance change. Therefore, each 1 µl of a 0.1 M K-acetate solution was applied on a sensitive layer and the experiment involved a concentration range of 0.8–1.9 ppm NO_2 in 10 % RH @ 25 °C at 250, 300 and 350 °C, which is similar to the procedure reported in [52]. From the results in Figure 4.8 it is clear that this K concentration (approximately 0.04 at.%) is already sufficient for the peculiar response to NO_2 since at every temperature a clear decrease in resistance is

observed. However, from 1 ppm NO_2 the resistance increases again, which was similarly observed for QD in Figure 4.7 and in [52]. At 300 °C the response is occurring in two steps with the second step starting at 1 ppm NO_2, after which the resistance slightly increases again. A possible explanation for the observed minima and steps could be a concentration dependent change of conduction type. Gurlo et al. found an n- to p-type transition on α-Fe_2O_3 during the adsorption of oxygen and related to the formation of an inversion layer at the surface. This kind of layer is formed when at a certain target gas concentration, the band bending is such strong that the Fermi-level crosses the intrinsic level at the surface and the concentration of holes exceeds the concentration of electrons, resulting in a p-type conductance [75]. This phenomenon was also reported for ZnO with NO_2 [76]. Considering the results in Figure 4.8, this could be a p- to n-type transition in surface conductance. However, it is questionable that the reaction is p-type already at low NO_2 concentrations, although ZnO is an n-type semiconductor. Because of the acceptor property of K it is possible that the surface is initially p-type. Another explanation for the change in response could be different concentration-dependent reaction mechanisms that have increasing and decreasing effects on the resistance. Such a phenomenon is known for WO_3, where water vapor can have an oxidizing or a reducing effect depending on the operating temperature [77]. For the purpose of simplicity, the terms n- and p-type response are used in this and the next section, although at this point it is still unclear what exactly are the reasons for the peculiar response. Since the resistance decrease is largest at 250 °C, this operating temperature was chosen for further experiments.

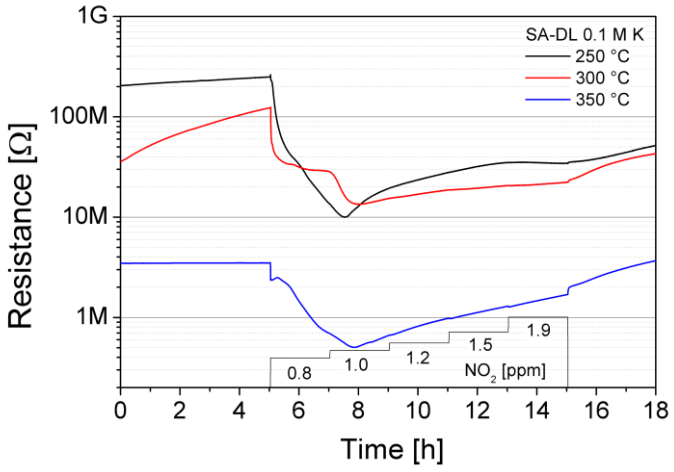

Figure 4.8 DC resistance measurement of SA-DL 0.1 M K in 0.8–1.9 ppm NO_2 (in 10 % RH @ 25 °C) at 250, 300 and 350 °C.

To get more details about the sensing behavior at 250 °C and to identify the K concentration that is necessary for the transition of the response type, two identically prepared sensors

were treated similarly with K as described in section 2.1.1 and measured simultaneously, while they were exposed to the same conditions as before. The results, represented in Figure 4.9, show that after 1 µl of the 0.01 M K-solution (approx. 0.004 at.%) the response is still n-type, while after 5 µl (approx. 0.02 at.%) the resistance initially slightly decreases but the resistance stays at the level of baseline resistance (mixture of both types). At 10 µl (approx. 0.04 at.%), which corresponds to the same total concentration as it was dosed in the experiment shown in Figure 4.8, a full p-type response is observed. So it is concluded that the transition takes place around 0.02 at.% K. It is conspicuous that both sensors differ significantly in their baseline resistances and show qualitatively but not quantitatively the same responses. Additionally, a lack of stability is observed, especially for the baselines of the dosage of 1 µl. It is not clear how much of the sensing layer was covered by the solution and how homogeneously it is distributed among the layer during drop loading. This explains why the samples prepared this way have a lack of reproducibility, which is observed as large differences in baseline resistance among identically prepared samples and differences in the shapes of response curves. Another drawback of this approach is the influence of irreversible changes caused by NO_2 exposure: when one and the same sensor is loaded and exposed to NO_2 several times, the insufficient recovery of the sensors from NO_2 will change the response of the next experiment. Therefore, it is recommended to use a fresh sensor for each NO_2 exposure. To overcome these shortcomings, a different approach to load ZnO and to investigate these samples was required.

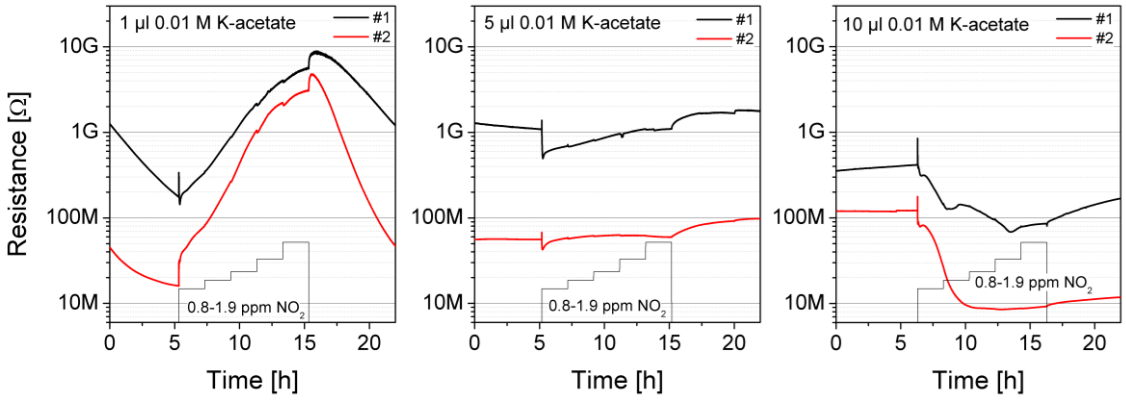

Figure 4.9 DC resistance measurement of SA-DL; the two identically prepared sensors were gradually loaded with various concentrations of 0.01 M K-acetate solution and exposed to 0.8 – 1.9 ppm NO_2 in 10 % RH @ 25 °C. The operating temperature was 250 °C.

4.2.3 Samples Based on Loaded Powder

To distribute K more homogeneously and to aim a better reproducibility, ZnO powder was loaded with K before screen printing, by using two different approaches. The target

concentrations of SA-SD and SA-UD were chosen based on the results from SA-DL and increased according to the method to compensate for losses due to residues or washing, for example. The results of both methods are discussed and compared with the aim to identify the most reliable method applied in this study. For the sake of comparison, some of the results obtained before for unloaded ZnO are considered and shown again next to results of K-loaded ZnO in this section.

4.2.3.1 Baseline Investigation

Initially, the baseline was investigated similarly as in section 3.2.1 in order to evaluate the reproducibility and to examine the sensing behavior in nitrogen and oxygen. In this way it will be possible to draw comparisons to reports about increased resistance [16], the findings for QD shown in Figure 4.6 and unloaded ZnO. Some of the results for SA-UD shown in this section were already published in [24].

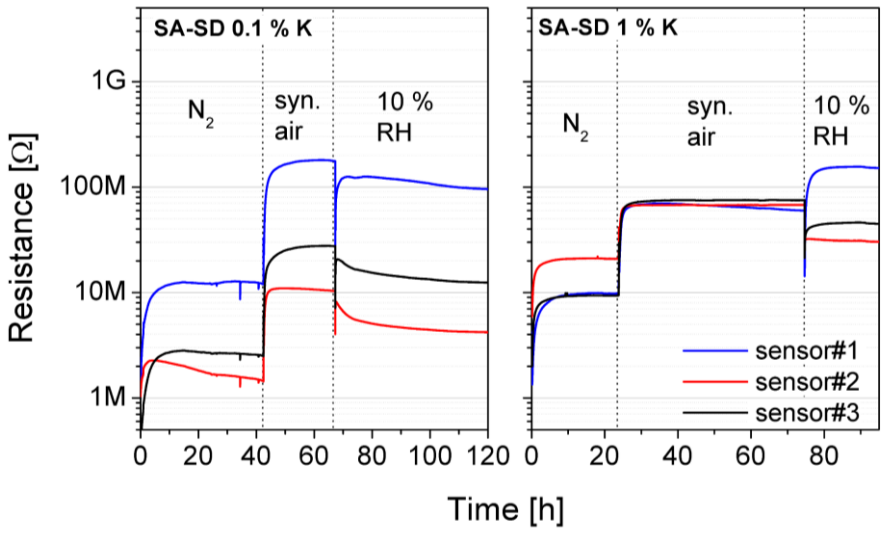

Figure 4.10 DC resistance measurement of SA-SD 0.1 and 1 % K in N_2, syn. air and 10 % RH @ 25 °C. Each three identically prepared sensors were measured simultaneously.

The results obtained on the samples prepared via simple dispersion (SD) are represented in Figure 4.10. The baseline resistance in nitrogen is in average higher for 1 % K than for 0.1 % K, which leads to a decreased response to oxygen for the higher K concentration. The phenomenon of increased resistance induced by K is a known phenomenon [16] and a reduced response to oxygen was observed for QD, as well. Conspicuous is the very low response to water vapor in comparison to unloaded SA-AR. Especially at 1 % K for two samples in humidity the resistance decreases whereas the third sample reacts with an increasing resistance.

The observations indicate that these samples show a lack of reproducibilty that increases as the K concentration increases. This is seen in large differences in the baseline resistances of the three sensors, observed in various conditions and the peculiar response to water vapor.

For a more homogeneous distributiuon, K was dispersed ultrasonically on the ZnO powder. The results in Figure 4.11 indicate the same trends as observed for SA-SD. However, in this case the baseline resistance increases even stronger in nitrogen with increasing K concentration as a higher K concentration was applied in this method. The higher resistance in oxygen compared to SA-SD is mainly explained by the material SA-UD itself similar as it was observed in section 3.2.1. The reproducibility seems to be higher for this sample as especially for 1 % K the resistances are very comparable. Still, they spread as the K concentration increases.

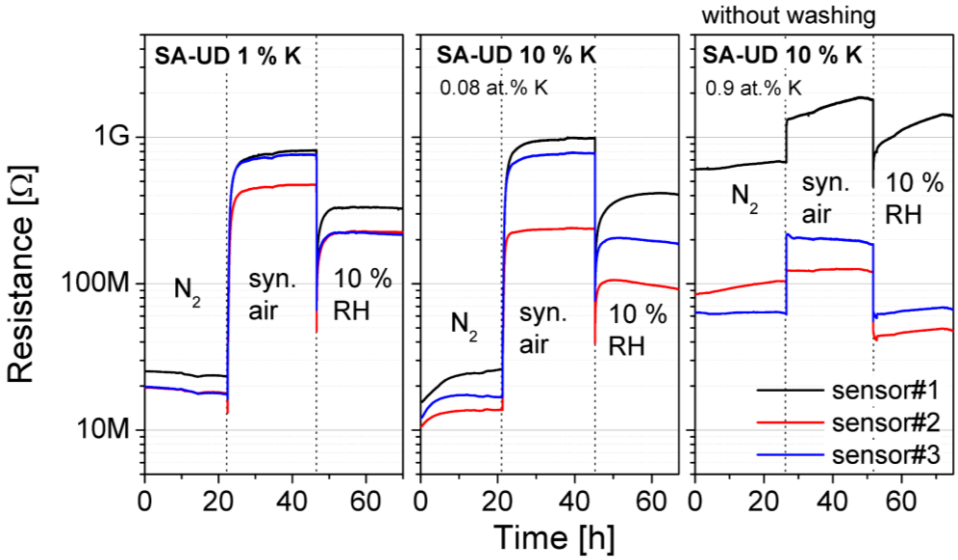

Figure 4.11 DC resistance measurement of SA-UD 1 % K, 10 % K and 10 % K (without washing) in N_2, syn. air and 10 % RH @ 25 °C. Each three identically prepared sensors were measured simultaneously.

For a more detailed comparison, the average, minimum and maximum signals for both methods and conditions are considered. Compared to unloaded ZnO, the signals to oxygen (see Figure 4.12) decrease for both SA-SD and SA-UD as the K concentration increases. The K related decrease in sensor signal is ascribed to the increased resistance in nitrogen and the result of the electron acceptor property. SA-UD shows a saturation effect between 1 % and 10 % K, which indicates that the maximum concentration of K is limited at the surface because of the washing process. Therefore the sample was prepared a second time without washing. The fact that the signal then decreased again supports this assumption. The extent to which the signal decreases differs depending on the

concentration and method, indicating that the true K concentrations are different for the same target concentration, which can be attributed to the different methods. Loaded samples show a similar spread as unloaded samples, with the exception of 10 % K SA-UD.

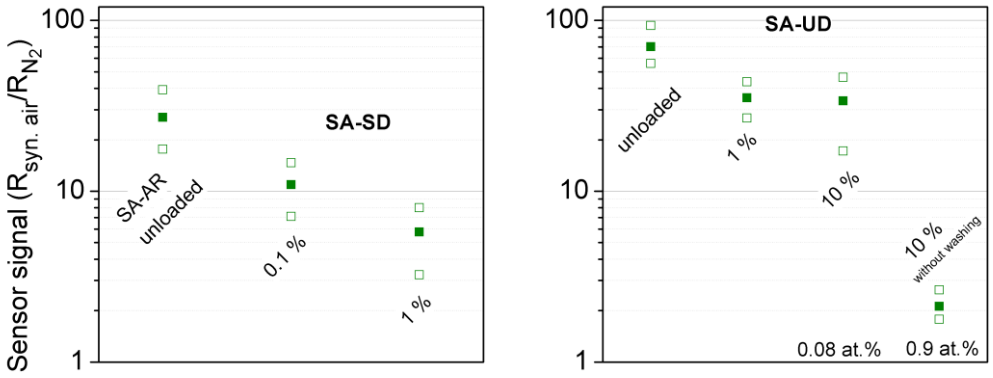

Figure 4.12 Sensor signals to 20.5 % oxygen for various unloaded and K-loaded ZnO samples. The filled squares represent the average signals of the three simultaneously measured sensors, whereas the blank squares represent minimum and maximum signals.

Even though the resistances for SA-AR and SA-SD are in parts strongly spread and not reproducible, it can be seen from the signals in oxygen that the range of minimum and maximum signals is comparable between the samples. For SA-UD the signals are even less spread, with the exception of 10 % K, indicating a higher reproducibility.

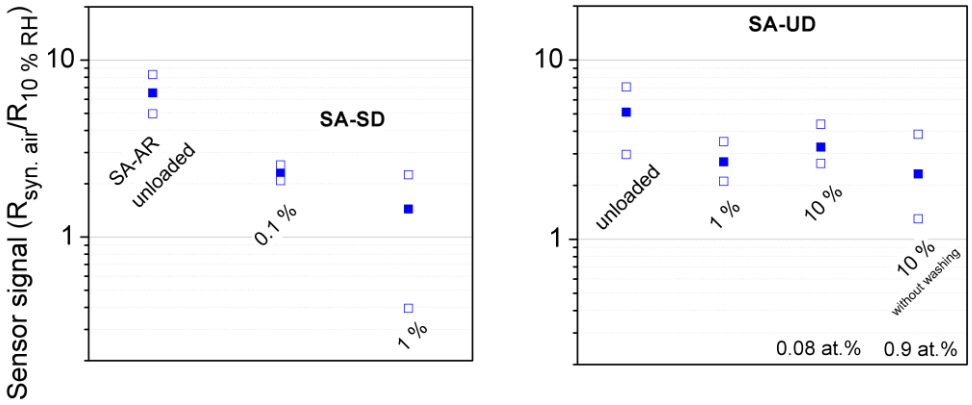

Figure 4.13 Sensor signals to 10 % RH for various unloaded and K-loaded ZnO samples. The filled squares represent the average signals of the three simultaneously measured sensors, whereas the blank squares represent minimum and maximum signals.

The sensor signals to humidity, shown in Figure 4.13, are also decreased by the presence of K for both SA-SD and SA-UD. Since the signal to oxygen was reduced before, less oxygen could be adsorbed and thus less oxygen species are available for the formation of

hydroxyls. However, the extent of decrease in signal is less pronounced for water vapor. Especially for SA-UD all loaded samples exhibit comparable signals, which indicates that the concentration of K has a minor impact. Rather the presence of K decreases the signals. The formation of hydroxyls can still take place on lattice oxygens that were not involved in the adsorption process of oxygen, which is why the signal to water vapor is comparable between the loaded SA-UD samples.

For both SA-SD and SA-UD, the signals indicate a lack of reproducibility, which tends to increase with increasing K concentration. This phenomenon is seen as increasing spreads of the minimum and maximum signals. Especially for 1 % K-loaded SA-SD the large differences of resistance values recorded during exposure to water vapor cause such spread signals with the minimum even below one.

Altogether the minimum, average and maximum signals are closer and more uniform between various K concentrations for SA-UD than for SA-SD, so the samples prepared via ultrasonic dispersion are considered as more reproducible.

4.2.3.2 Exposure to NO_2

Compared to before, the conditions were adjusted so that more time is available to achieve a state closer to equilibrium. The concentrations were limited to the lowest and the highest one (0.8 and 1.9 ppm NO_2) and the durations were extended to 5 h. This corresponds to the procedure applied in section 3.2.2 and thus enables a comparison to the results on unloaded ZnO and a detailed evaluation of the sensor response. Due to the lack of recovery, however, the exposures were not repeated.

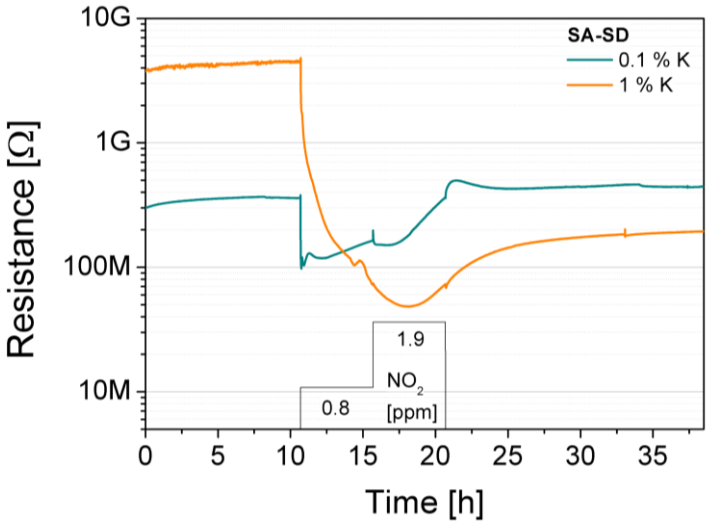

Figure 4.14 DC resistance measurement of SA-SD 0.1 and 1 % K in 0.8 and 1.9 ppm NO_2 in 10 % RH @ 25 °C.

The results for SA-SD in Figure 4.14 show a clear transition of response from n- to p-type with increasing K concentration. For SA-SD 0.1 % K the resistance initially decreases sharply, after which a slight increase during both NO_2 concentrations occurs until the baseline resistance of before the exposure is achieved. After NO_2 exposure the resistance slightly increases and stays at this value. This result resembles the one obtained for the middle concentration of SA-DL (Figure 4.9) and represents a mixture of both types of responses. At first glance, it seems as this sample almost fully recovers. However, it cannot be excluded that both types of responses electrically cancel out the effects of each other and make it look as if there is a real recovery with reversible surface reactions. The result of SA-SD 1 % K is clearly different and represents a p-type response: during exposure to 0.8 ppm NO_2 the resistance decreases by more than one order of magnitude and keeps increasing until the half time of 1.9 ppm NO_2, after which it slightly increases again. This phenomenon was already observed for QD and SA-DL before but there it occurred around 1–1.2 ppm NO_2. However, the measurement protocol involved different durations and combinations of concentrations, which makes an exact comparison difficult. Nevertheless, it can be summarized that in all cases the results indicate a concentration dependent mechanism. In addition, the mechanism could be depending on the duration of exposure since the resistances keep changing even after a few hours and practically never reached a steady state. During the recovery period of SA-SD 1 % K, the resistance slowly increases but stays clearly below the initial baseline resistance.

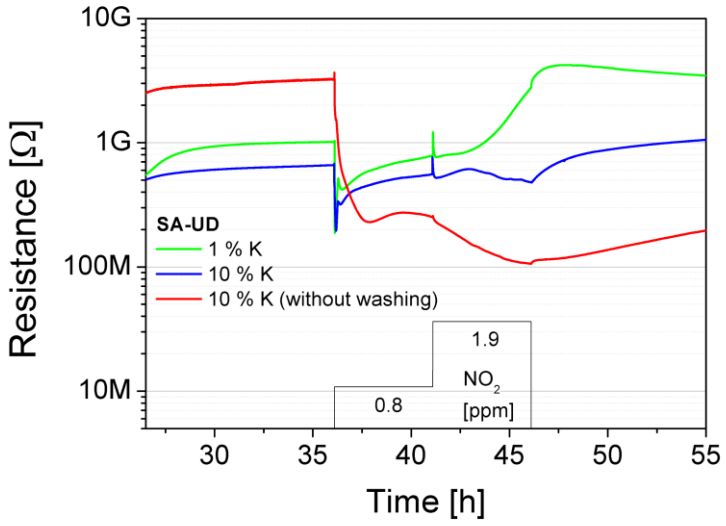

Figure 4.15 DC resistance measurement of SA-UD 1, 10 and 10 % K (without washing) in 0.8 and 1.9 ppm NO_2 in 10 % RH @ 25 °C.

Regarding the samples prepared via ultrasonic dispersion (Figure 4.15), with 1 % K the response is still rather comparable to the n-type response of unloaded SA-UD. Although,

the resistance increases less during 1.9 ppm NO_2 exposure. Afterwards, the resistance slightly increases and then slowly decreases but stays clearly above the initial baseline. The saturation effect observed in the signals to oxygen is seen here as well during exposure to 0.8 ppm NO_2: 10 % K responds very similar to 1 % K. However, during 1.9 ppm NO_2 the samples start to differ as 10 % K shows barely any resistance change. After the exposure stopped, the resistance increases to a value slightly above the initial baseline resistance. This response resembles a mixture of both types, comparable to SA-SD 0.1 % K. Thus, with washing it was not possible to achieve a clear inverse response as it was observed for example for 1 % K SA-SD. Even though the 10 fold concentration was dosed in this case, the responses between 1 and 10 % K SA-UD are comparable. Finally, dosing 10 % K without washing results in a clear p-type response. In contrast to the other previously discussed samples, after a strong resistance decrease it increases again already during 0.8 ppm NO_2, after which it continues decreasing. After the exposure, the resistance recovers a little but stays clearly below the initial baseline resistance.

Unloaded ZnO samples also showed an incomplete recovery. For the K-loaded ZnO with a p-type response, however, the deviation of the resistance after 9 h recovery to the initial baseline resistance is higher. Together with the fact that the resistance decreases, this indicates that compared to unloaded ZnO a different mechanism takes place and irreversible processes might occur. For more precise statements about which surface species are involved, DRIFTS investigations are necessary.

4.3 Spectroscopic Investigations

Based on the results obtained during the baseline investigation, SA-UD is considered as more reproducible than SA-SD, therefore these samples will be spectroscopically examined. For this purpose, both samples with the highest K concentration are chosen because this allows for the analysis of the inverse response and a mixture of both types of responses. Thus, ICP-OES analysis was made on exactly these two samples to link the true K concentration directly to the mechanism. In addition, QD was chosen for the spectroscopic investigation. The aim is to identify the species involved in the NO_2 sensing mechanism and to compare between the different samples. Based on that, a mechanism will be proposed and the role of potassium can be identified. For SA-UD samples, Zn-O and hydroxyl bands that appear during exposure to NO_2 in a humid background will be attributed based on the results obtained on the same base material in section 3.3. The relevant vibrations and wavenumbers for QD can be found in the appendix.

4.3.1 Reaction with NO_2

Most of the results for SA-UD presented and discussed in this section were already published [24]. The same conditions as in section 3.3.2 were applied here. Similar to rods, the protocol of QD slightly differs from the one of SA-UD, but still allows for a spectroscopic comparison of the relevant concentrations. Again, both NO_2 exposures are regarded separately in their absorbance spectra.

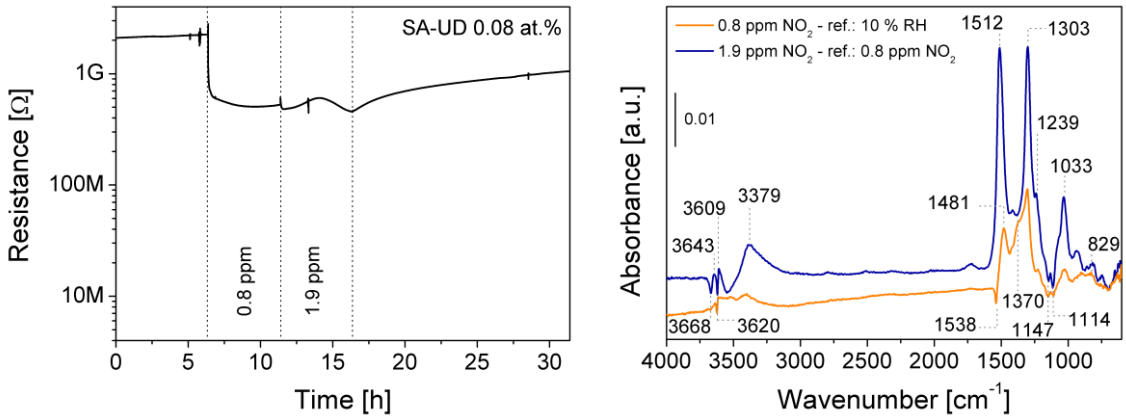

Figure 4.16 DC resistance (left) and simultaneously recorded DRIFTS measurement (right) of SA-UD 0.08 at.% K under exposure to 0.8 and 1.9 ppm NO_2 in a background of 10 % RH @ 25 °C. Reference spectra: 10 % RH and 0.8 ppm NO_2.

Concerning the DC resistance measurement recorded during DRIFTS of SA-UD 0.08 at.% (see Figure 4.16), the initial resistance decrease appears stronger as on the samples of the same batch discussed in section 4.2.3.2 (Figure 4.15). Nonetheless, the results are qualitatively comparable and minor differences are ascribed to common variations between identically prepared sensors in one batch.

In the hydroxyl region, increasing bands at 3643 and 3609 cm^{-1} and decreasing bands at 3668 and 3620 cm^{-1} are attributed to stretching vibrations of O-H. Furthermore, the broad band centered around 3379 cm^{-1} is assigned to interacting hydroxyls. This corresponds to the same situation as it was observed on unloaded SA-UD, similar bands were identified there and it was concluded that the hydroxyls rearrange when NO_2 is adsorbed. On this sample also the changes in the hydroxyl region get stronger as the NO_2 concentration increases, which is supporting this hypothesis. It is possible that this rearrangement correlates especially with monodentate and bidentate nitrate and nitro-nitrite, since it appeared mainly when these bands were observed on unloaded and SA-UD 0.08 at.% K.

In the region between 1750 and 1000 cm^{-1}, bands were attributed to wavenumbers based on the literature [20],[61],[66],[67],[78],[79], as it was summarized in [24]. SA-UD 0.08 at.% K is to some extent comparable to unloaded SA-UD: nitro-nitrite (1239 cm^{-1}) and monodentate and bidentate nitrate (1481, 1303, 1033 cm^{-1}) vibrations were found at both concentrations with the nitrates as dominant species. In this case, only one of the two typical nitro-nitrite vibrations could be clearly attributed, as it is assumed that the other is covered by the large band centered around 1512 cm^{-1}. In addition, during exposure to 0.8 ppm NO_2 free nitrate (1370 and 829 cm^{-1}) was identified and the decreasing band at 1538 cm^{-1} was attributed to monodentate carbonate. At 1.9 ppm NO_2, the nitro-nitrite and monodentate and bidentate nitrate vibrations appear much stronger whereas the free nitrate and monodentate carbonate are not observed anymore. It is possible though, that they are hidden due to the broadness of the other bands. Moreover, during both concentrations, two decreasing bands at 1114 and 1147 cm^{-1} were identified as Zn-O overtone vibrations. Their assignment was possible by considering the bands identified un unloaded SA-UD in Figure 3.7. Only the most dominant bands were listed in that section, thus the relevant part of the spectrum was magnified and every relevant peak was marked in the appendix (SF 12).

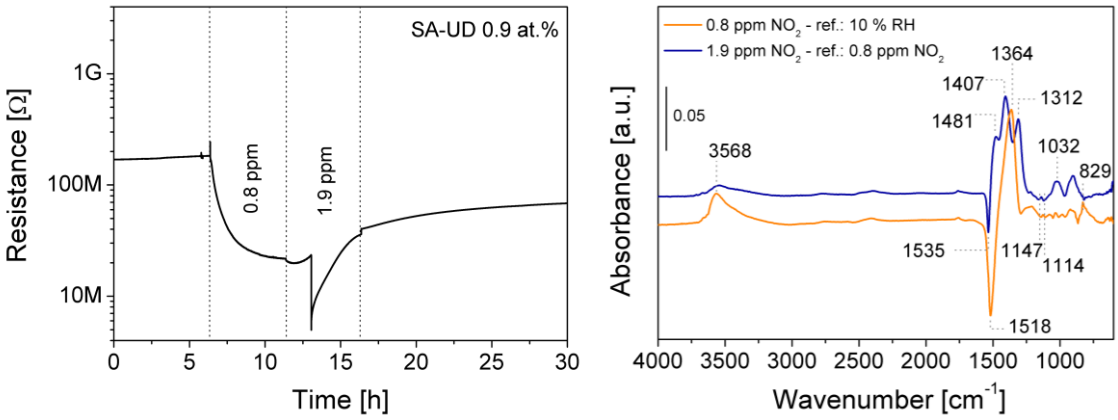

Figure 4.17 DC resistance (left) and simultaneously recorded DRIFTS measurement (right) of SA-UD 0.9 at.% K under exposure to 0.8 and 1.9 ppm NO_2 in a background of 10 % RH @ 25 °C. Reference spectra: 10 % RH and 0.8 ppm NO_2.

For SA-UD 0.9 at.% K during exposure to 0.8 ppm NO_2 the resistance decreases continuously and reaches an almost stable value in the end (Figure 4.17). When the concentration is increased, the resistance increases. During the DC resistance measurement discussed in the previous section, the change in response occurred already during the low NO_2 concentration. These differences between identically prepared samples were observed in particular with K-loaded ZnO samples and indicate that the distribution of K on the surface is not reproducible. Since the sensors were made with the same paste, it

is assumed that K agglomerated into particles of different sizes, each of them contributing differently to the resistance. As they were distributed by chance it is possible that the absolute K concentration slightly varies between the sensors, explaining the different results. The sudden drop in resistance at 13 h was caused by a change in the appropriate measurement range and is not ascribed to changes in the surface chemistry or the atmosphere. Neglecting this event, during exposure to 1.9 ppm NO_2 the resistance slightly increases.

The vibrations in the hydroxyl region are clearly different to both other unloaded and 0.08 at.% SA-UD samples: only one broad band at 3568 cm^{-1} that is stronger at lower NO_2 concentration was observed. At the same time, the species in the nitrite and nitrate region clearly differ from the other samples. This indicates that the changes in the hydroxyl region are depending on the respective nitrite and nitrate species.

At low NO_2 concentration, again free nitrate (1364 and 829 cm^{-1}) and monodentate carbonate (1518 cm^{-1}) were identified, being the dominant species now and appearing both much stronger as for 0.08 at.% K. Different species are observed at higher NO_2 concentration: the bands at 1407 and 1312 cm^{-1} are attributed to nitro groups and the vibrations at 1481 and 1032 cm^{-1} are assigned to monodentate nitrites. The monodentate carbonate band at 1535 cm^{-1} is still present but decreases less as for lower NO_2 concentration. It cannot be excluded that free nitrate is formed as well because it could be masked by the broad overlapping bands of nitro and monodentate nitrites. The two Zn-O bands at 1114 and 1147 cm^{-1} are identified on this sample as well, however, in relation to the large changes in the nitrate region they appear less pronounced.

Typically, free nitrates are present together with alkali or earth alkali metals [66]. Thus, the identification of free nitrate together with the presence of K indicates the formation of KNO_3. Simultaneously to the formation of free nitrate, the decomposition of monodentate carbonate, indicated by decreasing bands, is observed. It was also found in the single channel spectra recorded in 10 % RH (see SF 13, left): in order to make the K-related differences visible, the single channel spectra of the loaded samples were referenced to the spectrum of the unloaded sample. In the resulting spectrum (see SF 13, right), bands at 1530, 1360 and 1306 cm^{-1} were observed and assigned to monodentate carbonate vibrations [79], which proves its presence in the loaded samples. According to the different K concentrations in the samples, they appeared much stronger for 0.9 at.% K. They originate from the incomplete combustion of the precursor potassium acetate to K_2CO_3 and from the absorption of CO_2 from laboratory air. Similar to this phenomenon, Zhu et al. recently published that K_2CO_3 doped layered double oxides exhibited an increased CO_2

adsorption in comparison to unloaded samples [80]. The broadness of the monodentate carbonate bands indicates that both potassium and zinc carbonate are present, which is in accordance with the XPS results. Moreover, that the carbonate is monodentate indicates that it must be bound at the surface, e.g. as a Zn-K-carbonate complex. A separate phase of carbonate as K_2CO_3 or $ZnCO_3$ would result in free carbonate species. The decomposition of carbonates simultaneously to the formation of free nitrate was also observed on K-doped CoMgAlO catalysts [81]. In that study, it was found that their formation is beneficial because they are stable. It is possible that the carbonate leaves the surface in order to provide enough space for the free nitrate.

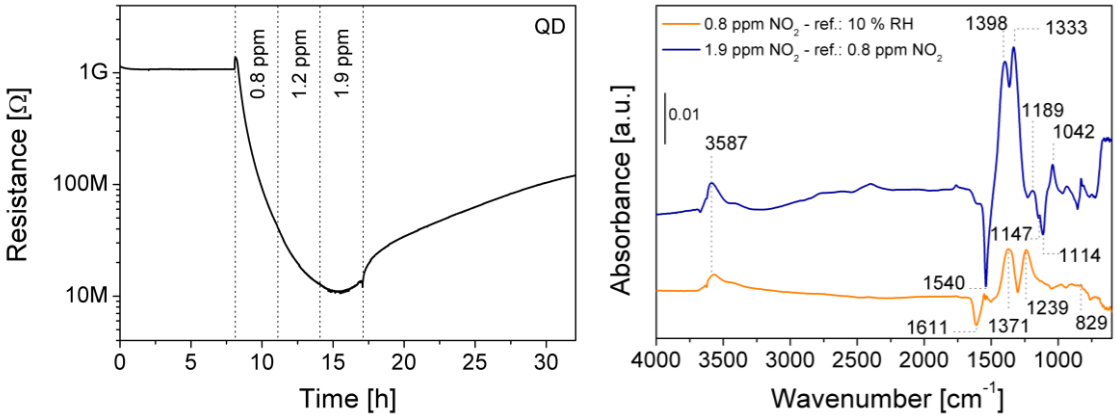

Figure 4.18 DC resistance (left) and simultaneously recorded DRIFTS measurement (right) of QD under exposure to 0.8 and 1.9 ppm NO_2 in a background of 10 % RH @ 25 °C. Reference spectra: 10 % RH and 0.8 ppm NO_2.

During exposure to NO_2, the resistance of QD (Figure 4.18) continuously decreases and from 1.9 ppm it slightly increases.

Similar as for SA-UD 0.9 at.%, in the hydroxyl region only one broad band at 3587 cm^{-1} appears, however, here it is stronger for higher NO_2 concentration. The presence of this band could be related to the concentration of K or to the different kinds and amounts of species found on these samples in contrast to unloaded and 0.08 % at.% K SA-UD.

Comparable with the other K-loaded samples, free nitrate (1371 and 829 cm^{-1}) is formed at low NO_2 concentration. In addition, the band at 1239 cm^{-1} is assigned to nitro-nitrite. Moreover, a decreasing band appears at 1611 cm^{-1}. In contrast to for SA-UD 0.9 at.%, it cannot be monodentate carbonate since it is not contained in QD, as the XPS analysis showed. Considering the Zn-O bands during exposure to oxygen (SF 14), it is noticeable that there is an overlap and thus, the band at 1611 cm^{-1} is assigned to a Zn-O overtone vibration. At higher NO_2 concentration, in addition to nitro-nitrite (1189 cm^{-1}), nitro (1389 and

1333 cm^{-1}) and monodentate nitrite (1042 cm^{-1}) species are formed. At the same time, three decreasing bands appear at 1540, 1147 and 1114 cm^{-1} that are attributed to Zn-O overtone vibrations (SF 14). The free nitrate vibration at 829 cm^{-1} is very small compared to the one at 1370 cm^{-1} [78], therefore it is barely visible at 0.8 ppm NO_2. At 1.9 ppm, the band at 829 cm^{-1} appears higher, which indicates the presence of free nitrate. Hence, it is assumed that the other free nitrate band is masked by the broad band centered around 1333 and 1398 cm^{-1}.

For all three samples the found nitrite, nitrate, nitro and carbonate bands are listed in Table 4.2.

Table 4.2 Summary of the nitrite, nitrate, nitro and carbonate groups observed on 0.08 and 0.9 at.% K-loaded SA-UD and QD with the corresponding wavenumbers and literature.

Sample	NO_2 [ppm]	Species	Wavenumbers [cm^{-1}]	References
0.08 at.% K-ZnO	0.8	monodentate carbonate	1538	[61][79]
		free nitrate	1370, 829	[20][61][78]
		monodentate and bidentate nitrate	1481, 1303, 1033	[61][67]
		nitro-nitrite	1239	[61][66]
	1.9	monodentate and bidentate nitrate	1512, 1303, 1033	[61][67]
		nitro-nitrite	1239	[61][66]
0.9 at.% K-ZnO	0.8	monodentate carbonate	1518	[61][79]
		free nitrate	1364, 829	[20][61][78]
	1.9	monodentate carbonate	1535	[61][79]
		nitro	1407, 1312	[61][66]
		monodentate nitrite	1481, 1032	[20][61]
QD	0.8	free nitrate	1371, 829	[20][61][78]
		nitro-nitrite	1239	[61][66]
	1.9	nitro	1389, 1333	[61][66]
		nitro-nitrite	1189	[61][66]
		monodentate nitrite	1042	[20][61]

From the electrical and spectroscopic results, the formation of different species will be explained and mechanisms will be proposed, as it was published in [24]. A (0001) K-loaded ZnO surface is assumed for this. The formation of nitro-nitrite, monodentate nitrite, monodentate and bidentate nitrate and nitro species was discussed in section 3.3.2 (see Figure 3.13) and is expected to occur similar as proposed there. Free nitrate formation on K-loaded ZnO together with the decomposition of monodentate carbonate and a resistance

decrease is explained as follows (see Figure 4.19 a). Due to the synthesis and from laboratory air, monodentate carbonates are bound to Zn and K atoms at the surface. When NO_2 molecules approach, CO_2 molecules are desorbed to provide enough space for the adsorption, which results in decreasing monodentate carbonate bands. For the free nitrate formation, an additional oxygen atom is necessary. Potential sources are NO_2 or O_2 molecules or surface oxygens after the desorption of CO_2 took place. The strong resistance decrease under exposure to NO_2 indicates that surface oxygen is involved in the mechanism and desorbed to form the free nitrate. When oxygen desorbs, electrons are transferred back to the conduction band of ZnO, which is equivalent to the reaction with reducing gases and explains why the resistance decreases. Without the involvement of surface carbonates, the formation of free nitrate takes place directly on surface oxygen atoms and the resistance decreases, as well (see Figure 4.19 b).

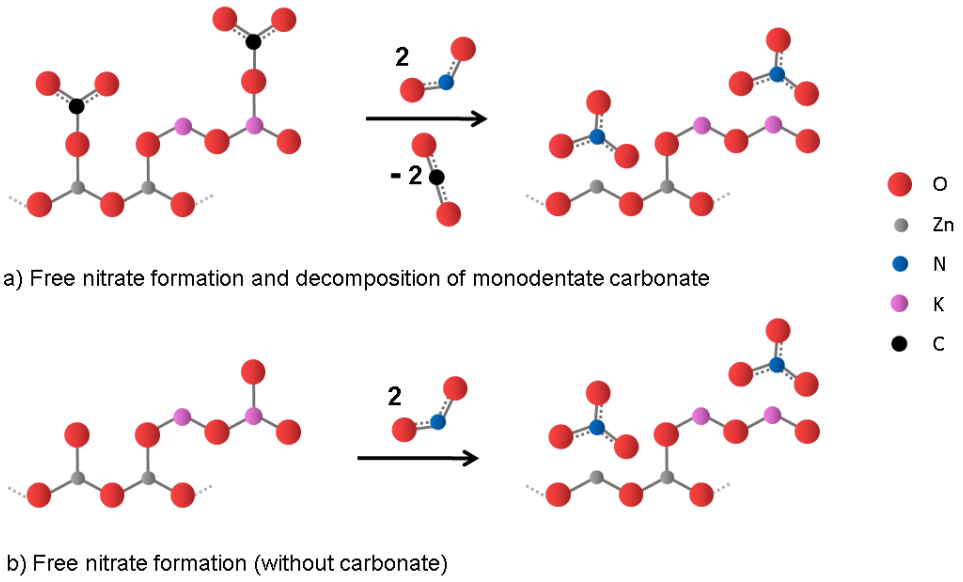

Figure 4.19 Schemes of the proposed mechanisms for the reaction of K-loaded ZnO with NO_2, including the formation of free nitrate with the participation of monodentate carbonate (a) and without (b).

That the surface reactions on SA-UD 0.08 at.% involve both the transfer of electrons from the conduction band to the surface (nitro-nitrite) and vice versa (free nitrate) explains why the resistance decreases initially and then predominantly stays at this value. It is assumed that the formation of nitro-nitrite and transformation to monodentate and bidentate nitrate takes place in a similar manner as observed on unloaded SA-UD. That the monodentate carbonate band decreases to a relatively small extent compared to the resistance decrease is explained by the partial overlap with nitrate bands (around 1481 cm^{-1}) which cancels out the decrease at 1538 cm^{-1}. Additionally, the decreasing Zn-O bands are in line with the

proposed mechanism including the desorption of surface oxygens during free nitrate formation, explaining the resistance decrease.

For SA-UD 0.9 at.%, the changes in monodentate carbonate and free nitrate bands are even stronger, especially at low NO_2 concentration, which indicates a dependence on the K concentration. At higher NO_2 concentration, less carbonate is desorbed and the formation of nitro and monodentate nitrite species is observed additionally. This explains why the resistance starts to increase again at this point. The change in dominant surface reactions indicates that at a certain point most of the surface K did react to KNO_3. Therefore, the adsorption of NO_2 molecules needs to occur differently and nitro and monodentate nitrite species were formed. This also provides an explanation as to why the free nitrate bands of SA-UD 0.08 at.% were rather small and did not increase during the higher NO_2 concentration. The decreasing carbonate band at 1518 cm^{-1} appears broader and at lower wavenumbers for SA-UD 0.9 at.%, which indicates an overlap of more than one species. It is assumed that the second species contributing to this band is a Zn-O overtone vibration. From the DRIFTS results on unloaded ZnO discussed in section 3.3.1 (see Figure 3.7), this Zn-O overtone vibration was identified at 1520 cm^{-1}. The presence of additional decreasing Zn-O bands explains the stronger decrease in resistance found on this sample.

In contrast to SA-UD, on QD the mechanism takes place without the participation of carbonate, the electrical results and surface reactions are however comparable in many parts, e.g. the formation of free nitrate under desorption of oxygen up to a certain point, after which the resistance increases again and different species are formed at the surface. This indicates that the proposed mechanism is not affected by the surface carbonates and depends predominantly on the presence of K. The strong resistance decrease during 0.8 ppm NO_2 is however not fully explained by only the Zn-O band at 1611 cm^{-1}. It is possible that further Zn-O bands are masked and cancelled out by free nitrate or nitro-nitrite bands. A Zn-O overtone vibration was identified at 1360 cm^{-1} during exposure to oxygen in a background of nitrogen (SF 14). An overlap with the free nitrate vibration at 1371 cm^{-1} would explain the discrepancy between resistance measurement and absorbance spectrum. After 0.8 ppm NO_2, the resistance continues to decrease. At the same time, the formation of additional species starts. That the resistance slightly increases again during 1.9 ppm NO_2 is explained by the formation of nitro-nitrite and monodentate nitrite. This change in mechanism indicates that at some point, similar as observed for SA-UD, most of the K reacted to KNO_3 and NO_2 needs to adsorb differently. The fact that at least three different decreasing Zn-O vibrations are observed indicates that the free nitrate formation can take place with oxygen atoms of various sites.

4.3.2 Recovery and Effect of CO_2

The evaluation of recovery was performed similar to section 3.3.3. For a better overview of the various processes occurring on K-loaded ZnO, the relevant bands were attributed schematically.

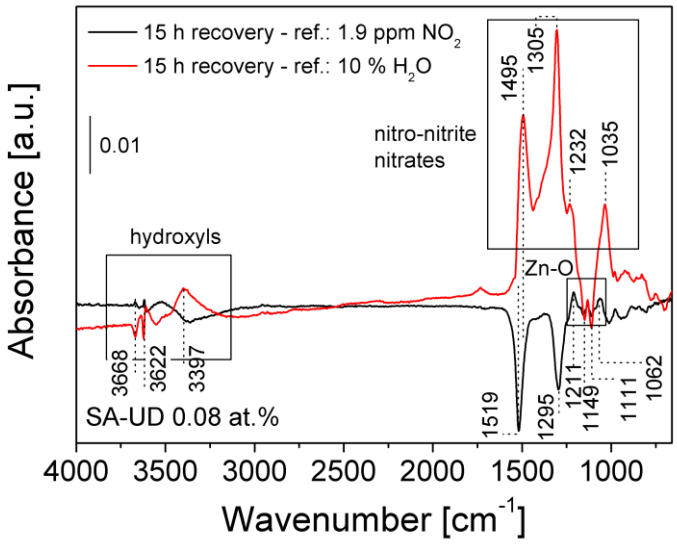

Figure 4.20 Absorbance spectra of SA-UD 0.08 at.% K during the recovery period; reference spectra: 1.9 ppm NO_2 and 10 % H_2O.

The recovery spectra of SA-UD 0.08 at.% K are shown in Figure 4.20. Similar as for unloaded SA-UD, after the recovery still rearranged hydroxyls and nitrates are present at the surface. During the recovery period the rearranged hydroxyls partially recover, as indicated by increasing and decreasing bands in the black spectrum. However, compared to the situation before NO_2 exposure, most of the hydroxyl vibrations that appeared together with NO_2 adsorption stay at the surface, seen in the red spectrum. This is in line with the fact that nitro-nitrite and nitrates are also still present. During the recovery period some of them were desorbed, represented by decreasing bands in the black spectrum. But this does not explain why the resistance increases during the recovery (Figure 4.16). In the Zn-O region two increasing bands are observed, they are attributed to Zn-O overtone vibration and indicate the partial re-oxidation of the surface by atmospheric oxygen. They were assigned based on SF 12, where they are part of series of peaks overlapping to broad bands. In between, two decreasing bands in the red spectrum, attributed to Zn-O, explain why the resistance is still lower after recovery than before exposure to NO_2. They were already observed during NO_2 exposure (Figure 4.16). The band around 1300 cm^{-1} is broad and asymmetric to higher wavenumbers, which indicates an overlap with the free nitrate

band that was observed in Figure 4.16. As it is not represented in the decreasing black bands in this region, it is assumed that the free nitrate formation is irreversible.

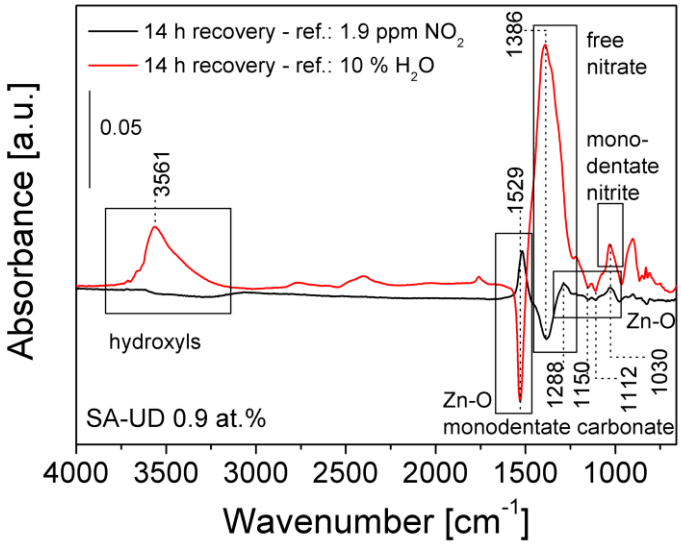

Figure 4.21 Absorbance spectra of SA-UD 0.9 at.% K during the recovery period; reference spectra: 1.9 ppm NO_2 and 10 % H_2O.

SA-UD 0.9 at.% K was given only 14 h instead of 15 h to recover, which is still considered as comparable to the other samples since the resistance almost reached equilibrium at that time. In the spectrum shown in Figure 4.21 the large band in the hydroxyl region (red spectrum) without any decrease in the black spectrum indicate that these OH groups did not recover. In addition, the large free nitrate band still exists at the surface after recovery together with the large decreasing monodentate carbonate and Zn-O band. Small peaks in the black spectrum into the opposite direction indicate that only small amounts of these groups left the surface or were recovered, which demonstrates the irreversible character of these reactions. The increasing black band in the monodentate carbonate region appears slightly shifted to lower wavenumbers. Since no CO_2 was in the atmosphere, it is attributed to Zn-O vibrations and shows a re-oxidation of the surface. This is an additional proof that the decreasing band in Figure 4.17 was composed of both monodentate carbonate and Zn-O overtone vibrations. The slight increase of two further Zn-O bands during the recovery period explains why the resistance slightly increases. However, that the resistance after recovery is still below the value before exposure, is explained by the decreasing Zn-O bands in the red spectrum (1529, 1150 and 1112 cm^{-1}). The band centered around 1030 cm^{-1}, which was attributed to a Zn-O overtone vibration, overlaps with monodentate nitrite. This makes a clear separation of both species difficult. Based on the different conditions that are included in both spectra, it is assumed that the band in the red spectrum predominantly

indicates the presence of monodentate nitrite species after recovery, whereas in the black spectrum the formation of Zn-O bonds during recovery is seen.

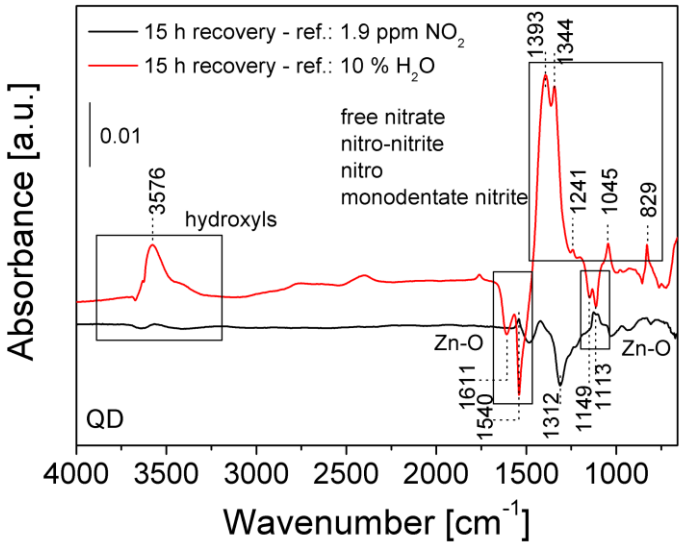

Figure 4.22 Absorbance spectra of QD during the recovery period; reference spectra: 1.9 ppm NO_2 and 10 % H_2O.

The surface of QD after recovery (Figure 4.22) to some extent resembles the one of SA-UD 0.9 at.% K. Both materials have the formation of hydroxyls and free nitrate together with the decrease in Zn-O vibrations in common. However, since no carbonate is involved in the mechanism for QD, in this case pure decreasing Zn-O bands are observed. Moreover, the variety of nitrite and nitrate species found at the surface after recovery is higher. The increasing resistance during the recovery period is explained again by the formation of Zn-O bonds at 1540 and 1113 cm^{-1}, exactly the bands that decreased during NO_2 exposure. However, compared to the surface before, most of the desorbed oxygen is not recovered, indicated as large decreasing bands at 1611, 1540 and 1149 and 1113 cm^{-1}. This is in line with the lower resistance after recovery. At 1312 cm^{-1} a broad decreasing band is observed. It is assumed that it is a combination of various nitrite and nitrate species and indicates the partial desorption of them during the recovery period. The two vibrations at 1149 and 1113 cm^{-1} were identified on each K-loaded sample but not on unloaded ZnO. Therefore, it is concluded that their vibrational changes are related to K. The proximity of K could increase the reactivity at the respective Zn sites.

The recovery of the surface on K-loaded ZnO takes place much slower than on unloaded ZnO. There are two main reasons for this. First, due to the electron acceptor property of K, generally less electrons are available for the typical surface reactions, which slows down adsorption and desorption processes. Second, the formation of KNO_3 is energetically

favorable because of its negative formation enthalpy [82] and the high symmetry of the free nitrate ion. The former also explains the irreversibility of the reaction.

Finally, it should be verified whether the reaction is reversible under the influence of CO_2. It was reported that alkali metal nitrates deposited on MgO showed a relatively high adsorption rate of CO_2 [83]. Hence, at the surface of 0.9 at.% K SA-UD an interaction between the formed KNO_3 and CO_2 could be possible. Therefore, after exposure to 1.9 ppm NO_2 and a partial recovery in 10 % RH for 15 h, highly loaded SA-UD was exposed to 500 ppm CO_2. In the absorbance spectrum, shown in Figure 4.23, large increasing M-O and monodentate carbonate bands and a decreasing free nitrate band are observed. At the same time, the resistance increases stronger than during the recovery period in only 10 % RH. This result demonstrates the interaction between CO_2 and free nitrate and proves the re-oxidation of the surface with the help of CO_2, by forming Zn-O bonds and carbonates. It is assumed that the formation of carbonates leads to the desorption of NO_2 while the remaining oxygen atom bonds again to a Zn atom. This corresponds to the reverse mechanism in Figure 4.19 a).

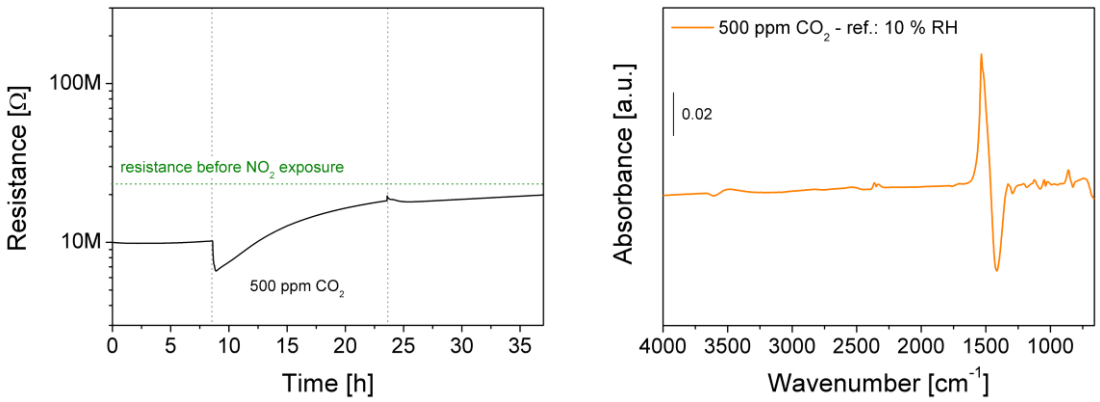

Figure 4.23 DC resistance (left) and simultaneously recorded DRIFTS (right) measurement of SA-UD 0.9 at.% K under exposure to 500 ppm CO_2 in a background of 10 % RH @ 25 °C (after exposure to 1.9 ppm NO_2 and a partial recovery in 10 % RH for 15 h). Reference spectrum: 10 % RH.

4.4 Summary and Outlook

ZnO nanopowder was loaded with various concentrations of K via drop loading the sensors or dispersing the powder before screen printing. During the baseline characterization via DC resistance measurements in N_2, O_2 and humidity, most of the K-loaded ZnO samples showed a lack of stability and reproducibility, especially for high K concentrations. Due to the acceptor property of K, the baseline in N_2 increased, which resulted in decreased signals

to O_2. The results obtained during exposure to humidity demonstrated that the concentration of K has a minor effect on the signals to humidity, suggesting that the formation of hydroxyls takes place mainly on lattice oxygen atoms that were already present before the exposure to oxygen. In contrast to unloaded ZnO, K-loaded ZnO responds with a decreasing resistance to NO_2 and recovers extremely slowly, indicating irreversible surface reactions. A transition of the response type was identified from low to high K concentration. From the electrical results it was concluded that the ultrasonic dispersion of K on the powder resulted in the most reproducible sensors; hence the two samples with the highest K concentrations were chosen for spectroscopic investigations. For comparison, QD, a K-contaminated sample was characterized as well. The formation of hydroxyl groups was observed together with the formation of NO_2 related species. Among these, especially free nitrate was formed on the K-loaded samples, suggesting the formation of KNO_3. The presence of carbonate that was introduced during the loading process was proven via XPS and DRIFTS. Monodentate carbonate vibrations demonstrated that it is bound to the K- and Zn- sites and not isolated.

Reaction mechanisms were proposed for the electrical and spectroscopic findings. The decreasing resistance in K-ZnO was explained by the formation of free nitrate via desorption of oxygen from the surface. To provide enough space, CO_2 leaves the surface. On QD, the surface reactions occur similar, but without the involvement of carbonate, proving that mainly K is dominating the mechanism. Instead, surface oxygen atoms are participating directly and the electrical results are the same. When all K reacted to KNO_3, additional NO_2 molecules adsorb in the form of other nitrite species and the resistance increases again. Furthermore, after the recovery period most of the nitrite and nitrate groups stayed at the surface, especially free nitrate was barely desorbed, proving the irreversibility of the reaction. The surface was only partially re-oxidized. It was concluded that the recovery is such slow because of the electron acceptor property of K that slows down the reception processes and due to the energetically favorable formation of KNO_3. In addition, it was demonstrated that the dosage of CO_2 during the recovery period assists to remove free nitrate from the surface and enables a certain reversibility of the reaction.

To conclude, it was proven that the inverse response of K-ZnO to NO_2 is due to a changed surface chemistry that was induced by K, so a p-type sensing behavior can be excluded. These findings and the understanding of the sensing mechanism could help in future research to improve the storage of NO_2 in NO_x storage/reduction catalysts.

Still, some improvements will be necessary in future investigations, such as the homogeneity and reproducibility of the samples. This could be addressed by synthesizing

K-loaded ZnO directly from the precursors. Additionally, due to the overlap of Zn-O, monodentate carbonate and nitrite/nitrate species it was not always possible to clearly separate the bands. Investigations during exposures to additional gases such as O_3, CO or CO_2 could be helpful to better distinguish these vibrations. Particularly the interaction between NO_2 and CO_2 could be of great importance for the improvement of recovery processes and is worth further research.

5 Light-Activated Sensing with ZnO

The results presented and discussed in this section are part of the research project „Photologic“, which was supported by the German Research Foundation (DFG). As part of the project work, a much more extensive characterization was carried out with additional materials and conditions, as it is published in [46]. The focus here will be on ZnO and NO_2 in particular.

5.1 Material Characterization

The results for SEM and XRD shown and discussed in this section have been published in [46].

Figure 5.1 shows a SEM image taken from the cross section of the sprayed layer. The obtained height was 47 µm, which is comparable to the thickness of a screen printed layer. However, due to the high porosity of the layer, there is a significantly lower amount of ZnO and a larger surface area overall.

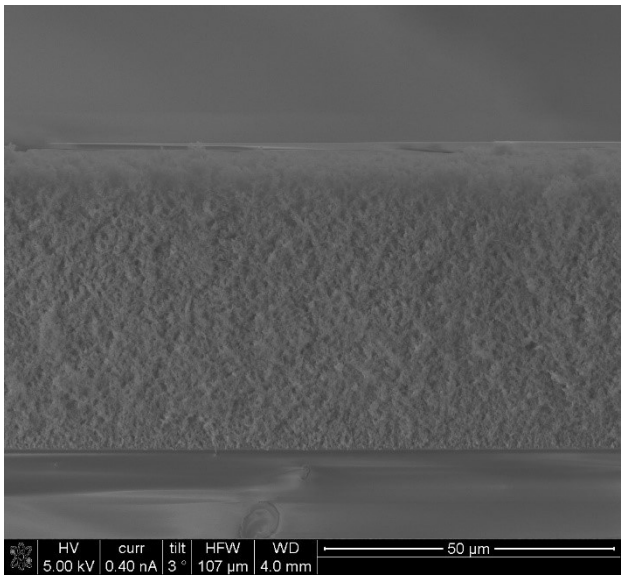

Figure 5.1 SEM image of cross section of a ZnO layer prepared via FSP.

The XRD measurement revealed a hexagonal wurtzite structure. The diffractograms and the corresponding reference pattern JCPDS 96-900-4181 can be found in the appendix (SF 15). With the Scherrer equation [84], the average crystallite size was estimated to be 15.9 nm.

From the DRUVS results a direct band gap of 3.34 eV was determined, which is in good agreement with the values reported in literature (3.25–3.35 eV) [85],[86]. The Tauc plot can be found in the appendix (SF 16). Furthermore, the band gap is comparable with the energy of the UV LED (375 nm or 3.31 eV). This indicates that a band-to-band transition is possible with the dUV LED since its photon energy (310 nm or 4 eV) is higher than the band gap. All other LEDs could excite states within the band gap if they exceed the respective energy.

5.2 DC Resistance Measurements

Each 0.5 and 0.75 ppm NO_2 were dosed in dry synthetic air, 10 % RH, 30 % RH and 70 % RH. This experiment was performed in seven different illumination conditions at 70 °C, as described in section 2.4.1. Preliminary investigations revealed that the FSP prepared sensors respond with large resistance changes to NO_2. In order to still record the entire response and mostly maintain the limit of measurement range, the concentrations were selected lower than for the screen printed ZnO gas sensors.

Figure 5.2 shows the DC resistance measurements in NO_2 with various levels of humidity and illumination conditions. From dark to UV, with increasing photon energy, the baseline resistance decreases. This indicates an activation of charge carriers already by red light. That the resistance decreases slightly more for each LED in this row from low to high photon energy shows that there are various defect states in the band gap that can be accessed by visible and UV light. In dUV the resistance increased again. To explain this behavior, adsorption and desorption processes are considered. It is known that UV light can induce the adsorption or desorption of surface species [87],[88], which is often correlated with a resistance change. In relation to the presented results, dUV light seems to induce additional processes, which results in an increased baseline resistance in dry air. The adsorption of oxygen species or desorption of remaining surface hydroxyls are considered as possible mechanisms. The final measurement in the dark is very comparable to the initial one, which demonstrates that the surface was recovered from the exposure to various photon energies and light-induced degradation of the material, as it is sometimes found especially in UV light [89], can be widely excluded.

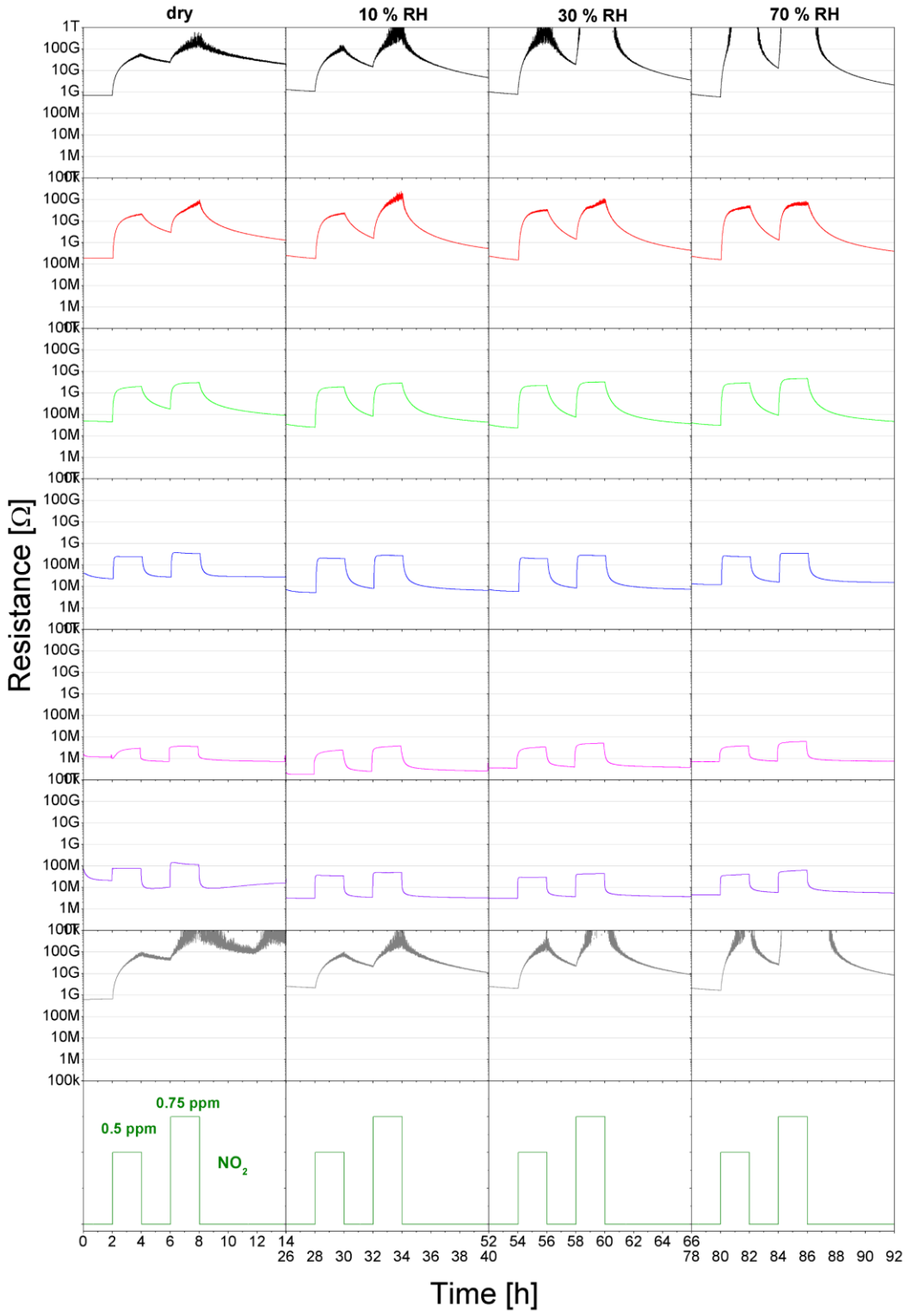

Figure 5.2 DC resistance measurement of FSP prepared ZnO. The sensor was exposed to 0.5 and 0.75 ppm NO_2 in 0, 10, 30 and 70 % RH @ 25 °C. Various illumination conditions were applied, from top to bottom dark start, red, green, blue, UV, dUV, dark end. The sensor was operated at 70 °C.

The varying level of RH has barely any effect on the baseline resistance in the dark or in red and green light. In contrast, during exposure to blue, UV and dUV light, the resistance decreases from 0 to 10 % RH, which is the common reaction to humidity. However, increasing the humidity level further, increases the resistance again without exceeding the initial resistance in dry air. This indicates that on the light-activated ZnO surface water vapor still has a reducing effect. That the resistance slightly increases only during the presence of water vapor suggests that an additional mechanism takes place in these conditions.

The response to NO_2 is very strong in the dark, so that the maximum measurable resistance was exceeded, as it is shown by the noisy responses and resistances up to the TΩ range. With increasing photon energy, the response to NO_2 is reduced. At the same time, the response and recovery are faster with increasing photon energy, as indicated by the steeper curves at the beginning and end of NO_2 exposures. This is explained by the enhancing effect light has on the adsorption and desorption speed of NO_2 [90]. Moreover, the response seems to be barely affected by the various levels of humidity. For a more precise comparison, the sensor signals in 0.75 ppm NO_2 were calculated, which are shown in Figure 5.3.

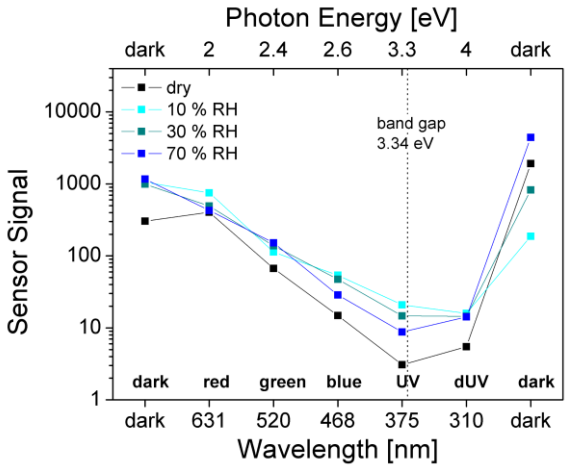

Figure 5.3 Sensor signals to 0.75 ppm NO_2 in different humidity levels and during various illumination conditions.

The sensor signals are decreasing with increasing photon energy, with a minimum in UV and dUV. A similar trend was observed in the baseline resistances. Ideally, it would be expected that the signal was increased by the application of light, however, the opposite was observed in this case. That the signals decrease already in red, green and blue light suggests a decomposition of NO_2 which is supported by the highly porous ZnO surface [91] and additionally enhanced by the light. As the photon energy increases, less NO_2 is available for the adsorption. This effect is strongest in UV and dUV. Below a wavelength of

approximately 420 nm, NO_2 is decomposed to NO and O. In the presence of O_2 the formation of O_3 occurs, which re-oxidizes the components again to NO_2 and O_2. This process decreases the effective concentration of NO_2 at the surface [92]. The interplay of both processes explains the reduced signals with increasing photon energy.

Furthermore, the signals are dependent on the level of humidity. For most of the illumination conditions they are lowest in 0 % RH and highest in 10 % RH. The peculiar trend of the baseline resistance in various RH is represented in the signals as well, especially in blue, UV and dUV. It explains the variations of signals with humidity.

The signals of both measurements in the dark are very comparable, which indicates a good recovery from the different applied photon energies. However, the dependency on RH is stronger in the end, with the highest signal for 70 % RH. Otherwise than initially expected from the raw data, this indicates that irreversible, light induced processes changed the surface slightly throughout the experiment.

5.3 Summary and Outlook

In this chapter it was demonstrated that light in the UV-Vis range changes the sensing behavior of FSP-prepared ZnO. Already red light provided sufficient photon energy for the activation of charge carriers, which indicates the presence of defect states in the band gap. It was observed that especially dUV has a different effect on the baseline resistance and suggested that it induced adsorption and desorption processes. Additionally, the results indicated slight degradation effects by illumination. During the exposure to various humidity levels, untypical resistance changes were observed that are not fully understood yet.

The applied light stabilized and speeded up the response and recovery in NO_2 with increasing photon energy. However, at the same time the sensor signal was decreased, which is the contrary to the expectations based on the literature. It was suggested that NO_2 was decomposed due to the large surface area in combination with the applied light.

The results demonstrated that many processes are not yet fully understood. A spectroscopic study of the reactions with water vapor and NO_2 will be key elements of future research. They will help to identify the reasons for the different sensing behavior compared to conventionally operated sensors. By changing the respective parameters during the material synthesis, improvements in the sensor performance will be possible.

6 Bibliography

[1] A. F. Holleman, E. Wiberg, *Lehrbuch Der Anorganischen Chemie*, 102nd edition, Walter de Gruyter & Co., Berlin, **2007**.

[2] J. Kolar, *Stickstoffoxide und Luftreinhaltung: Grundlagen, Emissionen, Transmission, Immissionen, Wirkungen*, Springer, **2013**.

[3] B. Ritz, B. Hoffmann, A. Peters, *Dtsch. Arztebl. Int.* **2019**, *116*, 881–886.

[4] "Stickoxidgrenzwerte der Aussenluft und am Arbeitsplatz", Deutscher Bundestag, 2018.[Online]. Available: https://www.bundestag.de/resource/blob/531762/6a7d2a26e62fab08cef1ebe7c79961be/WD-8-035-17-pdf-data.pdf. [Accessed: 15-Dec-2023]

[5] N. Barsan, D. Koziej, U. Weimar, *Sensors Actuators B Chem.* **2007**, *121*, 18–35.

[6] G. Heiland, *Zeitschrift für Phys.* **1954**, *138*, 459–464.

[7] N. Barsan, in *8th Gospel Work. Gas Sensors Based Semicond. Met. Oxides Basic Underst. Appl. Fields*, MDPI, Basel Switzerland, **2019**, p. 53.

[8] S. Tyagi, M. Chaudhary, A. K. Ambedkar, K. Sharma, Y. K. Gautam, B. P. Singh, *Sensors & Diagnostics* **2022**, *1*, 106–129.

[9] R. Kumar, O. Al-Dossary, G. Kumar, A. Umar, *Nano-Micro Lett.* **2015**, *7*, 97–120.

[10] E. Mollwo, *Zeitschrift für Phys.* **1954**, *138*, 478–488.

[11] N. Saito, K. Watanabe, H. Haneda, I. Sakaguchi, K. Shimanoe, *J. Phys. Chem. C* **2018**, *122*, 7353–7360.

[12] X. Xing, X. Xiao, L. Wang, Y. Wang, *Sensors Actuators B Chem.* **2017**, *247*, 797–806.

[13] N. Saito, H. Haneda, K. Watanabe, K. Shimanoe, I. Sakaguchi, *Sensors Actuators B Chem.* **2021**, *326*, 128999.

[14] E.-C. Lee, K. J. Chang, *Phys. Rev. B* **2004**, *70*, 115210.

[15] B. W. C. Au, K. Y. Chan, *Appl. Phys. A Mater. Sci. Process.* **2017**, *123*, 1–9.

[16] N. S. Parmar, C. D. Corolewski, M. D. McCluskey, K. G. Lynn, *AIP Adv.* **2015**, *5*.

[17] L. Zhu, W. Zeng, *Sensors ActuatorsA Phys.* **2017**, *267*, 242–261.

[18] S. Maeng, S. W. Kim, D. H. Lee, S. E. Moon, K. C. Kim, A. Maiti, *ACS Appl. Mater. Interfaces* **2014**, *6*, 357–363.

[19] A. Staerz, U. Weimar, N. Barsan, *Sensors Actuators B Chem.* **2022**, *358*, 131531.

[20] M. Chen, Z. Wang, D. Han, F. Gu, G. Guo, *Sensors Actuators, B Chem.* **2011**, *157*, 565–574.

[21] M. Chen, Z. Wang, D. Han, F. Gu, G. Guo, *J. Phys. Chem. C* **2011**, *115*, 12763–12773.

[22] B. Zhang, J. Y. Sun, P. X. Gao, *ACS Sensors* **2021**, *6*, 2979–2987.

[23] K. Khamfoo, A. Staerz, M. Boepple, A. Wisitsoraat, C. Liewhiran, U. Weimar, N. Barsan, *Sensors Actuators B Chem.* **2022**, *371*, 132495.

[24] C. Ewald, N. Saito, U. Weimar, N. Barsan, *Sensors Actuators B Chem.* **2023**, *393*, 134321.

[25] A. Saaédi, R. Yousefi, *J. Appl. Phys.* **2017**, *122*.

[26] Y. Gu, Z. Ye, N. Sun, X. Kuang, W. Liu, X. Song, L. Zhang, W. Bai, X. Tang, *J. Mater. Sci. Mater. Electron.* **2019**, *30*, 18767–18779.

[27] G. Liu, P. X. Gao, *Catal. Sci. Technol.* **2011**, *1*, 552–568.

[28] Q. Geng, Z. He, X. Chen, W. Dai, X. Wang, *Sensors Actuators B Chem.* **2013**, *188*, 293–297.

[29] N. M. Vuong, N. D. Chinh, T. T. Hien, N. D. Quang, D. Kim, H. Kim, S.-G. Yoon, D. Kim, *J. Nanosci. Nanotechnol.* **2016**, *16*, 10346–10350.

[30] Y. Chen, X. Li, X. Li, J. Wang, Z. Tang, *Sensors Actuators B Chem.* **2016**, *232*, 158–164.

[31] B. P. J. de Lacy Costello, R. J. Ewen, N. M. Ratcliffe, M. Richards, *Sensors Actuators B Chem.* **2008**, *134*, 945–952.

[32] Z. Zou, Y. Qiu, J. Xu, P. Guo, Y. Luo, C. Wang, *J. Alloys Compd.* **2017**, *695*, 2117–2123.

[33] A. Chizhov, P. Kutukov, A. Gulin, A. Astafiev, M. Rumyantseva, *Chemosensors* **2022**, *10*, 147.

[34] J. Wang, Y. Shen, X. Li, Y. Xia, C. Yang, *Sensors Actuators B Chem.* **2019**, *298*, 126858.

[35] K. Matsumoto, N. Saito, T. Mitate, J. Hojo, M. Inada, H. Haneda, *Cryst. Growth Des.* **2009**, *9*, 5014–5016.

[36] H. Jung, W. Cho, R. Yoo, H. sook Lee, Y. S. Choe, J. Y. Jeon, W. Lee, *Sensors Actuators B Chem.* **2018**, *274*, 527–532.

[37] J. Kappler, *Characterisation of high-performance SnO_2 gas sensors for CO detection by in situ techniques*, Dissertation, Eberhard Karls Universität Tübingen, **2001**.

[38] S. Rank, *The Influence of the Electrode Material on the Sensor Characteristics of SnO_2 Thick Film Gas Sensors*, Dissertation, Eberhard Karls Universität Tübingen, **2014**.

[39] L. Mädler, A. Roessler, S. E. Pratsinis, T. Sahm, A. Gurlo, N. Barsan, U. Weimar, *Sensors Actuators B Chem.* **2006**, *114*, 283–295.

[40] M. Sokolowski, A. Sokolowska, A. Michalski, B. Gokieli, *J. Aerosol Sci.* **1977**, *8*, 219–230.

[41] K. Okuyama, Y. Kousaka, N. Tohge, S. Yamamoto, J. J. Wu, R. C. Flagan, J. H. Seinfeld, *AIChE J.* **1986**, *32*, 2010–2019.

[42] S. Chung, Y. Sheu, M. Tsai, *J. Am. Ceram. Soc.* **1992**, *75*, 117–123.

[43] Y. Xia, L. Zhou, J. Yang, P. Du, L. Xu, J. Wang, *ACS Appl. Electron. Mater.* **2020**, *2*, 580–589.

[44] D. Degler, H. W. Pereira de Carvalho, U. Weimar, N. Barsan, D. Pham, L. Mädler, J.-D. Grunwaldt, *Sensors Actuators B Chem.* **2015**, *219*, 315–323.

[45] J. Kemmler, S. O. Schopf, L. Mädler, N. Barsan, U. Weimar, *Procedia Eng.* **2014**, *87*, 24–27.

[46] B. Junker, A. Kobald, C. Ewald, P. Janoschek, M. Schalk, U. Weimar, L. Mädler, N. Barsan, *ACS Sensors* **2024**, *9*, 1584–1591.

[47] J. M. Olinger, P. R. Griffiths, *Anal. Chem.* **1988**, *60*, 2427–2435.

[48] G. Ballerini, K. Ogle, M. G. Barthés-Labrousse, *Appl. Surf. Sci.* **2007**, *253*, 6860–6867.

[49] Q. Feng, S. Wen, *J. Alloys Compd.* **2017**, *709*, 602–608.

[50] H. Noei, C. Wöll, M. Muhler, Y. Wang, *J. Phys. Chem. C* **2011**, *115*, 908–914.

[51] J. Zhao, C. Xie, L. Yang, S. Zhang, G. Zhang, Z. Cai, *Appl. Surf. Sci.* **2015**, *330*, 126–133.

[52] C. Ewald, *Evaluating the Sensor Response of ZnO Based Gas Sensors to NO_2*, Master Thesis, Eberhard Karls Universität Tübingen, **2020**.

[53] Lontio Fomekong, Saruhan, *Chemosensors* **2019**, *7*, 42.

[54] M. Tonezzer, L. Van Duy, *Gas Sensors*, in *Encycl. Sensors Biosens.*, Elsevier, **2023**, pp. 185–208.

[55] C. Liu, Q. Ma, H. He, G. He, J. Ma, Y. Liu, Y. Wu, *Environ. Sci. Nano* **2017**, *4*, 2388–2394.

[56] L. D'Arsié, V. Alijani, S. T. S. Brunelli, F. Rigoni, G. Di Santo, M. Caputo, M. Panighel, S. Freddi, L. Sangaletti, A. Goldoni, *Sci. Rep.* **2018**, *8*, 10028.

[57] B. S. de Lima, W. A. S. Silva, A. L. Ndiaye, V. R. Mastelaro, J. Brunet, *Chemom. Intell. Lab. Syst.* **2022**, *220*, 104460.

[58] D. Degler, *Spectroscopic Insights in the Gas Detection Mechanism of Tin Dioxide Based Gas Sensors*, Dissertation, Eberhard Karls Universität Tübingen, **2017**.

[59] E. Schmitt, *Surface Reaction Mechanisms of Volatile Organic Compounds on WO_3 - based Gas Sensors*, Master Thesis, Eberhard Karls Universität Tübingen, **2022**.

[60] D. Degler, S. Wicker, U. Weimar, N. Barsan, *J. Phys. Chem. C* **2015**, *119*, 11792–11799.

[61] A. Davydov, N. Sheppard, *Molecular spectroscopy of oxide catalyst surfaces*, Wiley, Chichester, **2003**.

[62] W. M. Hlaing, Infrared Spectroscopy of Zinc Oxide and Magnesiumnanostructures, Dissertation, Washington State University, **2007**.

[63] G. Heiland, D. Kohl, in *Chem. Sens. Technol.*, Elsevier, **1988**, pp. 15–38.

[64] J. A. Rodriguez, T. Jirsak, J. Dvorak, S. Sambasivan, D. Fischer, *J. Phys. Chem. B* **2000**, *104*, 319–328.

[65] S. Roso, D. Degler, E. Llobet, N. Barsan, A. Urakawa, *ACS Sensors* **2017**, *2*, 1272–1277.

[66] K. I. Hadjiivanov, *Catal. Rev. - Sci. Eng.* **2000**, *42*, 71–144.

[67] G. Busca, V. Lorenzelli, *J. Catal.* **1981**, *72*, 303–313.

[68] M. Kantcheva, *Appl. Catal. B Environ.* **2003**, *42*, 89–109.

[69] D. M. L. Goodgame, M. A. Hitchman, *Inorg. Chem.* **1965**, *4*, 721–725.

[70] K. Shingange, Z. P. Tshabalala, O. M. Ntwaeaborwa, D. E. Motaung, G. H. Mhlongo, *J. Colloid Interface Sci.* **2016**, *479*, 127–138.

[71] N. Kalinke, *Untersuchung von ZnO Quantenpunkten bezüglich ihrer Teilchengröße und gassensitiven Eigenschaften in Abhängigkeit der Kalziniertemperatur*, Bachelor Thesis, Eberhard Karls Universität Tübingen, **2019**.

[72] M. Afzal, H. Ahmad, F. Mahmoud, *Jour. Chem. Soc. Pak.* **1991**, *13*, 219–222.

[73] A. V. Shchukarev, D. V. Korolkov, *Cent. Eur. J. Chem.* **2004**, *2*, 347–362.

[74] T. P. Dirkse, C. Postmus, R. Vandenbosch, *J. Am. Chem. Soc.* **1954**, *76*, 6022–6024.

[75] A. Gurlo, N. Bârsan, A. Oprea, M. Sahm, T. Sahm, U. Weimar, *Appl. Phys. Lett.* **2004**, *85*, 2280–2282.

[76] J. X. Wang, X. W. Sun, Y. Yang, C. M. L. Wu, *Nanotechnology* **2009**, *20*, DOI 10.1088/0957-4484/20/46/465501.

[77] A. Staerz, A. Kobald, T. Russ, U. Weimar, A. Hémeryck, N. Barsan, *ACS Appl. Electron. Mater.* **2020**, *2*, 3254–3262.

[78] N. F. Khadiran, M. Z. Hussein, R. Ahmad, T. Khadiran, Z. Zainal, W. R. W. A. Kadir, S. S. Hashim, *J. Porous Mater.* **2021**, *28*, 1797–1811.

[79] J. Wu, T. Su, Y. Jiang, X. Xie, Z. Qin, H. Ji, *Appl. Surf. Sci.* **2017**, *412*, 290–305.

[80] X. Zhu, C. Chen, Q. Wang, Y. Shi, D. O'Hare, N. Cai, *Chem. Eng. J.* **2019**, *366*, 181–191.

[81] Q. Li, M. Meng, N. Tsubaki, X. Li, Z. Li, Y. Xie, T. Hu, J. Zhang, *Appl. Catal. B Environ.* **2009**, *91*, 406–415.

[82] V. Fantauzzo, *Exploring KNO_3 behaviour and Formation through Simulation,* Dissertaion, The University of Sheffield, **2023**.

[83] T. Harada, F. Simeon, E. Z. Hamad, T. A. Hatton, *Chem. Mater.* **2015**, *27*, 1943–1949.

[84] M. Birkholz, *Thin Film Analysis by X-Ray Scattering*, Whiley-VCH, Weinheim, **2005**.

[85] W. H. Strehlow, E. L. Cook, *J. Phys. Chem. Ref. Data* **1973**, *2*, 163–200.

[86] V. Srikant, D. R. Clarke, *J. Appl. Phys.* **1998**, *83*, 5447–5451.

[87] J. B. Cantuária, G. Gozzi, L. F. Santos, *MRS Adv.* **2019**, *4*, 111–117.

[88] M. Takeuchi, G. Martra, S. Coluccia, M. Anpo, *J. Phys. Chem. C* **2007**, *111*, 9811–9817.

[89] Q. Zhang, Z. Pang, W. Hu, J. Li, Y. Liu, Y. Liu, F. Yu, C. Zhang, M. Xu, *Appl. Surf. Sci.* **2021**, *541*, 148418.

[90] M. Benamara, S. S. Teixeira, M. P. F. Graça, M. A. Valente, S. K. Jakka, H. Dahman, E. Dhahri, L. El Mir, M. Debliquy, D. Lahem, *Appl. Phys. A* **2021**, *127*, 706.

[91] J. A. Rodriguez, J. Hrbek, *J. Vac. Sci. Technol. A Vacuum, Surfaces, Film.* **1994**, *12*, 2140–2144.

[92] I. B. Pollack, B. M. Lerner, T. B. Ryerson, *J. Atmos. Chem.* **2010**, *65*, 111–125.

Appendix

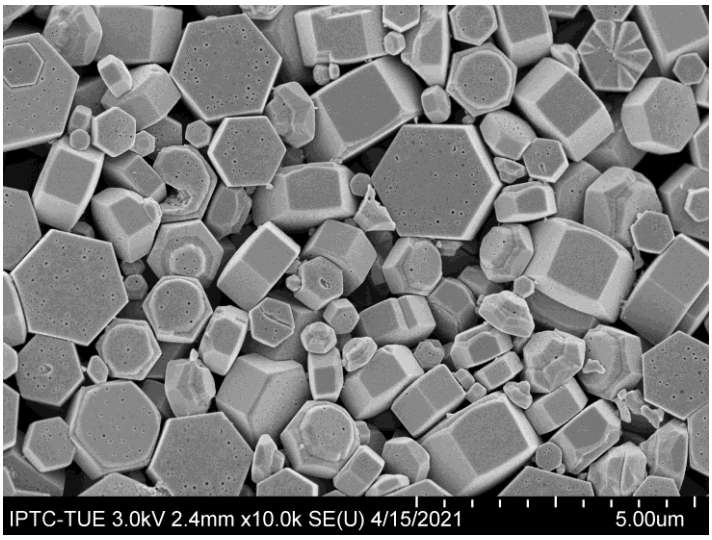

SF 1 SEM image of rods in lower magnification than in section 3.1 for a better overview of the particle size.

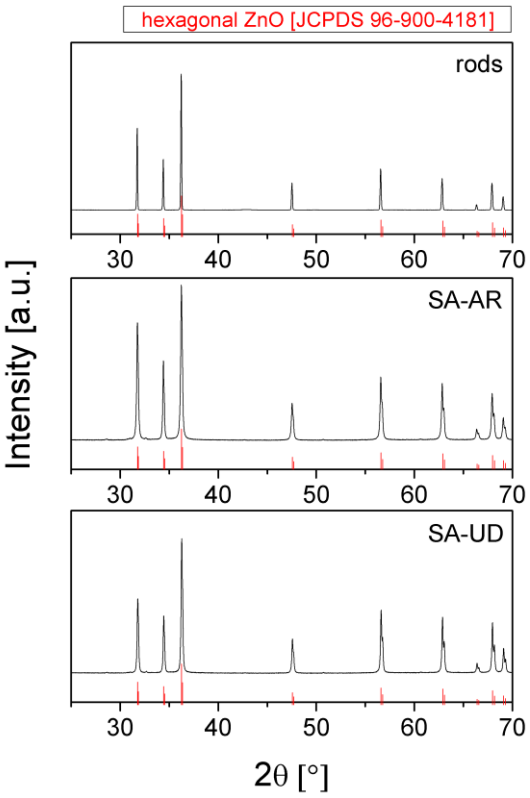

SF 2 XRD patterns of rods, SA-AR and SA-UD with hexagonal ZnO as reference.

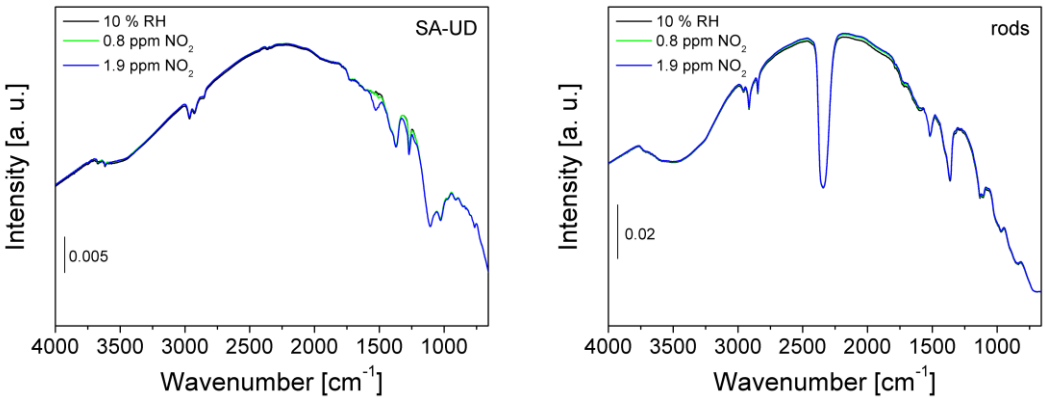

SF 3 Single channel spectra in 10 % RH, 0.8 and 1.9 ppm NO_2 for SA-UD (left) and rods (right). Below 1000 cm^{-1} the intensity decreases strongly.

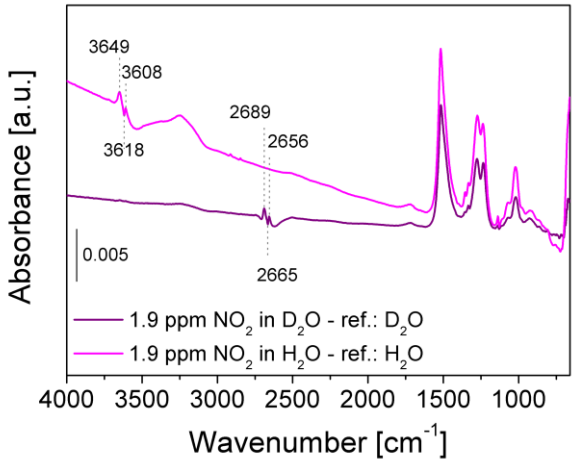

SF 4 Absorbance spectra of SA-UD during exposure to NO_2 in 10 % D_2O @ 25 °C and in 10 % H_2O @ 25 °C to demonstrate the hydroxyl rearrangement.

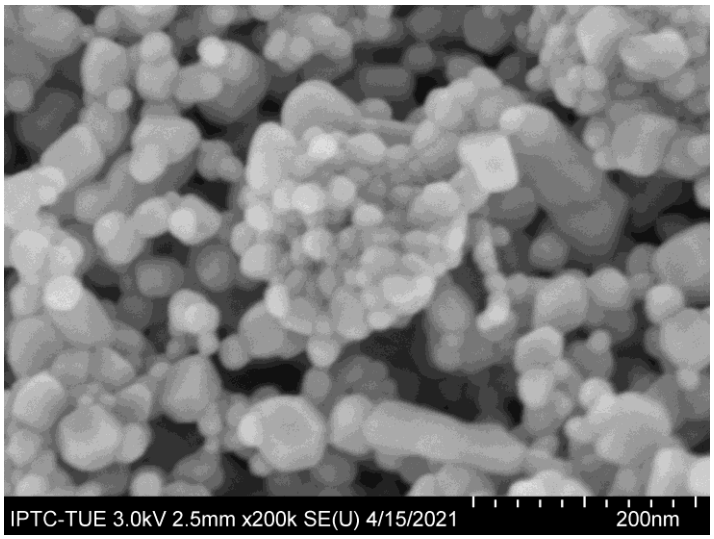

SF 5 SEM image of QD in higher magnification than in section 4.1 for a better overview of the particle size.

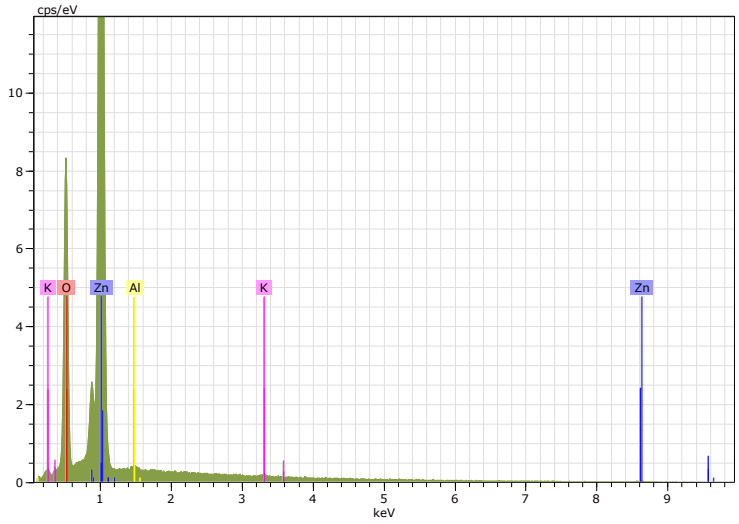

SF 6 EDX spectrum of QD p1.

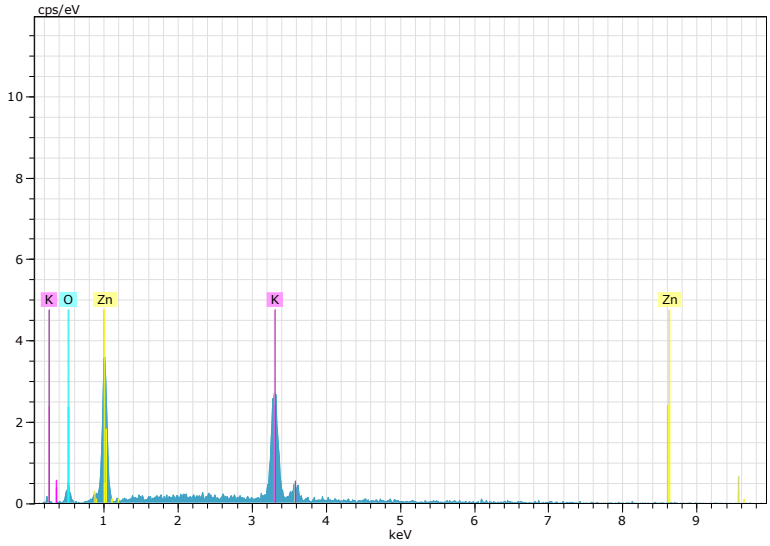

SF 7 EDX spectrum of QD p2.

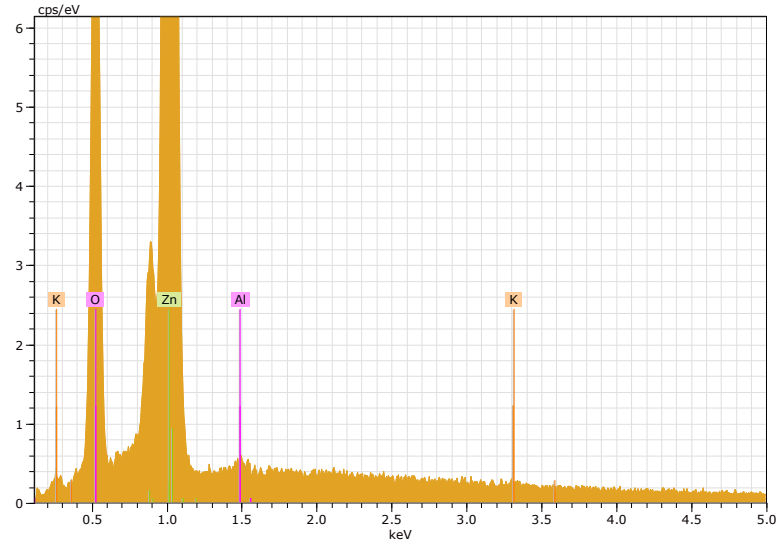

SF 8 EDX spectrum of SA-UD p1.

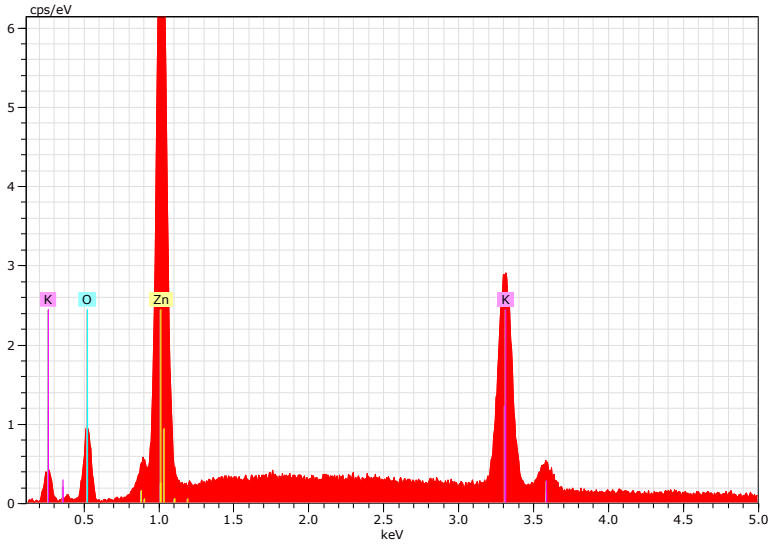

SF 9 EDX spectrum of SA-UD p2.

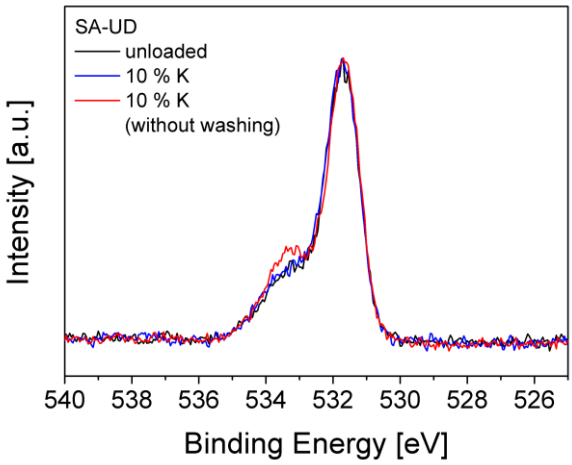

SF 10 O1s XPS results of unloaded and K-loaded SA-UD samples; the spectra were scaled for comparison.

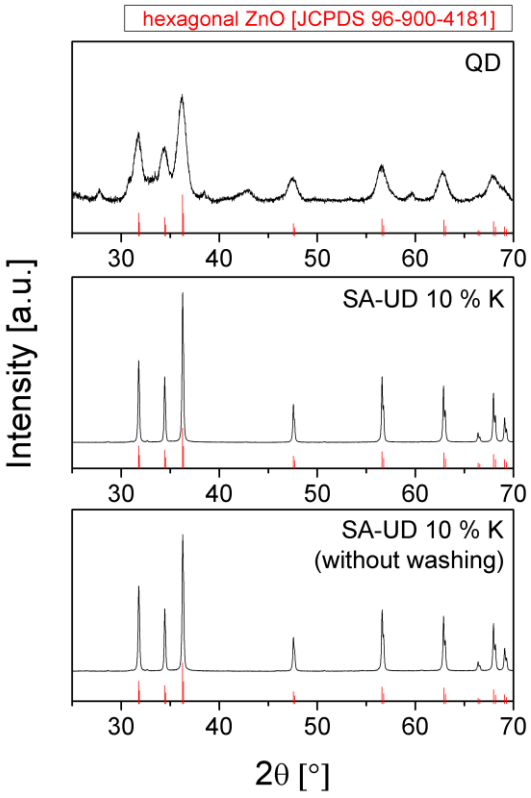

SF 11 XRD patterns of QD, SA-UD 10 % K and 10 % K (without washing) with hexagonal ZnO as reference.

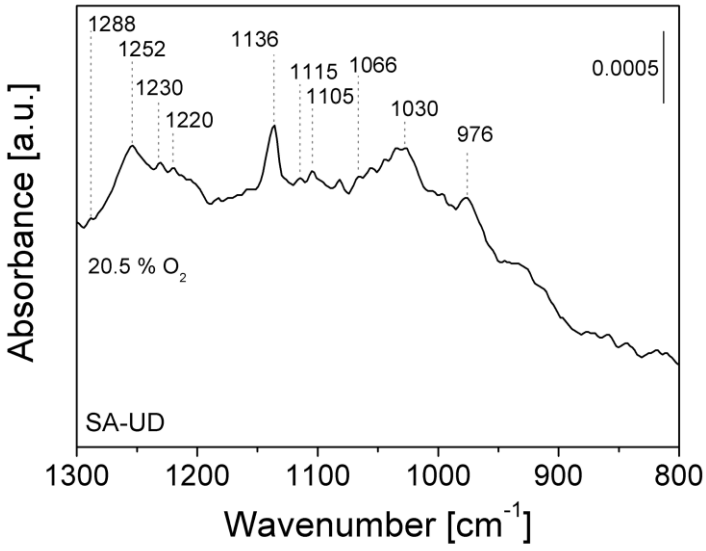

SF 12 Section of the absorbance spectrum depicted in Figure 3.7 in order to show additional Zn-O bands. Reference spectrum: nitrogen.

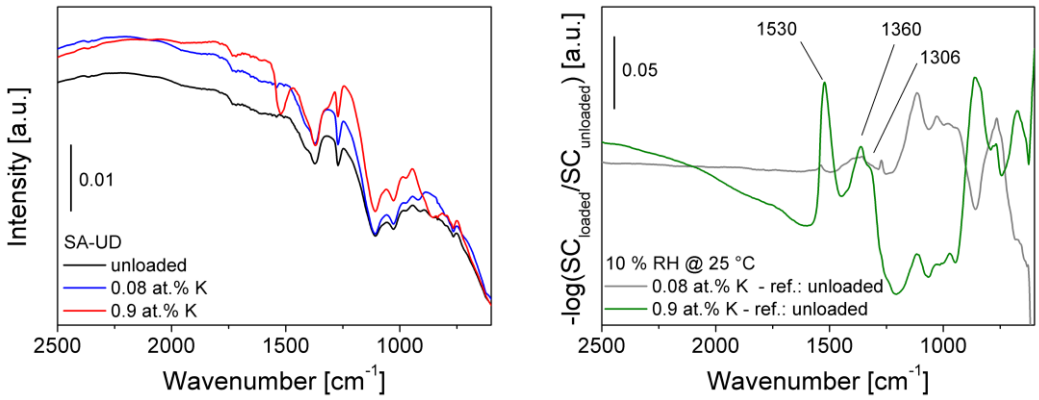

SF 13 Single channel spectra of SA-UD samples recorded in 10 % RH @ 25 °C (left) and referenced spectra of 0.08 and 0.9 at.% K SA-UD; reference spectrum: unloaded SA-UD.

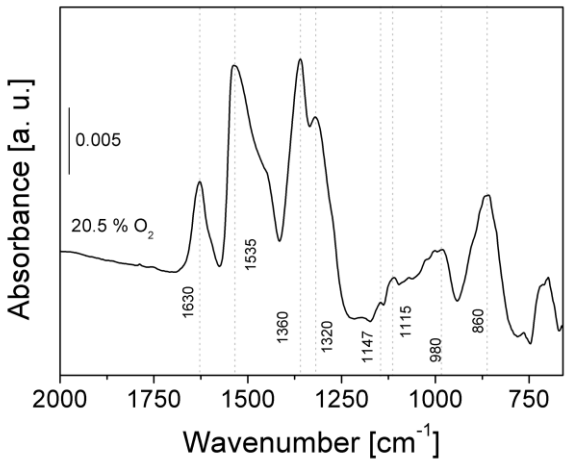

SF 14 Zn-O bands in QD during exposure to 20.5 % oxygen in nitrogen; reference spectrum: nitrogen.

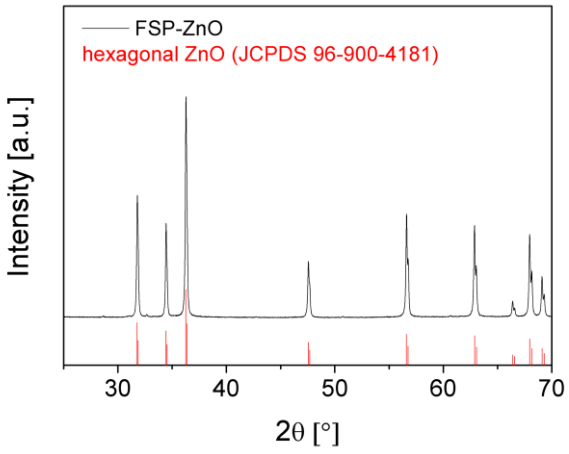

SF 15 XRD pattern of ZnO prepared via FSP with hexagonal ZnO as reference.

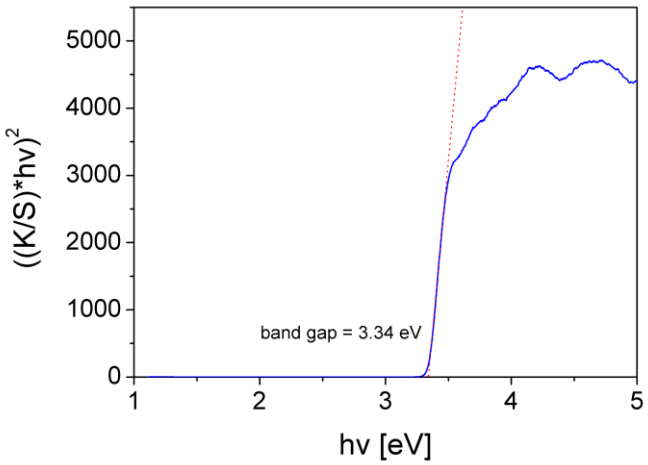

SF 16 Tauc plot of FSP ZnO for the determination of the band gap with data measured via DRUVS.

Publications

Full papers

B. Junker, A. Kobald, C. Ewald, P. Janoschek, M. Schalk, U. Weimar, L. Mädler, N. Barsan, Multivariate Analysis of Light-Activated SMOX Gas Sensors, ACS Sensors 9 (2024) 1574–1591.

C. Ewald, N. Saito, U. Weimar, N. Barsan, Role of potassium loading in ZnO-based gas sensors under NO_2 exposure – Operando diffuse reflectance infrared Fourier transform spectroscopic study, Sensors Actuators B Chem. 393 (2023) 134321.

X.-X. Wang, B. Junker, C. Ewald, U. Weimar, X. Guo, N. Barsan, Proof of Concept for Operando Infrared Spectroscopy Investigation of Light-Excited Metal Oxide-Based Gas Sensors, J. Phys. Chem. Lett. 13 (2022) 3631–3635.

Talks

C. Ewald, N. Saito, U. Weimar, N. Barsan, ZnO based gas sensors and the response to NO_2: role of potassium contamination, PhD GOSPEL Workshop 2021-2022: Gas sensors based on semiconducting metal oxides: basic understanding & application fields (Virtual Edition), 2022.

Academic Teachers

R. Anwander, N. Barsan, H. Bettinger, T. Chassé, K. Eichele, R. Fink, G. Gauglitz, J. Glaser, S. Grond, C. Huhn, M. Kramer, D. Kunz, M. E. Maier, H. A. Mayer, A. J. Meixner, H.-J. Meyer, B. Nachtsheim, U. Nagel, A. Oprea, H. Peisert, M. Scheele, A. Schnepf, E. Schweda, M. Seitz, P. Sirsch, B. Speiser, U. Weimar, L. Wesemann, D. Wistuba, K.-P-. Zeller, D. Zhang, T. Ziegler

Danksagungen

Herrn Dr. Nicolae Barsan möchte ich an erster Stelle für die Betreuung und Unterstützung während meiner Doktorarbeit danken. Die konstruktive Kritik und die regelmäßigen Diskussionen haben das Gelingen dieser Arbeit erst möglich gemacht.

Außerdem danke ich Herrn Prof. Dr. Udo Weimar für die Bereitstellung des interessanten Dissertationsthemas sowie die herzliche Aufnahme in die Arbeitsgruppe.

Bei Herrn Prof. Dr. Reinhold Fink bedanke ich mich für die Übernahme des Zweitgutachtens sowie die Bereitschaft, zusammen mit Prof. Dr. Doris Kunz und Prof. Dr. Marcus Scheele die mündlichen Prüfer*innen bei der Verteidigung zu sein.

Herrn Dr. Alexandru Oprea danke ich für seine Unterstützung bei technischen Problemstellungen.

Ein großer Dank geht an alle Kolleg*innen der Arbeitsgruppe Weimar, die mir durch das konstruktive Miteinander und die angenehme Arbeitsatmosphäre die letzten Jahre zu einer unvergesslichen Zeit gemacht haben. Ganz besonders danke ich Benjamin Junker für die stetige Bereitschaft für (nicht nur) wissenschaftliche Gespräche und Diskussionen sowie Hilfestellungen bei Versuchsaufbauten. Außerdem danke ich herzlich meinen Bürokollegen Ugur Geyik und Peter Janoschek, die immer ein offenes Ohr haben. Leah Schynowski und Jonas von Festenberg danke ich für die Unterstützung bei Laborarbeiten.

Der Deutschen Forschungsgemeinschaft (DFG) möchte ich herzlich für die finanzielle Unterstützung im Rahmen des Forschungsprojektes „Photologic“ während der letzten Jahre danken.

Unseren „Photologic“-Projektpartnern von der Universität Bremen, Herrn Prof. Dr. Lutz Mädler und Malte Schalk danke ich für die konstruktive und wertschätzende Zusammenarbeit in dieser Zeit.

Dem NIMS (National Institute for Materials Science) in Tsukuba, Japan möchte ich für die Möglichkeit und finanzielle Unterstützung eines dreimonatigen Forschungspraktikums danken.

Ganz herzlich danke ich Frau Dr. Noriko Saito vom NIMS, die meinen Aufenthalt in Japan wissenschaftlich und persönlich bereichert hat. Unsere Kooperation hat mir viele wichtige Erkenntnisse für diese Arbeit geliefert.

Frau Elke Nadler von der Arbeitsgruppe Chassé möchte ich für die zahlreichen Aufnahmen am Rasterelektronenmikroskop danken.

Der Arbeitsgruppe von Herrn Prof. Dr. H.-J. Meyer danke ich für die Hilfsbereitschaft bei den Aufnahmen und Auswertungen von Röntgendiffraktogrammen.

Außerdem gilt mein Dank meinen Kommilitonen Axel Daikeler, Jürgen Gliebe, Lars Hirneise, Marc Junge, Theo Maulbetsch, Fabio Mazzotta, Heiko Wetzel und Max Widemann für die angenehme gemeinsame Zeit während und außerhalb des Studiums.

Schließlich möchte ich mich bei meiner Familie bedanken, allen voran meinen Eltern, die mich stets unterstützen und hinter mir stehen.

Mein ganz besonderer Dank gilt meinem Lebensgefährten Steven Wodrich für die gegenseitige Unterstützung und das schöne Zusammenleben.